SURFACTANT EFFECTS ON POLYELECTROLYTE BRUSH SWELLING AND EMULSION FILTRATION THROUGH BRUSH-COATED MEMBRANES

By

Zhefei Yang

A DISSERTATION

Submitted to
Michigan State University
in partial fulfillment of the requirements
for the degree of

Chemistry—Doctor of Philosophy

2017

ABSTRACT

SURFACTANT EFFECTS ON POLYELECTROLYTE BRUSH SWELLING AND EMULSION FILTRATION THROUGH BRUSH-COATED MEMBRANES

By

Zhefei Yang

This dissertation investigates the swelling and fouling resistance of polyanionic and polyzwitterionic brushes in the presence of surfactants and surfactant-stabilized oil-in-water (O/W) emulsions. Such emulsions are an undesired byproduct of many processes, the largest of which is the massive oil and gas extraction industry. Among the three existing forms of oil (free oil, dispersions and emulsions), emulsions are the most difficult to treat due to the small oil droplet size (< 20 μm) and surfactant-enhanced emulsion stability. Membrane filtration is an effective method for removing oil from emulsions, but fouling induces a rapid decline in permeate flux that may make such separations impractical.

Polyelectrolyte brushes can potentially resist oil fouling because they are superoleophobic in aqueous solutions due to their strong water affinity. This research employs surface-initiated atom transfer radical polymerization for relatively controlled growth of polyanionic and polyzwitterionic films. Poly(3-sulfopropyl methacrylate potassium salt) (PSPMK) brushes formed on Au surfaces show underwater hexadecane contact angles of nearly 180°. Due to electrostatic repulsion, these polyanionic brushes do not adsorb the anionic surfactant sodium dodecyl sulfate (SDS). Moreover, with SDS-stabilized O/W emulsions, microfiltration membranes modified with PSPMK brushes show ~100% oil rejection and a constant permeate flux, indicating minimal fouling during 12-h, dead-end filtrations. In contrast, electrostatic attraction causes strong adsorption of the cationic surfactant cetrimonium bromide (CTAB) to PSPMK brushes, and this leads to

brush collapse and no oil rejection during filtration. Thus, polyanionic brushes effectively resist oil fouling, but only for emulsion stabilized with anionic surfactants.

To investigate whether zwitterionic films can resist adsorption of both cationic and anionic surfactants, this work employed poly(sulfobetaine methacrylate) (PSBMA) brushes. Unfortunately, both cationic and anionic surfactants adsorb to these brushes, and swelling in surfactant solutions depends on surfactant charge and concentration, as well as brush thickness. Preliminary data show that during the filtration of O/W emulsions, the permeate flux is much lower than the pure water flux, presumably because of fouling. Moreover, the permeate flux increases during filtration, implying brush collapse after oil adsorption. Compared with the strong fouling resistance of anionic PSPMK brushes to negatively charged oil droplets, the nearly neutral zwitterionic brushes have little charge repulsion to oil droplets and show low resistance to fouling.

During filtration with PSBMA-modified membranes, oil coalescence occurs. As an alternative approach to separate O/W emulsions, membrane coalescence traditionally employs hydrophobic membranes to prompt oil attachment and coalescence on the surface. Preliminary data show that superoleophobic membranes can also induce oil coalescence and are less fouled than traditional hydrophobic membranes.

I dedicate this dissertation to my parents, Yi Yang and Hui Ma, for their endless love and support.

ACKNOWLEDGEMENTS

We gratefully acknowledge financial support from the U.S. Environmental Protection Agency (Science to Achieve Results grant RC-83518301) and from the U.S. National Science Foundation (Partnerships for International Education and Research Grant IIA-1243433).

This dissertation would not have been completed without the support from so many people. I would first like to thank my family. They are always believing and supporting me in my every decision, which is very important to me. I would like to thank my advisor Dr. Merlin Bruening and my co-advisor Dr. Volodymyr Tarabara. They are always there to give me suggestions not only in research, also in presenting and writing. I've got much inspiration from them. I would also like to thank my labmates and friends for their help and company. They made my Ph.D. life much more interesting. Finally, I want to thank everyone else who gave me help in both research and daily life during these 5 years.

TABLE OF CONTENTS

LIST OF TABLES

LIST OF FIGURES

KEY TO ABBREVIATIONS

SBMA	sulfobetaine methacrylate
O/W emulsion	oil-in-water emulsion
SI-ATRP	surface-initiated atom transfer radical polymerization
CRP	controlled radical polymerization.
SPMK	3-sulfopropyl methacrylate potassium salt
MEDSAH	[2-(methacryloyloxy)ethyl]dimethyl-(3-sulfopropyl) ammonium hydroxide
PDA	polydopamine
FTIR	Fourier-transform infrared spectroscopy
SDS	sodium dodecyl sulfate
CTAB	cetrimonium bromide
DTAB	dodecyltrimethylammonium bromide
BSA	bovine serum albumin
BIBB	α-bromoisobutyryl bromide
PPEGMA	poly(poly(ethylene glycol) methacrylate)
PHEMA	poly(2-hydroxyethyl methacrylate)
XPS	X-ray photoelectron spectroscopy

SEM	scanning electron microscope
AFM	atomic force microscope

Chapter 1. Introduction

This dissertation aims to develop polyanionic and polyzwitterionic brushes as superoleophobic coatings that resist fouling during filtration of surfactant-stabilized oil-in-water (O/W) emulsions. Polyanionic brushes swell greatly in water and do not adsorb anionic surfactants due to electrostatic repulsion. Remarkably, microfiltration membranes modified with these brushes reject >99.9% of the oil from emulsions stabilized by anionic surfactants, and the permeate flux does not decline over time, which demonstrates excellent resistance to fouling. In contrast, electrostatic attraction induces strong adsorption of cationic surfactants or cationic surfactant-stabilized oil droplets to polyanionic brushes. Thus, I examined zwitterionic poly(sulfobetaine methacrylate) (PSBMA) brushes as coatings that may resist fouling in solutions containing either cationic or anionic surfactants. However, these brushes adsorb both anionic and cationic surfactants, and this sorption strongly depends on thickness of the swollen brushes, surfactant charge and surfactant concentration. The swelling of PSBMA brushes in surfactant solutions results from a combination of charge-screening, disordering of water molecules around zwitterions and the surfactant hydrophobicity. While developing these brushes, I obtained preliminary filtration data that suggest that oil droplets coalesce on some membrane surfaces, which could provide another approach for combatting fouling.

This chapter first introduces O/W submicron emulsions and describes the importance of removing oil from these mixtures. The second section of this introduction reviews common approaches for oil-water separation, emphasizing membrane filtration as an effective method, especially for submicron O/W emulsions. I then present background on polyelectrolyte brushes as effective anti-fouling materials, and briefly explore their

synthesis and underwater superoleophobicity. Finally, the fourth section gives a brief description of oil coalescence on membranes, which is a much less common strategy than membrane filtration but may provide an effective alternative mechanism for separating O/W emulsions. At the end of this chapter, I briefly outline the rest of this dissertation.

1.1. O/W Emulsions in Produced Water

1.1.1. Oil and Grease in Produced Water

Produced water, the wastewater that stems from oil and gas extraction from underground deposits, is a massive, unwanted byproduct in the oil industry.[1] According to a 2012 market study, fossil fuel extraction creates more than 115 billion barrels of produced water each year. Generation of each barrel of oil leads to around 3 barrels of produced water. This ratio was 8/1 (barrels of produced water/barrels of oil) for the United States in 2012 and will likely reach 12/1 by 2027. In the worst cases, this ratio may increase to 50/1.[2] Oil and grease are among the major components in produced water, with a wide concentration range from 20-200000 mg/L.[3] As discharged oil and grease may significantly damage the environment, the US Environmental Protection Agency issues regulations governing their discharge. For example, the maximum concentration of oil and grease in the effluents of any new oil and gas facilities cannot exceed 42 mg/L at any time. Meanwhile, the average concentration in effluents for 30 successive days cannot exceed 29 mg/L.[4] These tight regulations of oil discharge along with the growth of oil and gas industries require new advances in efficient oil-water separations.

1.1.2. Surfactant-Stabilized Oil-in-Water (O/W) Emulsions

Based on the sizes of oil droplets, oil and grease in produced water exist in three categories: free oil (> 150 μm), dispersed oil (20-150 μm) and emulsified oil (< 20 μm).[5] Emulsions

with oil droplets smaller than 1 μm are termed submicron emulsions[6] and are common in drug delivery,[7, 8] pesticide formulations,[9] food processing,[10] cosmetics[11] and emulsion polymerization.[12, 13] Separation of these tiny oil droplets from water is very challenging, particularly because surfactants stabilize these droplets.

Surfactants are amphiphilic compounds with both hydrophilic and hydrophobic moieties. According to the charge on the hydrophilic groups, surfactants fall into four groups: cationic, anionic, nonionic and zwitterionic (Figure 1.1). The amphiphilicity of surfactants allows them to reside at the oil-water interface, increasing oil solubility in water and preventing coalescence of oil droplets (Figure 1.2).

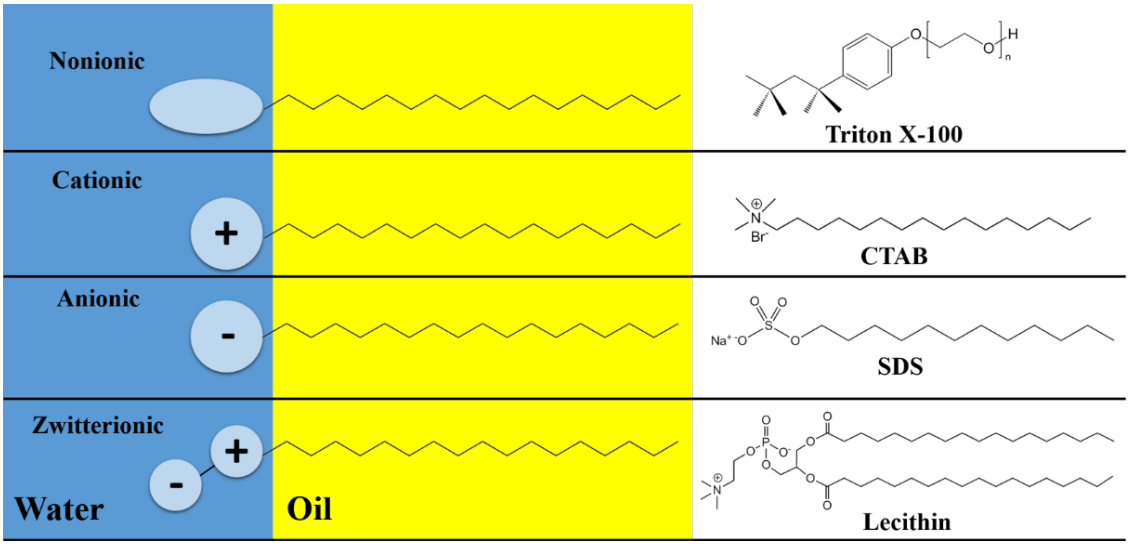

Figure 1.1. Surfactant classification based on the charge of the hydrophilic head group, and specific examples. SDS-sodium dodecyl sulfate; CTAB-cetrimonium bromide.

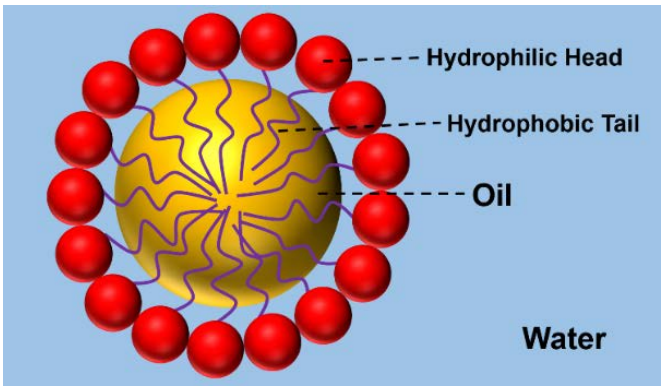

Figure 1.2. Surfactant-stabilized oil droplets in an O/W emulsion.

1.2. Separation of O/W Emulsions

1.2.1. Common Oil-Water Separation Methods

For produced water, oil-water separation typically occurs in three stages.[14, 15] The primary treatment relies on the density difference between oil and water and uses instruments such as the American Petroleum Institute gravity separator. In general, solid particles will settle to the bottom and the oil will rise to the surface, leaving the wastewater in the middle phase. However, the primary treatment can only isolate free oil (droplets larger than 150 μm).[16] The remaining oil droplets are too small to separate from water using density differences. Stokes' equation (Eq. 1.1) illustrates this point as it describes droplets' vertical velocity, V,

$$V = \frac{d^2 g(\rho_w - \rho_o)}{18\mu_w} \qquad \text{Eq. 1.1}$$

as a function of the droplet diameter, d, the densities of water and oil, ρ_w and ρ_o respectively, and the dynamic viscosity of water, μ_w. (The variable g represents the acceleration due to gravity.) Although oil droplets will float to the surface due to their low density relative to water, small droplet diameters lead to a low flotation rate and a low separation efficiency.

Thus, the secondary separation stage aims to coalesce the oil droplets. Common methods include gas flotation and the use of plate separators. Gas flotation induces gas

bubbles to contact and coalesce with oil droplets, and the oil-gas aggregates rise to the surface rapidly due to their low densities and large sizes.[17] As their name implies, plate separators employ plates to provide more surface area for oil attachment and coalescence, leading to more separation than in simple gravity separators. However, these conventional coalescing methods focus on oil droplets between 50 and 100 μm in the absence of surfactants.[18, 19]

Treatment of surfactant-stabilized emulsified oil occurs primarily at the tertiary stage. One common method in this stage is membrane filtration. This technique effectively separates oil from emulsions, even submicron O/W emulsions, and is becoming more common in both lab-scale and industrial applications. Section 1.2.3 discusses membrane filtration in more detail.

1.2.2. Conventional Methods for Demulsification

Due to the stability of emulsified oil, breaking emulsions into oil and water phases, termed demulsification, is often indispensable before separation. The traditional demulsification methods mainly include chemical addition and thermal treatment (evaporation and incineration). Both of these techniques are effective under certain conditions but suffer from shortcomings.[20] Chemical demulsification is very effective when a proper demulsifier is available. For example, addition of HCl to emulsions stabilized by ester surfactants will destabilize the system due to the surfactant decomposition.[21] However, chemical demulsification is highly susceptible to changes in the influents. Analysis of the emulsion chemical composition is vital for choosing the right demulsifier. Other limitations include mechanical problems due to clogging of chemical feeding lines, sludge generation and corrosion. Thermal treatment is more universal since it doesn't rely on specific chemical

interactions. However, heating leads to high energy costs, and oil evaporation may produce a contaminated condensate.

1.2.3. Membrane Filtration

Compared to conventional oil-water separation methods, membrane filtration has several advantages:[20, 21] (1) It doesn't require extraneous chemicals in most cases. (2) Energy costs are much lower than in thermal treatment. (3) The operation is amenable to automation. (4) Low weight and small space requirements give rise to low installation costs. (5) Because of the sieving-based barrier technology, the quality of the treated stream is not highly susceptible to the properties of the influent stream, especially when compared with chemical demulsification. (6) Membrane filtration has the potential to combine with other separation methods such as hydrocyclones.

Membrane filtration can be divided into four categories according to the membrane pore size: microfiltration (MF), ultrafiltration (UF), nanofiltration (NF) and reverse osmosis (RO). As Figure 1.3 shows, as the pore size decreases, membrane filtration requires higher operating pressures but the minimum size of the rejected species decreases.[22, 23]

Like all the other methods for oil-water separation, membrane filtration has its limitations. Most importantly, fouling greatly decreases the water-permeability of membranes. Oil droplets will attach to the membrane and block the pores during filtration, leading to decreased hydrophilicity and a permeate flux that declines with filtration time (Figure 1.4). Thus, fouling requires membrane cleaning or even replacement, which leads to a high maintenance cost. Several approaches may reduce fouling, including the use of

vibratory or centrifugal devices,[24, 25] membrane modification,[26-28] and pretreatment of feed

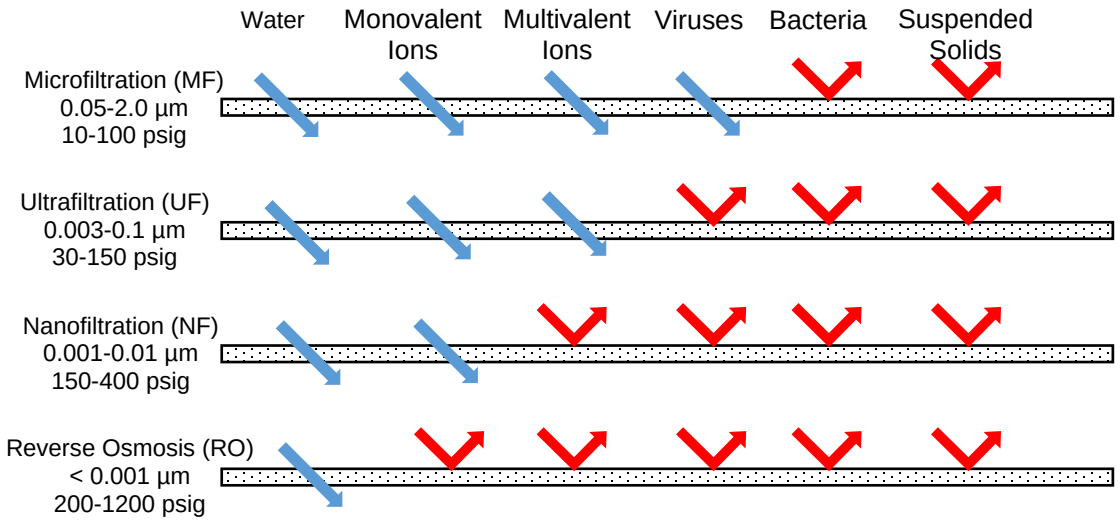

Figure 1.3. Membrane filtration classification based on the membrane pore size. The column at the left lists the method, the range of pore diameters, and typical operating pressures, whereas the figure shows solutes that the membrane rejects (bent red arrows) or allows to pass (blue arrows).

solutions.[29] Among these methods, membrane modification may prove the least expensive if modifications are stable. This work focuses on modifying membranes with polyelectrolyte brushes, so the next section introduces methods for preparing and characterizing such coatings.

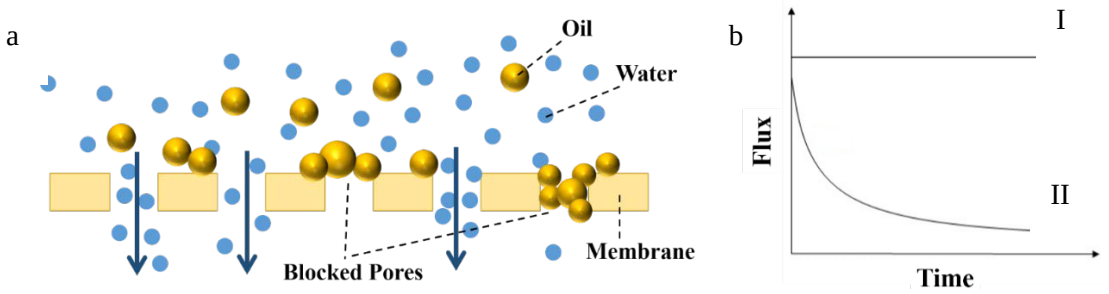

Figure 1.4. (a) Diagram of membrane fouling when oil droplets attach to the surface. (b) Qualitative plot of the fouling-induced decline in flux with time (curve II) during constant-pressure filtration. In contrast, the flux through membranes that do not foul is constant with time (b, line I).

1.3. Polyelectrolyte Brushes

1.3.1. Synthesis via Surface-Initiated Atom Transfer Radical Polymerization (SI-ATRP)

Polyelectrolyte brushes are among the most popular and well-studied anti-fouling coatings.[30-33] They consist of polyelectrolytes with one end attached to an interface,[34] and both *grafting to* and *grafting from* strategies can yield such structures (Figure 1.5).[35] The *grafting to* strategy refers to the attachment of prefabricated polymers via either physisorption or covalent bonds to a substrate. Although this strategy is feasible, it cannot produce thick and dense polymer brushes because steric repulsion between the coating and incoming chains limits the chain attachment.[36, 37] In the *grafting from* method, polymerization occurs directly from immobilized initiators. This enables the growth of thick, dense brushes because small incoming monomers can readily diffuse to initiators or growing chain ends. Controlled radical polymerization (CRP) techniques are particularly attractive for the *grafting from* strategy because they allow control over the thickness, composition and architecture of polymer brushes and are compatible with many functional groups in both aqueous and organic media.[34] Among different CRP techniques for brush fabrication, surface-initiated atom transfer radical polymerization (SI-ATRP) is especially versatile as it provides controlled polymerization of a wide range of functional monomers.

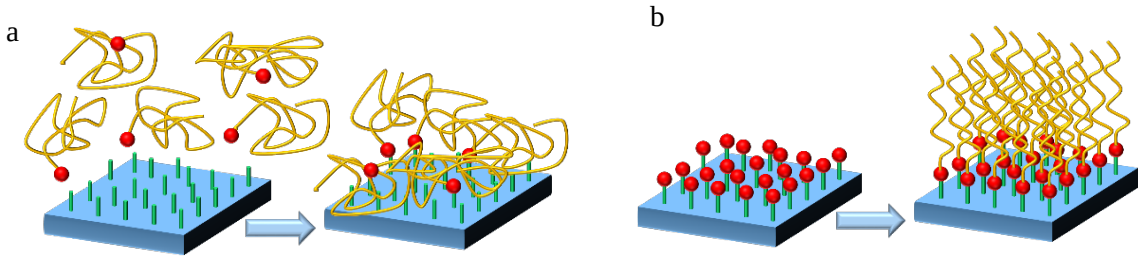

Figure 1.5. Synthetic strategies for the preparation of polymer brushes: (a) *grafting to* strategy, polymer synthesis occurs before attachment to the surface; (b) *grafting from* strategy, monomers are polymerized from initiators anchored to the surface.

ATRP relies on the reversible redox activation of a dormant alkyl halide (R-X), which is either the initiator or the end-group on a growing polymer chain, using a transition metal complex (M_t^n-Y/Ligand, Y is the counterion or another ligand and M_t is a transition metal ion). Scheme 1.1 shows a general mechanism of ATRP.[38] Homolytic cleavage of the

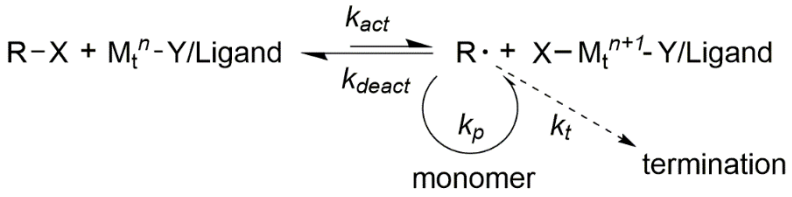

Scheme 1.1. Transition-metal-catalyzed ATRP.[38]

R-X bond through a one-electron oxidation of the transition metal complex reversibly produces a reactive radical. The rate constants for the forward and reverse reactions are k_{act} and k_{deact}, respectively. Meanwhile, in addition to deactivation the generated radicals may undergo both polymerization with a rate constant k_p and termination with a rate constant k_t. To achieve well-controlled ATRP, the concentration of radicals should be low to minimize radical termination, and this requires a rapid reversible deactivation. Moreover, fast initiation is also necessary for uniform polymer growth. A successful SI-ATRP reaction with uniform and adjustable brush growth needs optimization of the various constituents of the reaction such as the initiator, catalyst and solvent. Among these factors, the catalyst is the key to ATRP since it determines the equilibrium state of the radical formation and deactivation reactions.[39]

Despite excellent control of polymerization under many conditions, SI-ATRP suffers two major problems in the fabrication of polyelectrolyte brushes on membranes. Considering the chemical compatibility of membrane substrates, water is the preferred solvent. However, prior studies report that the ATRP catalyst deactivates by forming

complexes with charged monomers in water (Scheme 1.2).[40] Moreover, water will accelerate the disproportionation of Cu (I), leading to the loss of catalyst.[41] These side reactions may lead to a less controlled polymerization and a relatively rough brush surface.

$$M_t^n\text{-Y/Ligand} + R\text{-}SO_3^- K^+ \overset{H_2O}{\rightleftharpoons} R\text{-}SO_3^- - M_t^n\text{/Ligand} + K^+Y^-$$

$$X\text{-}M_t^{n+1}\text{-Y/Ligand} + R\text{-}SO_3^- K^+ \overset{H_2O}{\rightleftharpoons} R\text{-}SO_3^- - M_t^n\text{-Y/Ligand} + K^+X^-$$

Scheme 1.2. Catalyst deactivation by charged monomers in water.[40]

1.3.2. Wettability of Polyelectrolyte Brushes

Several studies reported that polyelectrolyte brushes form underwater superoleophobic surfaces,[42-44] which are defined as surfaces with an oil contact angle larger than 150° with contact angle hysteresis < 10°.[45, 46] For example, as Figure 1.6 shows, silicone oil spreads on polyelectrolyte brushes in air, whereas in water oil will bead up and detach from same

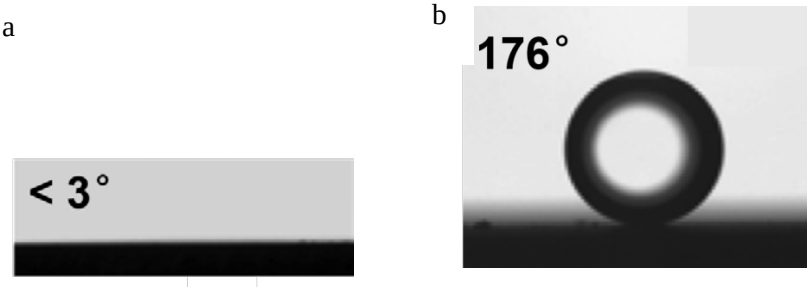

Figure 1.6. Wetting of a silicon wafer modified with PSPMK (poly(3-sulfopropyl methacrylate potassium salt)) brushes. (a) In air, the silicone oil droplet spreads on the surface to give a low contact angle. (b) In water, silicone oil forms contact angles of nearly 180°, and the oil droplet may detach from the surface. Reprinted from reference 44 with permission of the American Chemical Society.

surface. This phenomenon results from a small work of adhesion, which is the reversible work needed to separate a unit area of one phase from another.[47, 48] As shown in Figure 1.7, the work of adhesion for oil and a surface in water can be expressed as:

$$W_{ows} = \gamma_{sw} + \gamma_{ow} - \gamma_{so} \quad \text{Eq. 2}$$

where W_{ows} is the work of adhesion needed to separate oil from a solid surface. The terms γ_{sw}, γ_{ow} and γ_{so} represent the surface free energies of a solid-water interface, an oil-water interface and a solid-oil interface, respectively. Combining Eq. 2 and Young's Equation (Eq. 3) yields a more useful expression relating the work of adhesion with the contact angle (Eq. 4).

$$\gamma_{sw} - \gamma_{so} = \gamma_{ow}\cos\theta \quad \text{Eq. 3}$$

$$W_{ows} = \gamma_{ow}(1 + \cos\theta) \quad \text{Eq. 4}$$

where θ is the contact angle between oil and the solid surface under water.

Because of their strong affinity for water, polyelectrolyte brushes become superoleophobic with a large contact angle of oil under water.[42] According to Eq. 4, a large oil contact angle leads to a small work of adhesion, indicating that oil can detach from the surface easily. Thus, polyelectrolyte brushes are good choices as materials that resist fouling with oil.

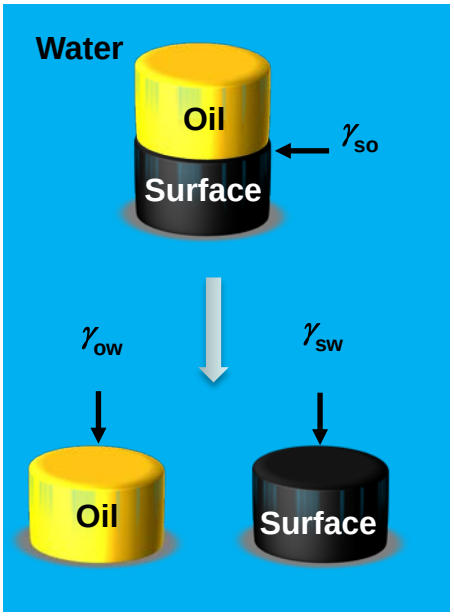

Figure 1.7. The work of adhesion needed to separate oil from a surface in water.

1.4. Membrane Coalescence for Separation of O/W Emulsions

As discussed above, conventional coalescence techniques can hardly separate surfactant-stabilized O/W emulsions, especially submicron emulsions. However, Nitsch and coworkers reported that emulsified oil droplets will coalesce as they are pumped through a hydrophobic membrane.[18, 49] They proposed a mechanism for this process assuming that

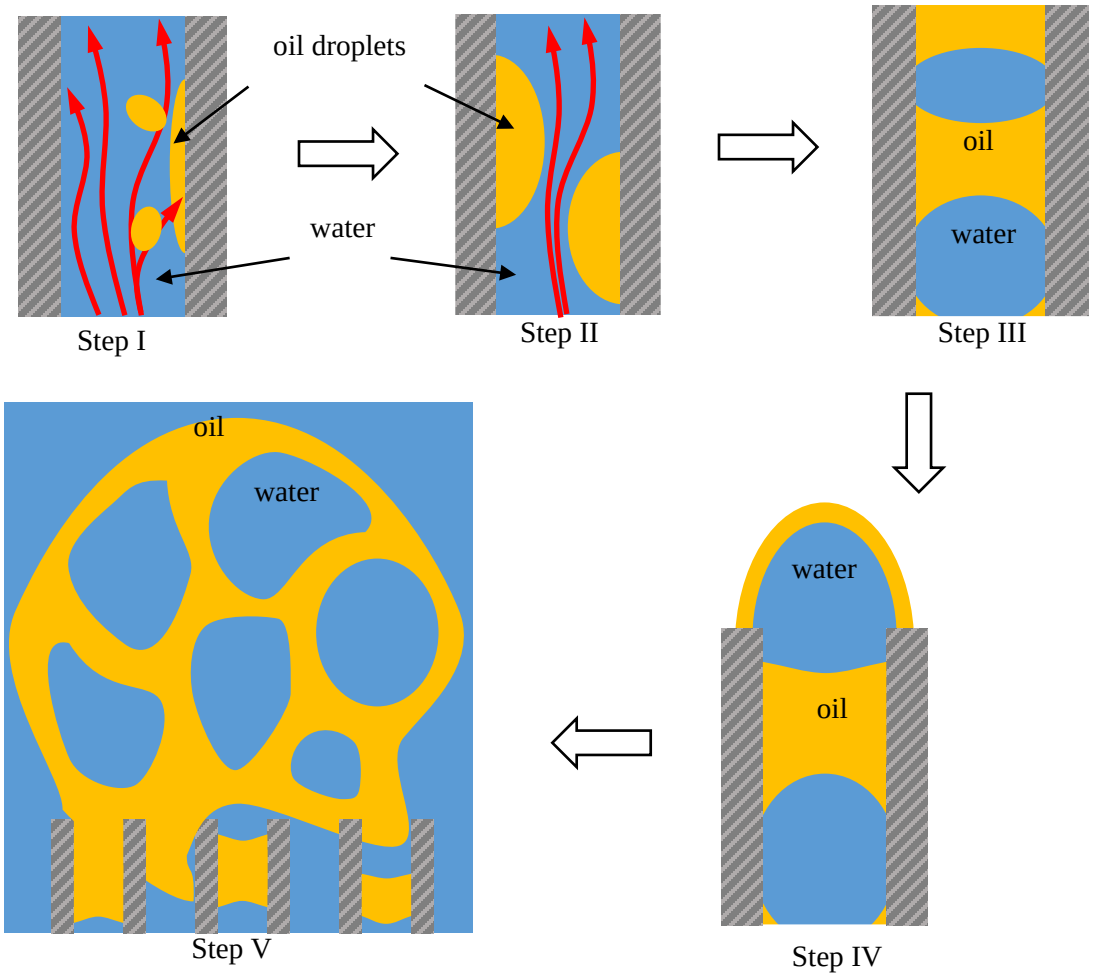

Figure 1.8. Proposed process of oil coalescence during flow through a porous hydrophobic membrane. I. Oil droplets (yellow) adsorb and coalesce on the pore surface (dashed gray). II and III. Oil droplets grow and eventually block the pores creating water occlusions (blue). IV and V. Oil and water occlusions pass through the membrane creating water-in-oil droplets, which are large enough to detach from membrane.[18]

the porous membrane is a network of capillaries. As Figure 1.8 shows, emulsified oil droplets first attach to the hydrophobic membrane surface (Step I), followed by contact and coalescence with nearby oil droplets (Step II). As the oil aggregates become large enough to cover the membrane pores, water occlusion occurs (Step III) and leads to the formation of W/O (water-in-oil) droplets at the membrane outlet (Steps IV, V). Compared with the original tiny oil droplets, these W/O aggregates are much larger. Therefore, they can float to the surface rapidly according to Stokes' equation (Eq. 1).

Using several filtration membranes, Agarwal and co-workers investigated the factors that affect oil coalescence including filter pore size, surface roughness and surface wettability.[50, 51] They found that an effective coalescing filter should meet the following criteria. Firstly, the filter should be hydrophobic to enable oil attachment and coalescence. Secondly, flow through the membrane should occur vertically since in this direction oil droplets will possess high mobility. This configuration may also enhance oil droplet contact and coalescence. Thirdly, the filter should have a rough surface to promote oil adhesion that induces oil coalescence. Based on these fundamental studies, several groups successfully fabricated hydrophobic coalescing membranes for emulsion separation.[52-55] Nevertheless, as a technique in development, in-membrane coalescence still faces several challenges, such as low coalescence of submicron oil droplets or droplets stabilized by mixed surfactants. Still, membrane coalescence was already more effective in coalescing oil than a common fiber bed coalescer, as shown in Table 1.1.[18] For example, membrane coalescence can separate surfactant-stabilized oil droplets whereas a fiber bed coalescer is only effective for oil droplets with not enough or even no surfactants. In addition,

membrane coalescence provides a higher flow rate and better separation efficiency, which is defined as

$$\eta = \frac{V_{org,\omega}}{V_{org,\alpha}} \times 100\% \qquad \text{Eq. 5}$$

where $V_{org,\ \omega}$ and $V_{org,\ \alpha}$ represent separated and initial volume of organic phase, respectively.

Table 1.1. The comparison between membrane coalescence and fiber bed coalescer.

Membrane Coalescence		Fiber bed Coalescer	
Surfactant	yes	partial	No
O/W conc. (vol, %)	0.1-7	2-5	0.1-0.2
Droplet size (μm)	1-10	< 100	10-100
Flow rate (m^3/m^2h)	3-660	2.5-6.5	7-47
Separation efficiency (%)	80-98	complete/partial	50-98

1.5. Outline of This Dissertation

As shown in Table 1.2., Chapter 2 describes (a) the controlled growth of polyanionic brushes composed of poly(3-sulfopropyl methacrylate salts) (PSPMK), (b) brush swelling and surfactant adsorption in solutions containing either anionic or cationic

Table 1.2. Titles of the remaining chapters of this dissertation.

Chapter 2	Adsorption of Anionic or Cationic Surfactants in Polyanionic Brushes and Its Effect on Brush Swelling and Fouling Resistance during Emulsion Filtration
Chapter 3	Aqueous Swelling of Zwitterionic Poly(Sulfobetaine Methacrylate) Brushes in the Presence of Ionic Surfactants
Chapter 4	Oil Coalescence on Porous Membrane Surfaces during Dead-End Filtration
Chapter 5	Summary and Future Work

surfactant and (c) separation of O/W submicron emulsion using microfiltration membranes modified with PSPMK brushes. In short, the polyanionic brushes show minimal surfactant sorption or oil fouling when using an anionic surfactant, but high sorption and fouling when using a cationic surfactant. In an effort to create brushes that resist sorption of both cationic and anionic surfactants, I began investigating the properties of polyzwitterionic brushes. Specifically, chapter 3 discusses the swelling of poly[2-(methacryloyloxy)ethyl dimethyl-(3-sulfopropyl)ammonium hydroxide] (PMEDSAH) films in the presence of anionic and cationic surfactants. These brushes show sorption of both cationic and anionic surfactants, leading a more swelling or collapsed brush layer, depending on the surfactant charge and concentration, as well as brush thickness. Chapter 4 shows preliminary oil coalescence data using membranes with different coatings, focusing on oil coalescence on less hydrophilic membranes. Preliminary data suggest oil coalescence can be adjusted by changing membrane substrate, surface modification, pore size and filtration pressure. Finally, Chapter 5 summarizes my PhD research and its potential application in the separation of O/W submicron emulsions.

REFERENCES

REFERENCES

1. Stephenson, M. A Survey of Produced Water Studies. In *Produced Water*; Springer, 1992; pp 1-11.

2. BCC Research The North American Market for Produced Water Treatment Equipment. https://www.bccresearch.com/pressroom/env/north-american-market-produced-water-treatment-equipment-reach-nearly-$1.2-billion-2017 (accessed Aug 9, 2017).

3. Duong, P. H.; Chung, T.-S. Application of Thin Film Composite Membranes with Forward Osmosis Technology for the Separation of Emulsified Oil–Water. *J. Membr. Sci.* **2014**, *452*, 117-126.

4. Environmental Protection Angency 40 Cfr 435.15. https://www.gpo.gov/fdsys/pkg/CFR-2010-title40-vol29/pdf/CFR-2010-title40-vol29-sec435-15.pdf (accessed Aug 9, 2017).

5. Rhee, C.; Martyn, P.; Kremer, J. In *Removal of Oil and Grease in the Hydrocarbon Processing Industry*, Proceedings 42 nd Industrial Waste Conference. Purdue University, 1987; pp 143-150.

6. Calvo, P.; Remunan-Lopez, C.; Vila-Jato, J.; Alonso, M. Development of Positively Charged Colloidal Drug Carriers: Chitosan-Coated Polyester Nanocapsules and Submicron-Emulsions. *Colloid Polym.r Sci.* **1997**, *275*, 46-53.

7. Lovelyn, C.; Attama, A. A. Current State of Nanoemulsions in Drug Delivery. *J.Biomater. Nanobiotechnol.* **2011**, *2*, 626.

8. Benita, S.; Levy, M. Submicron Emulsions as Colloidal Drug Carriers for Intravenous Administration: Comprehensive Physicochemical Characterization. *J. Pharm. Sci.* **1993**, *82*, 1069-1079.

9. Wang, L.; Li, X.; Zhang, G.; Dong, J.; Eastoe, J. Oil-in-Water Nanoemulsions for Pesticide Formulations. *J. Colloid Interface Sci.* **2007**, *314*, 230-235.

10. Quintanilla-Carvajal, M. X.; Camacho-Díaz, B. H.; Meraz-Torres, L. S.; Chanona-Pérez, J. J.; Alamilla-Beltrán, L.; Jimenéz-Aparicio, A.; Gutiérrez-López, G. F. Nanoencapsulation: A New Trend in Food Engineering Processing. *Food Eng. Rev.* **2010**, *2*, 39-50.

11. Bernardi, D. S.; Pereira, T. A.; Maciel, N. R.; Bortoloto, J.; Viera, G. S.; Oliveira, G. C.; Rocha-Filho, P. A. Formation and Stability of Oil-in-Water Nanoemulsions Containing Rice Bran Oil: In Vitro and in Vivo Assessments. *J. Nanobiotechnol.* **2011**, *9*, 44.

12. Asua, J. M. Miniemulsion Polymerization. *Prog. Polym. Sci.* **2002**, *27*, 1283-1346.

13. Bechthold, N.; Tiarks, F.; Willert, M.; Landfester, K.; Antonietti, M. In *Miniemulsion Polymerization: Applications and New Materials*, Macromolecular Symposia, 2000; Wiley Online Library: 2000; pp 549-555.

14. Duhon, H. Produced Water Treatment: Yesterday, Today, and Tomorrow. *Oil and Gas Facilities* **2012**, *1*, 29-30.

15. Frankiewicz, T. In *Understanding the Fundamentals of Water Treatment, the Dirty Dozen-12 Common Causes of Poor Water Quality*, 11th produced water seminar, Houston, TX, Jan, 2001; 2001.

16. Rhee, C. H.; Martyn, P. C.; Kremer, J. Removal of Oil and Grease in Oil Processing Wastewater. *Sanitation District of Los Angeles County, USA* **1989**.

17. Moosai, R.; Dawe, R. A. Gas Attachment of Oil Droplets for Gas Flotation for Oily Wastewater Cleanup. *Sep. Purif. Technol.* **2003**, *33*, 303-314.

18. Hoffmann, S.; Nitsch, W. Membrane Coalescence for Phase Separation of Oil-in-Water Emulsions Stabilized by Surfactants and Dispersed into Smallest Droplets. *Chem. Eng. Technol.* **2001**, *24*, 22-27.

19. Beychok, M. R. Aqueous Wastes from Petroleum and Petrochemical Plants. **1967**.

20. Cheryan, M.; Rajagopalan, N. Membrane Processing of Oily Streams. Wastewater Treatment and Waste Reduction. *J. Membr. Sci.* **1998**, *151*, 13-28.

21. Katnik, K. E.; Pavilcius, A. M. In *Novel Chemical Approach for the Treatment of Oily Wastewaters*, 33rd Ind. Waste Conf. Proc.;(United States), 1978; Nalco Chemical Co., Northbrook, IL: 1978.

22. Fane, A. Membranes for Water Production and Wastewater Reuse. *Desalination* **1996**, *106*, 1-9.

23. General Electric Water & Process Technologies, Filtration and Separation Spectrum. http://products.pargreen.com/Asset/Filtration-spectrum.pdf (accessed Aug 9, 2017).

24. Petala, M.; Zouboulis, A. Vibratory Shear Enhanced Processing Membrane Filtration Applied for the Removal of Natural Organic Matter from Surface Waters. *J. Membr. Sci.* **2006**, *269*, 1-14.

25. Shi, W.; Benjamin, M. M. Membrane Interactions with Nom and an Adsorbent in a Vibratory Shear Enhanced Filtration Process (Vsep) System. *J. Membr. Sci.* **2008**, *312*, 23-33.

26. Rana, D.; Matsuura, T. Surface Modifications for Antifouling Membranes. *Chem. Rev.* **2010**, *110*, 2448-2471.

27. Zhou, R.; Ren, P.-F.; Yang, H.-C.; Xu, Z.-K. Fabrication of Antifouling Membrane Surface by Poly (Sulfobetaine Methacrylate)/Polydopamine Co-Deposition. *J. Membr. Sci.* **2014**, *466*, 18-25.

28. Kang, G.-d.; Cao, Y.-m. Development of Antifouling Reverse Osmosis Membranes for Water Treatment: A Review. *Water Research* **2012**, *46*, 584-600.

29. Gryta, M. Chemical Pretreatment of Feed Water for Membrane Distillation. *Chem. Pap.* **2008**, *62*, 100-105.

30. Gleason, K. K.; Zafarullah, K.; Shafi, H. Z.; Yang, R., Development of Zwitterionic Coatings That Confer Ultra Anti-Biofouling Properties to Commercial Reverse Osmosis Membranes. U.S. Patents: 9,598,598, Mar. 21, 2017.

31. Wang, Z.; van Andel, E.; Pujari, S. P.; Feng, H.; Dijksman, J. A.; Smulders, M. M.; Zuilhof, H. Water-Repairable Zwitterionic Polymer Coatings for Anti-Biofouling Surfaces. *J. Mater. Chem. B* **2017**.

32. Yang, W. J.; Neoh, K.-G.; Kang, E.-T.; Teo, S. L.-M.; Rittschof, D. Polymer Brush Coatings for Combating Marine Biofouling. *Prog. Polym. Sci.* **2014**, *39*, 1017-1042.

33. Yang, Z.; Tarabara, V. V.; Bruening, M. L. Adsorption of Anionic or Cationic Surfactants in Polyanionic Brushes and Its Effect on Brush Swelling and Fouling Resistance During Emulsion Filtration. *Langmuir* **2015**, *31*, 11790-11799.

34. Barbey, R.; Lavanant, L.; Paripovic, D.; Schüwer, N.; Sugnaux, C.; Tugulu, S.; Klok, H.-A. Polymer Brushes Via Surface-Initiated Controlled Radical Polymerization: Synthesis, Characterization, Properties, and Applications. *Chem. Rev.* **2009**, *109*, 5437-5527.

35. Zhao, B.; Brittain, W. J. Polymer Brushes: Surface-Immobilized Macromolecules. *Prog. Polym. Sci.* **2000**, *25*, 677-710.

36. Balazs, A. C.; Singh, C.; Zhulina, E.; Chern, S.-S.; Lyatskaya, Y.; Pickett, G. Theory of Polymer Chains Tethered at Interfaces. *Prog. Surf. Sci.* **1997**, *55*, 181-269.

37. Rühe, J.; Knoll, W. Functional Polymer Brushes. *J. Macromol. Sci. Polym. Rev.* **2002**, *42*, 91-138.

38. Matyjaszewski, K.; Xia, J. Atom Transfer Radical Polymerization. *Chem. Rev.* **2001**, *101*, 2921-2990.

39. Pintauer, T.; Matyjaszewski, K. Structural Aspects of Copper Catalyzed Atom Transfer Radical Polymerization. *Coord. Chem. Rev.* **2005**, *249*, 1155-1184.

40. Sankhe, A. Y.; Husson, S. M.; Kilbey, S. M. Direct Polymerization of Surface-Tethered Polyelectrolyte Layers in Aqueous Solution via Surface-Confined Atom Transfer Radical Polymerization. *J. Polym. Sci. Polym. Chem.* **2007**, *45*, 566-575.

41. Tsarevsky, N. V.; Braunecker, W. A.; Matyjaszewski, K. Electron Transfer Reactions Relevant to Atom Transfer Radical Polymerization. *J.Organomet. Chem.* **2007**, *692*, 3212-3222.

42. Kobayashi, M.; Terayama, Y.; Yamaguchi, H.; Terada, M.; Murakami, D.; Ishihara, K.; Takahara, A. Wettability and Antifouling Behavior on the Surfaces of Superhydrophilic Polymer Brushes. *Langmuir* **2012**, *28*, 7212-7222.

43. Zhu, Y.; Zhang, F.; Wang, D.; Pei, X. F.; Zhang, W.; Jin, J. A Novel Zwitterionic Polyelectrolyte Grafted Pvdf Membrane for Thoroughly Separating Oil from Water with Ultrahigh Efficiency. *J. Mater. Chem. A* **2013**, *1*, 5758-5765.

44. Liang, S.; Qi, G.; Xiao, K.; Sun, J.; Giannelis, E. P.; Huang, X.; Elimelech, M. Organic Fouling Behavior of Superhydrophilic Polyvinylidene Fluoride (Pvdf) Ultrafiltration Membranes Functionalized with Surface-Tailored Nanoparticles: Implications for Organic Fouling in Membrane Bioreactors. *J. Membr. Sci.* **2014**, *463*, 94-101.

45. Feng, X.; Jiang, L. Design and Creation of Superwetting/Antiwetting Surfaces. *Adv. Mater.* **2006**, *18*, 3063-3078.

46. Drelich, J.; Chibowski, E. Superhydrophilic and Superwetting Surfaces: Definition and Mechanisms of Control. *Langmuir* **2010**, *26*, 18621-18623.

47. Ström, G.; Fredriksson, M.; Stenius, P. Contact Angles, Work of Adhesion, and Interfacial Tensions at a Dissolving Hydrocarbon Surface. *J. Colloid Interface Sci.* **1987**, *119*, 352-361.

48. Wang, H.; Shi, H.; Li, Y.; Wang, Y. The Effects of Leaf Roughness, Surface Free Energy and Work of Adhesion on Leaf Water Drop Adhesion. *PLOS ONE* **2014**, *9*, e107062.

49. Daiminger, U.; Nitsch, W.; Plucinski, P.; Hoffmann, S. Novel Techniques for Iol/Water Separation. *J. Membr. Sci.* **1995**, *99*, 197-203.

50. Agarwal, S.; von Arnim, V.; Stegmaier, T.; Planck, H.; Agarwal, A. Role of Surface Wettability and Roughness in Emulsion Separation. *Sep. Purif. Technol.* **2013**, *107*, 19-25.

51. Agarwal, S.; von Arnim, V.; Stegmaier, T.; Planck, H.; Agarwal, A. Effect of Fibrous Coalescer Geometry and Operating Conditions on Emulsion Separation. *Ind. Eng. Chem. Res.* **2013**, *52*, 13164-13170.

52. Hu, D.; Li, X.; Li, L.; Yang, C. Designing High-Caliber Nonwoven Filter Mats for Coalescence Filtration of Oil/Water Emulsions. *Sep. Purif. Technol.* **2015**, *149*, 65-73.

53. Hu, D.; Li, L.; Li, Y.; Yang, C. Restructuring the Surface of Polyurethane Resin Enforced Filter Media to Separate Surfactant Stabilized Oil-in-Water Emulsions Via Coalescence. *Sep. Purif. Technol.* **2017**, *172*, 59-67.

54. Kulkarni, P. S.; Patel, S. U.; Patel, S. U.; Chase, G. G. Coalescence Filtration Performance of Blended Microglass and Electrospun Polypropylene Fiber Filter Media. *Sep. Purif. Technol.* **2014**, *124*, 1-8.

55. Tan, K. Y.; Hughes, T. L.; Nagl, M.; Huck, W. T. Nonfouling Capture–Release Substrates Based on Polymer Brushes for Separation of Water-Dispersed Oil Droplets. *ACS Appl. Mater. Interfaces* **2012**, *4*, 6403-6409.

Chapter 2. Adsorption of Anionic or Cationic Surfactants in Polyanionic Brushes and Its Effect on Brush Swelling and Fouling Resistance during Emulsion Filtration

Portions of this chapter are reprinted from our published paper in *Langmuir* (Yang, Z., Tarabara, V. V., and Bruening, M. L. *Langmuir* **2015**, *31* (43), 11790–11799).

2.1. Introduction

Oil and grease are common pollutants in wastewater from processes such as oil production, food processing, can manufacturing, and wool scouring,[1] and limitations on the release of oil in wastewater necessitate separation of oil-water mixtures prior to water discharge. According to U.S. regulations, new oil and gas facilities should limit the maximum concentration of oil and grease in wastewater to 42 mg/L, and the average of daily values over 30 consecutive days should not exceed 29 mg/L.[2] Density-based separation technology, e.g. flotation and hydrocyclones, can readily isolate free oil (droplets with diameters >150 μm) and dispersed oil (20-150 μm droplets) from water, but emulsified oil (droplets with diameters <20 μm) is more difficult to remove.[3] Demulsification of such surfactant-stabilized droplets through chemical or thermal treatments can increase droplet sizes under certain conditions, but these techniques have limitations.[1] Chemical treatment requires customization for a given feed and may introduce corrosion problems. Although thermal treatment is more universal, it incurs high energy costs, and evaporated oil may present another disposal issue.

Compared to other separation methods for removal of emulsified oil, membrane filtration offers several advantages including a relatively low energy cost, possible automation, and no addition of extraneous chemicals.[1, 4] However, fouling due to oil accumulation at the membrane surface or in membranes pores often rapidly decreases

permeate flux or increases filtration pressures. To solve this problem, a number of groups modified membrane surfaces to achieve both high flux and high oil rejection.[5-10] However, only a few studies examined the separation of micron and submicron-sized emulsions because the small oil droplets are difficult to separate from water.[11-12] Submicron emulsions are common in drug delivery,[13-14] pesticide application,[15] food processing,[16] cosmetics[17-18] and emulsion polymerization.[19-20] Considering the increasing popularity of submicron emulsions and tighter regulations on oil discharge, their separation from water will likely become increasingly important.

Two recent studies indicate that polyelectrolyte brushes on membranes limit fouling by oil emulsions while increasing oil rejection.[12, 21] Water sorption in these brushes creates extremely hydrophilic surfaces to which oil does not adhere. However, the fouling resistance of charged brushes may vary greatly with the surfactant that stabilizes the emulsion. Katleen and co-workers found that cationic surfactants readily foul unmodified negatively charged nanofiltration membranes.[22] At higher concentrations, even negatively charged surfactants foul these membranes, suggesting the need for higher surface charge density, such as that in polyelectrolyte brushes, to prevent fouling. Daniel and co-workers increased both the concentration of initiator and polymerization time during membrane modification to create a dense, neutral brush that shows strong antifouling ability.[23] A few experimental[24-26] and computational[27-28] studies examined adsorption of charged surfactants to polyelectrolyte brushes and suggest that a relatively low surfactant concentration and low brush density promote brush collapse. Moreover, surfaces modified with polyelectrolyte brushes become more hydrophobic after absorbing cationic surfactants.[29] However, these studies focused on adsorption of ionic surfactants to

oppositely charged or nonionic polymer brushes.[24, 30] A very recent paper (submitted at approximately the same time as the paper describing this research) focused on the adsorption of ionic surfactants to oppositely charged polymer brushes and the lubrication behavior after surfactant adsorption.[31]

This work examines interactions of cationic and anionic surfactants with brushes composed of poly(3-sulfopropyl methacrylate salts) (PSPMK, Scheme 2.1). We chose these brushes because Kobayashi et al. showed they are superoleophobic in water, although that study did not exam surfactant-stabilized oil droplets. Negatively charged polymer brushes are attractive because they may resist adsorption of anionic surfactants, which are the most common class of surfactants in the oilfield market.[32] We employ surface-initiated atom-transfer radical polymerization (SI-ATRP)[33] to grow these brushes on both Au-coated Si wafers and porous nylon membranes. The wafers enable studies of film thickness, swelling in water and surfactant solutions, surfactant adsorption, and wettability (contact angles), whereas dead-end filtration with membranes examines fouling, oil rejection, and

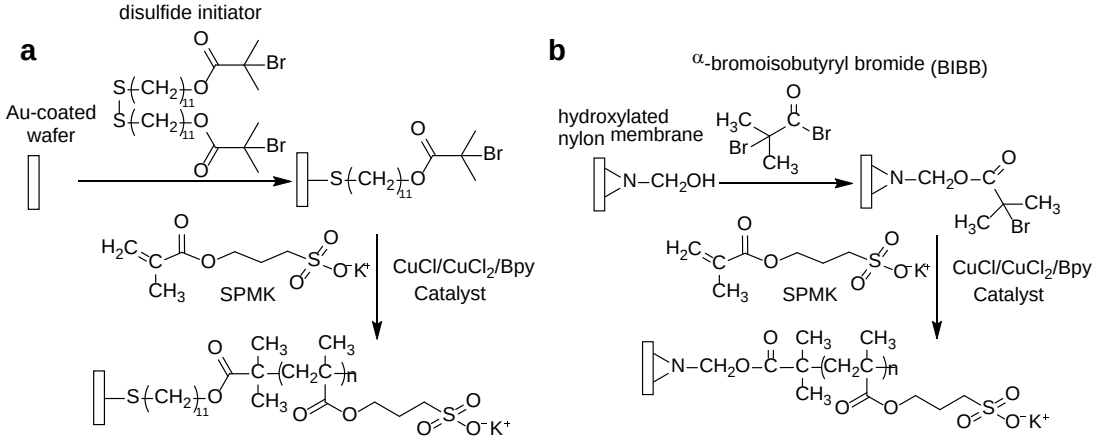

Scheme 2.1. SI-ATRP of SPMK on Au-coated wafers (a) and hydroxylated nylon membranes (b)

permeate flux as functions of surfactant composition and brush thickness. For comparison, we also perform dead-end filtration with commercial NF270 membranes.[34]

2.2. Experimental

2.2.1. Materials

Hydroxylated (LoProdyne LP) nylon membranes with 1.2 μm diameter pores were obtained from Pall Corporation, and NF270 membranes were a gift from Dow Chemical. All membranes were cut into 2-cm discs, and nylon membranes were exposed to UV/ozone for 15 min prior to modification. Au-coated Si wafers were prepared at LGA Thin Films (Santa Clara, CA) by sputtering 200 nm of gold on 20 nm of Cr on Si wafers. 3-sulfopropyl methacrylate potassium salt (98%, SPMK), 11-mercapto-1-undecanol (97%), ammonium chloride (≥99.5%), α-bromoisobutyryl bromide (98%, BIBB), 2,2'-bipyridine (≥99%, Bpy), decane (≥99%), hexadecane (99%), sodium dodecyl sulfate (98.5%, SDS), and cetrimonium bromide (≥99%, CTAB) were obtained from Sigma-Aldrich. Bromine (100.0%) and triethylamine (100%) were purchased from J.T. Baker, and copper (I) chloride (≥ 99.995%), copper (II) chloride dihydrate (≥ 99.0%) and dimethylformamide (≥ 99.8%, DMF) were acquired from Jade Scientific. Anhydrous dichloromethane (Macron Fine Chemicals) was used as received. Chloroform (Macron Fine Chemicals) and triethylamine were dried with molecular sieves (4 Å, Jade Science) before use. Aqueous solutions were prepared using deionized water (Milli-Q, 18.2 MΩ cm), and disulfide initiator, $(BrC(CH_3)_2COO(CH_2)_{11}S)_2$, was synthesized according to a literature procedure.[35]

2.2.2. Preparation of PSPMK Brushes on Au-Coated Wafers and Nylon Membranes

2.2.2.1.Initiator Immobilization

The protocol for immobilizing the disulfide initiator on Au-coated wafers included washing the substrate with ethanol, drying with N_2, cleaning with UV/ozone for 15 min, immersion

in a 1 mM ethanolic solution of $(BrC(CH_3)_2COO(CH_2)_{11}S)_2$ for 24 h, rinsing with ethanol and drying under a stream of N_2. Initiator immobilization on hydroxylated nylon membranes employed an esterification reaction with BIBB as described in the literature.[36] In this procedure, 30 mL of chloroform and 2.4 mL of triethylamine were mixed under N_2 and kept at 0 °C in a sealed round-bottom flask for 1 h. In a N_2-filled glovebag, this mixture was introduced into a 50-mL petri dish containing 6 hydroxylated nylon membrane discs, and 0.5 mL of BIBB was added to the solution. The reaction mixture was gently stirred with a magnetic stir bar for 20 min, and the BIBB-esterified membranes were removed from the glove bag and washed with copious amounts of acetone and then with a methanol/water (1/1, v/v) mixture prior to drying under a stream of N_2. The membranes were further dried under vacuum overnight before polymerization.

2.2.2.2.Polymerization of SPMK

The SI-ATRP is similar to a literature procedure.[37-38] In a typical synthesis, SPMK (36 mmol) was dissolved in a DMF/water mixture (1/1 v/v, 30 mL) in a round-bottom flask. The mixture was degassed via four freeze-pump-thaw cycles. A freshly prepared Cu-Bpy stock solution containing CuCl (0.002 mmol), $CuCl_2$ (0.002 mmol), and Bpy (0.01 mmol) in a DMF/water mixture (1/1 v/v, 5 mL) was degassed via four freeze-pump-thaw cycles and mixed with the monomer solution in a petri dish in a N_2-filled glove bag. Polymerization occurred after immersion of initiator-modified membranes or wafers in the mixed solution at room temperature. After the desired polymerization time, the modified substrates were removed from the glove bag, rinsed with 100 mL of water, and dried with N_2.

2.2.3. Characterization of Modified Au-Coated Wafers and Nylon Membranes

Wafers coated with disulfide initiator and PSPMK brushes were characterized by reflectance Fourier transform infrared spectroscopy (FTIR) (Nicolet 6700 FT-IR spectrometer, Thermo Scientific, with a Pike grazing angle (80 º) attachment). A UV/ozone-cleaned Au-coated wafer served as a background. Infrared spectra of membranes modified with BIBB and PSPMK brushes were obtained using a PerkinElmer FT-IR spectrometer (Spectrum One, PerkinElmer) with an attenuated total reflectance (ATR) accessory (Universal ATR-1 Reflection Top-Plate). The spectrum of an unmodified nylon membrane was subtracted from the spectrum of modified membranes to highlight absorbances due to newly grown films. To examine surfactant adsorption, PSPMK brush-modified wafers were transferred directly from water to surfactant-containing solutions. After an overnight immersion in the surfactant solution, the wafer was rinsed with 100 mL of water from a wash bottle for ~ 2 min prior to drying with N_2 and obtaining a reflectance FTIR spectrum.

The "dry" thickness and refractive indices of the polymer brushes on Au-coated wafers were determined in air using a rotating analyzer ellipsometer (model M-44, J.A. Woollam) at an incident angle of 75°. Similar thickness determinations for films immersed in water employed a homemade trapezoidal cell with glass windows.[39-40] In all experiments, the refractive index was fit using a Cauchy model. Ellipsometric measurements were performed on at least three spots on each wafer, with many different films.

Contact angles on surfaces were acquired using a dynamic contact angle analyzer (FTA 200, Firsttenangstroms). Hexadecane drops were placed on the modified and

unmodified Au-coated wafers both before and after immersion of substrates in water to determine contact angles. We attempted to measure a hexadecane contact angle directly in solutions containing either 0.36 mM SDS or 0.36 mM CTAB, but hexadecane droplets would not form at the end of the syringe needle due to the surfactants. As an alternative, the wafers were pretreated by immersion in the surfactant solutions overnight, followed by washing with 100 mL of water and drying with N_2. A drop of hexadecane was placed on these dry wafers, and they were immersed in surfactant solutions prior to determining the contact angle. The morphologies of membranes were also observed using a field-emission scanning electron microscope (JSM-7500F, JEOL). The membrane porosity was determined from the mass loss of wet membranes after drying. After polymerization, polymers physically adsorbed on the membrane were washed off by pumping pure water through the membrane for 5 h. Membranes were then patted dry with a Kimwipe to remove water on their surface, and immediately weighed (wet mass). To obtain the mass of a dry membrane, the wet membranes were dried in a vacuum oven for 24 h and weighed. The membrane porosity was calculated using Eq. 2.1[41]:

$$\text{Porosity} = \left(\frac{(W_w - W_d)/\rho_{water}}{(W_w - W_d)/\rho_{water} + W_d/\rho_{polymer}}\right) \times 100\% \qquad \text{Eq. 2.1}$$

where W_w and W_d are the masses of wet and dry membranes, respectively, ρ_{water} is the density of water (1 g/cm^3), and $\rho_{polymer}$ represents the density of nylon, which is 1.15 g/cm^3.[42]

2.2.4. Emulsion Preparation and Characterization

Hexadecane emulsions stabilized with SDS or CTAB were prepared as described previously.[43] Preparation of stable hexadecane-in-water emulsions with oil droplet

diameters smaller than 1 μm requires an oil content ≤10% (volume fraction).[1] SDS (0.0144 g) or CTAB (0.0182 g) was dissolved along with NaCl (0.0058 g) in a hexadecane/water mixture (1/9, v/v, 100 mL), and this mixture was sonicated for 3 min (1 min on, 0.5 min off) using a horn ultrasonicator (power setting: 6.5, power output: 57 W, Sonicator 3000, Misonix). The size distribution of the oil droplets was determined by light scattering using a Malvern Instruments particle size analyzer (Mastersizer 2000, Malvern Instruments) with a manually controlled pump and sample dispersion unit (Hydro SM, Malvern Instruments). These stock emulsions were stored for up to two weeks prior to dilution and filtration. At longer times phase separation occurs with CTAB emulsions, and even for shorter times, some phase separation may decrease the oil concentration.

2.2.5. Dead-End Filtration

The specific flux (L/(m^2·h·bar)), referred to as LMH/bar) and observed oil rejection (R, %) of the membranes were determined in dead-end filtration using a 15-mL Amicon cell (Model 8010, Millipore) with a suspended stir bar rotating at 45 rpm. The cell was connected to a stainless steel feed tank (standard 2 gallon pressure vessel, Pope Scientific) that contained deionized water (Figure 2.1),[44] and the applied pressure was always 1.4 bar. A stainless steel frit with nominal 1 μm pores (316LSS 1 μm Discs, Mott Corporation) supported the membrane. Initially, pure water flux was determined using deionized water as the feed. Permeate fractions were collected over specific times and weighed to determine the flux. In filtration of emulsions, the Amicon cell was filled with 13 mL of deionized

water and 1 mL of the 10% hexadecane emulsion. The solution was mixed with the hanging

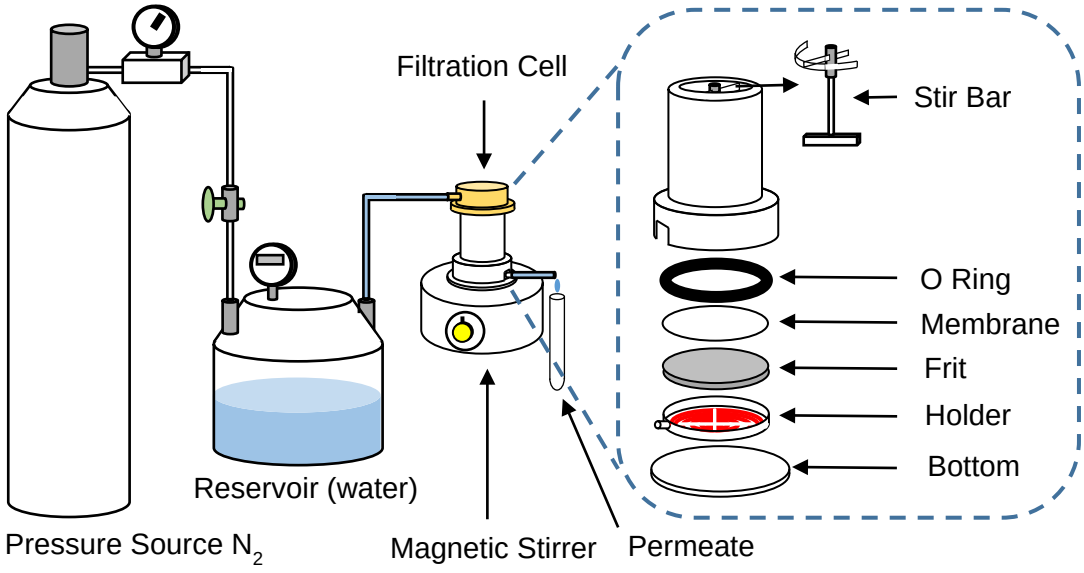

Figure 2.1. Diagram of the apparatus for dead-end filtration.

magnetic stir bar for 30 sec. The cap was placed on the Amicon cell, and pressurized N_2 was applied to the water-containing feed tank so deionized water entered the stirred Amicon cell to replace the permeate. Permeate fractions were collected over specific times and weighed to determine flux, and rejection values, R, were calculated using Eq. 2.2:

$$R = \left(1 - \frac{C_p}{C_f}\right) \times 100\% \qquad \text{Eq. 2.2}$$

where C_f and C_p are the hexadecane concentrations in the feed and the permeate, respectively. During the filtration, the volume of feed solution decreases slightly due to a small amount of air entering the cell so the feed concentration increases ~20% during experiments where the rejection is essentially 100%. For rejection calculations, C_f was the average of the feed concentration before and after filtration. Hexadecane concentrations were determined by gas chromatography (GC-17a, Shimadzu) using a hexadecane calibration curve with decane as an internal standard. To prepare GC samples, hexadecane in permeate solutions was extracted by mixing 1 mL of saturated NaCl solution, 5 drops of

1 M HCl, 1 mL of dichloromethane and 1 mL of the permeate solution for 30 s on a vortex mixer (BV1000, Benchmark Scientific). After phase separation, 0.5 mL of the organic phase was added to a GC vial containing 10 μL of decane as an internal standard. Figure 2.2 shows the calibration curve. Several blank solutions without hexadecane were analyzed to determine the minimum detectable signal (average of the blank signal plus three times the standard deviation of this signal.) Based on this minimum detectable signal and the calibration curve in Figure 2.2b, the detection limit of these analyses is 9 x 10^{-6} M hexadecane.

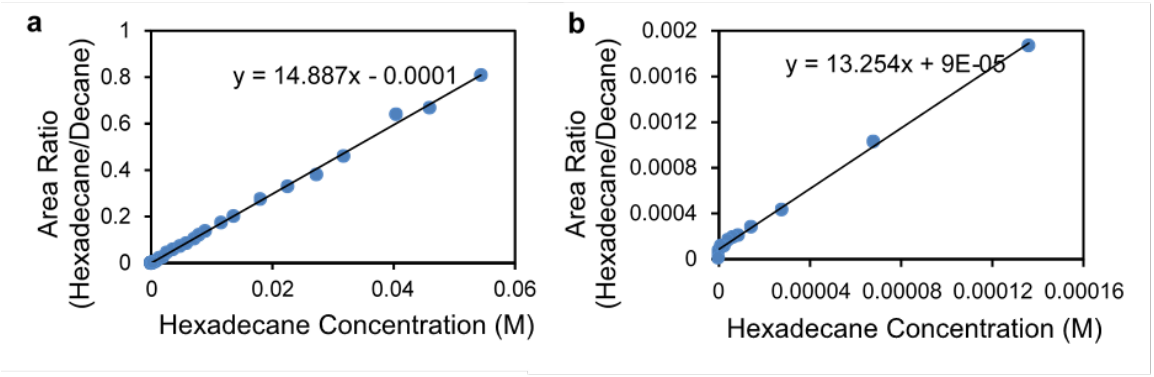

Figure 2.2. (a) GC calibration curve showing a linear relationship between the ratio of GC peak area (hexadecane/decane) and the concentration of hexadecane at high hexadecane concentration. Figure (b) shows the calibration curve at low concentration. Hexadecane concentrations in all filtrations were calculated using the left curve. Estimates of detection limits and low concentrations for determining high rejections were obtained using the right curve.

To examine whether oil adsorbed significantly to the filtration cell, a control experiment employed an impermeable transparency film (3M, PP2500) in place of a membrane. Because the film is impermeable, any change in the amount of hexadecane after the experiment represents oil adsorption on the Amicon cell or film. Table 2.1 describes these results and shows <20% adsorption to the cell. All of the filtration experiments were repeated with 2 or 3 membranes.

Table 2.1. Mass balance for the dead-end filtration of surfactant-stabilized emulsions using PSPMK-modified (1-h polymerization time) and NF270 membranes, and an impermeable transparency film. Values of n are the percentages of oil (relative to that in the initial feed) found in the total permeate and retentate fractions, and on the cell after the filtration. The value adsorbed on the cell was calculated by subtraction and represents the amount of oil not accounted for in the permeate and retentate. The total filtration time was 12 h. Initial studies with a teflon cell instead of the Amicon cell showed higher levels of adsorption.

Membrane	Surfactant	n (Permeate)	n (Retentate)	n (Cell)
PSPMK-modified membrane	SDS	1.7%	78.9%	19.4%
PSPMK-modified membrane	CTAB	81.0%	0.4%	18.6%
NF270	SDS	0.4%	87.0%	12.6%
NF270	CTAB	0.03%	84.7%	15.3%
Impermeable transparency film (3M, PP2500)	SDS	N/A	77.9%	22.1%

2.3. Results & Discussion

2.3.1. Brush Synthesis on Au-Coated Wafers and Nylon Membranes

Reproducible growth of polymer brushes is the first step in investigating both the interaction of brushes with surfactants and their use as membrane skins for emulsion filtration, and Scheme 2.1 shows the SI-ATRP strategy we employ to grow brushes on Au-coated wafers and nylon membranes. The Au surfaces enable brush characterization with reflectance IR spectroscopy and ellipsometry. IR spectra confirm both initiator adsorption and brush growth on the Au surface (Figure 2.3). In particular, sulfonate stretches at 1219 and 1049 cm^{-1} and a C=O stretch at 1737 cm^{-1} confirm the presence of PSPMK brushes. Figure 2.4 shows the peak height for the sulfonate stretch at 1219 cm^{-1} and the “dry” ellipsometric thickness of PSPMK brushes (on Au-coated wafers) as a function of

polymerization time. Both the peak height and the dry thickness increase approximately linearly with polymerization time, indicating continuous growth of PSPMK brushes.

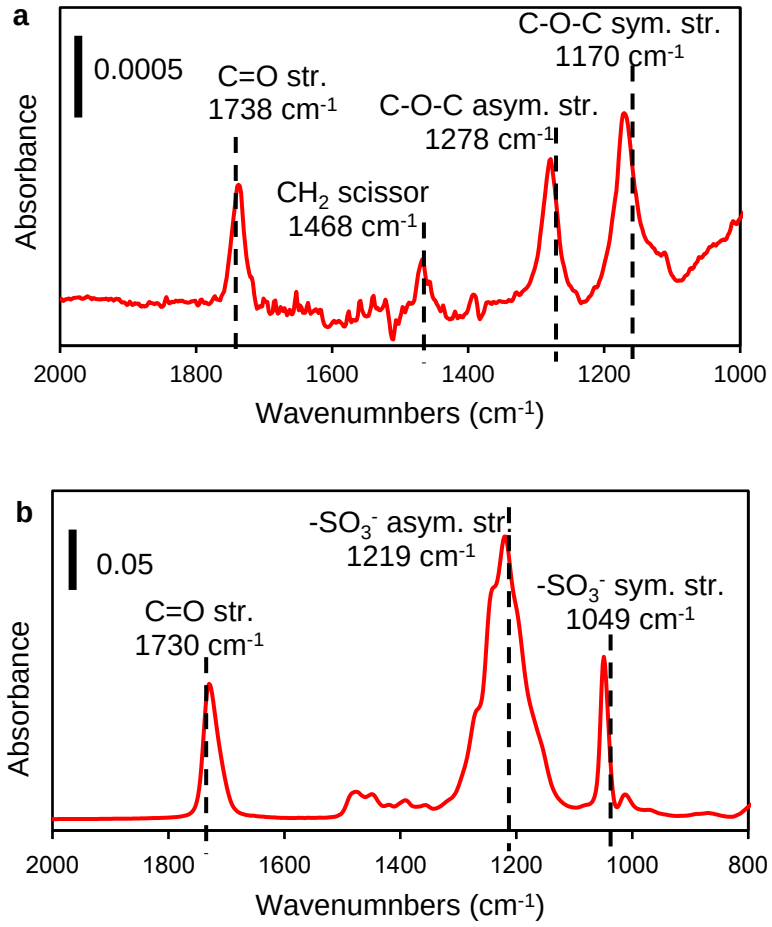

Figure 2.3. Reflectance FTIR spectrum of (a) the monolayer formed from treatment of a Au-coated wafer with a solution containing $(BrC(CH_3)_2COO(CH_2)_{11}S)_2$ and (b) PSPMK brushes on a Au-coated wafer.

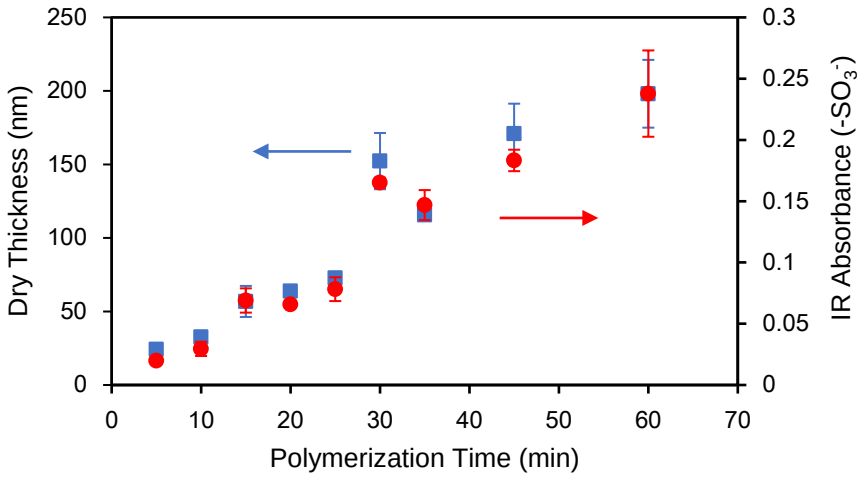

Figure 2.4. "Dry" ellipsometric thicknesses (blue squares) and sulfonate IR absorbances at 1219 cm^{-1} (red circles) as a function of polymerization time for PSPMK brushes grown from an initiator monolayer on Au. Error bars represent standard deviations (n=12 determinations on 4 wafers).

SI-ATRP on nylon membranes is difficult to characterize, but ATR-IR spectra clearly show the presence of C=O and sulfonate stretches after growth of PSPMK (Figure 2.5). The mass loss of wet membranes after drying also indicates a decrease in porosity from 66% for a bare membrane to around 56% after modification with PSPMK brushes (Table 2.2). Top-view SEM images (Figure 2.6a, b) suggest a lower porosity and smaller pore size at the membrane surface after the growth of polymer brushes. Cross-sectional SEM images (Figure 2.6c, d) also reveal a smaller pore size after polymerization, especially in the top layer of the membrane. Based on these images, pore size appears to decline after brush growth. However, pores in these spongy membranes are difficult to interrogate with microscopy. Additionally, SEM images show dry membranes whereas during filtration brushes will swell.

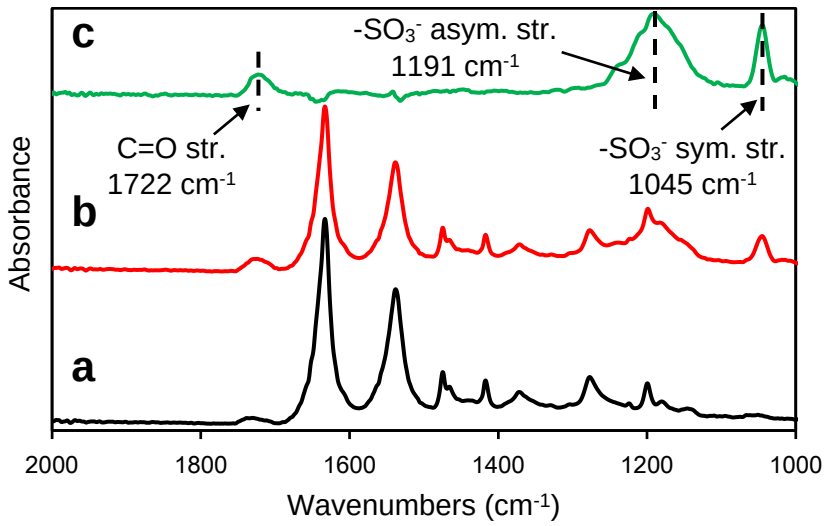

Figure 2.5. ATR-IR spectra of a hydroxylated membrane (a) before and (b) after growth of PSPMK brushes. Spectrum (c) results from subtracting 0.8 × spectrum (a) from spectrum (b) and shows absorbances due primarily to the PSPMK brush. We employed the factor of 0.8 to minimize infrared absorbances from the base nylon membrane.

Table 2.2. Membrane porosity determined by the mass loss of wet membranes after drying. The PSPMK-modified membranes show lower porosity than the bare membrane.

Polymerization Time		Dry Weight (g)	Wet Weight (g)	Porosity	Average Porosity
45 min	1	0.0374	0.0756	54.0%	54.4%
	2	0.0362	0.0745	54.9%	
1 h	1	0.0372	0.0860	60.1%	57.5%
	2	0.0372	0.0766	54.9%	
0 (bare)	1	0.0312	0.0850	66.5%	65.8%
	2	0.0332	0.0876	65.3%	
	3	0.0332	0.0884	65.6%	

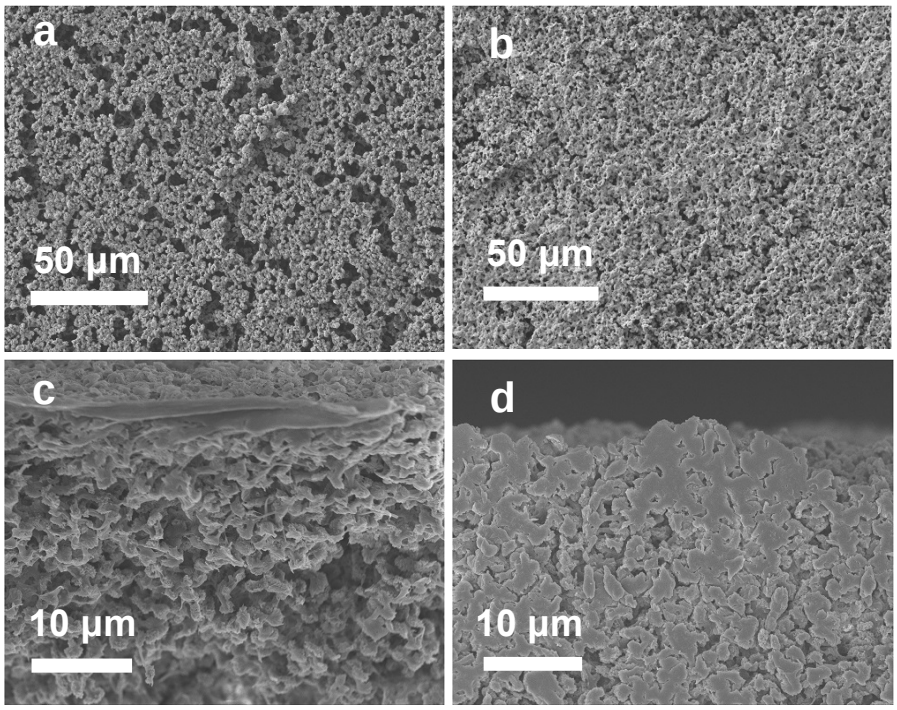

Figure 2.6. SEM images of (a, c) bare nylon membranes and (b, d) PSPMK-modified membranes. Figures a and c are the top views of the membranes, where figures b and d show cross sections of the membranes.

2.3.2. Film Swelling and Contact Angles

PSPMK brushes should resist oil adsorption in large part because they swell extensively in water. Figure 2.7 shows the thickness of water-swollen PSPMK brushes (on Au-coated wafers) and their percent swelling (percent increase in thickness after immersion in deionized water for 12 h) as a function of their "dry" thickness. Notably, films swell by up to 280%, and the maximum swollen thickness is around 340 nm. Some films increase in thickness as much as 240 nm due to water sorption. The swelling data are consistent with changes in the refractive index of the PSPMK brush after immersion in water (see Figure 2.8, higher swelling gives lower refractive indices). When the "dry" thickness of the brush is < ~100 nm, the percent swelling is essentially constant. Lower swelling at the higher

"dry" thicknesses may occur due to a lower chain density at the exterior of thicker films. (Some chain termination likely occurs during the polymerization.)

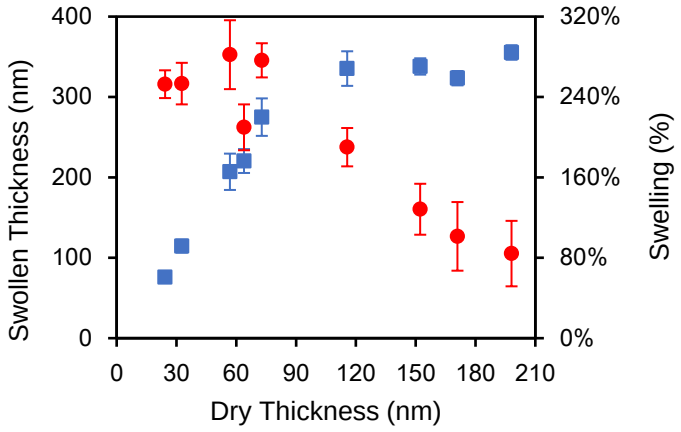

Figure 2.7. The water-swollen thickness (blue squares) and percent swelling (red circles) of PSPMK brushes as a function of their "dry thickness". Error bars represent standard deviations (n=12 determinations on 4 wafers).

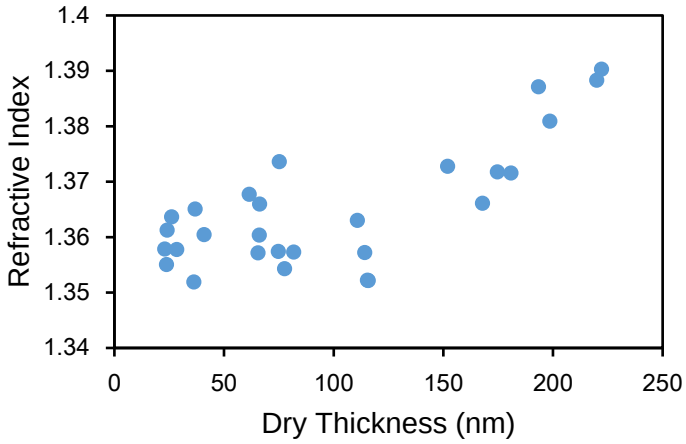

Figure 2.8. Refractive indices of water-swollen PSPMK brushes as a function of their dry thickness. When the dry thickness is <~100 nm, the refractive indices are around 1.36. Refractive indices increase from 1.36 to 1.39 when dry thicknesses surpass 100 nm and swelling decreases. Each point represents an average of refractive indices determined at wavelengths ranging from 410 to 740 nm.

Consistent with high aqueous swelling, the hexadecane contact angles on PSPMK-coated wafers increase from 50º in air to ~180º in water (Figures 2.9a and 2.9b). Kobayashi

and coworkers obtained similar results with hexadecane on PSPMK and other polyelectrolyte brushes.[45] Bare gold surfaces show hexadecane contact angles <5 º in both air and water (Figures 2.9c and 2.9d). Eq. 2.2, often known as Young' s equation, shows the surface tensions that affect hexadecane contact angles in air, θ_{HD-Air} , and in water, $\theta_{HD-Water}$, where γ_{FAir}, γ_{FHD}, γ_{HDAir}, γ_{FW}, and γ_{HDW} are the surface tensions between film and air, film and hexadecane, hexadecane and air, film and water, and hexadecane and water, respectively.

$$\cos\theta_{HD-Air} = \frac{\gamma_{FAir}-\gamma_{FHD}}{\gamma_{HDAir}} \qquad \cos\theta_{HD-Water} = \frac{\gamma_{FW}-\gamma_{FHD}}{\gamma_{HDW}} \qquad \text{Eq. 2.2}$$

Because $\gamma_{HDAir} < \gamma_{HDW}$, for values <90 º contact angles are often greater in water than air. In contrast, for contact angles >90 º, if it acted independently, the high value of γ_{HDW} would decrease the contact angle value compared to the contact angle in air. However, for a highly swollen, water-like film, γ_{FW} approaches zero and $\gamma_{FHD} \approx \gamma_{HDW}$, so $\cos\theta_{HD-water}$ approaches -1 (Figure 2.9b). Thus, oil droplets should dewet and detach easily on PSPMK surfaces in water. This superoleophobicity also occurs on modified nylon membranes, leading to a strong resistance to fouling.

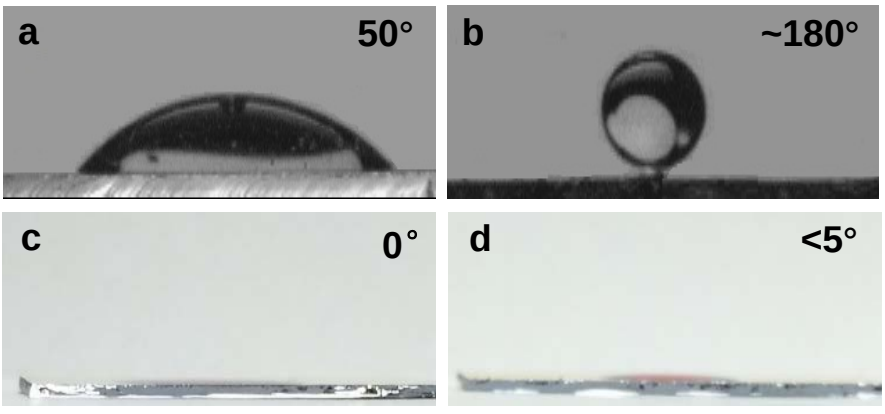

Figure 2.9. Contact angles of hexadecane on PSPMK-modified wafers (a, b) and bare Au-coated wafers (c,d). The images were obtained in air (a, c) and water (b,d).

2.3.3. Surfactant Interactions with PSPMK Brushes

Charged surfactants may adsorb to PSPMK brushes through hydrophobic interactions with brush alkyl backbones, but electrostatic forces between PSPMK side chains and surfactants will be repulsive for anionic surfactants and attractive for cationic surfactants. Thus, this section examines adsorption of anionic and cationic surfactants in PSPMK films and the effect of adsorption on brush swelling.

2.3.3.1.Anionic Surfactant

For studies of SDS adsorption to PSPMK brushes, we first polymerized SPMK for 1 h from many initiator-modified Au-coated wafers to create films with water-swollen thicknesses around 340 nm. The CMC of SDS is 8 mM.[46] Thus, to examine brush swelling

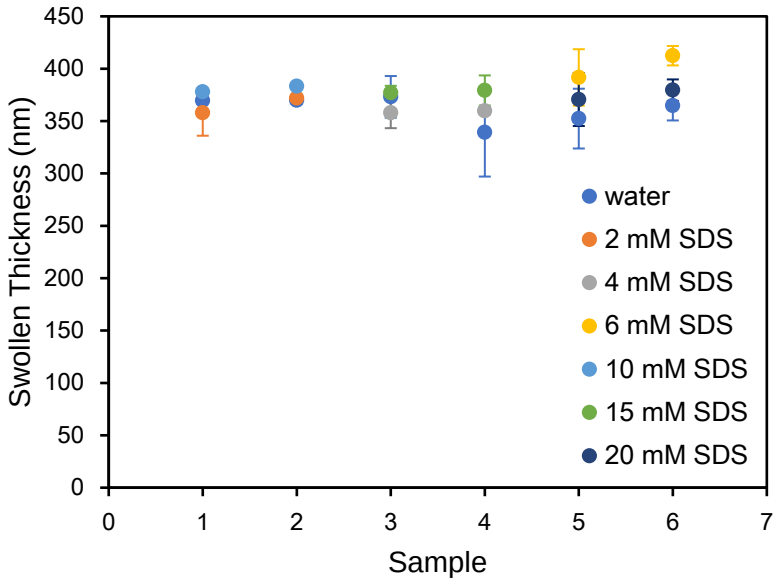

Figure 2.10. Swollen thicknesses of PSPMK brushes on Au-coated wafers in water and in solutions with different concentrations of SDS. Error bars represent standard deviations (n=12 measurements on 4 wafers).

at SDS concentrations above and below the CMC, we immersed the different films in aqueous solutions with SDS concentrations ranging from 2 to 20 mM and determined the

water-swollen thicknesses with in situ ellipsometry. In all cases the swollen thickness was around 340 nm (Figure 2.10) both in water and in the SDS solutions, suggesting that SDS does not affect the film architecture. Moreover, after a brief rinse with water, the reflectance IR spectra of these films showed no increase in the absorbance from CH_2 stretches, which indicates minimal SDS adsorption (Figure 2.11).

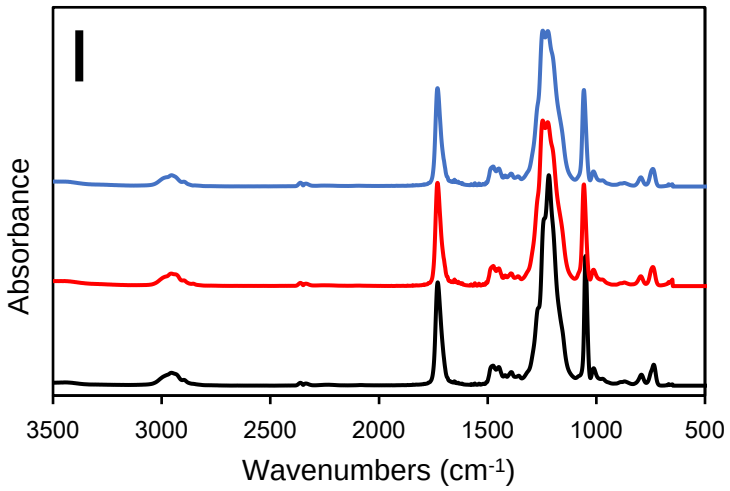

Figure 2.11. Reflectance IR spectra of PSPMK brushes on Au-coated wafers before (black line) and after immersion in 4 mM (red line) and 15 mM (blue line) SDS solutions. Small changes in the intensity of sulfonate stretches with minimal change in the carbonyl stretch may reflect a change in the film orientation or the environment around the sulfonates after immersion in surfactant solutions and rinsing with water. However, the spectra show no aliphatic stretches of surfactant around 2900 cm^{-1}.

Shorter polymerization times lead to lower "dry" film thicknesses and more swelling of PSPMK brushes (see Figure 2.4 and 2.7), so we also examined SDS adsorption in thinner films that have a lower polymer density in water. However, as Figure 2.12 shows, films with water-swollen thicknesses ranging from 75 to 350 nm exhibited no substantial change in their swollen thickness upon immersion in 20 mM SDS solutions.

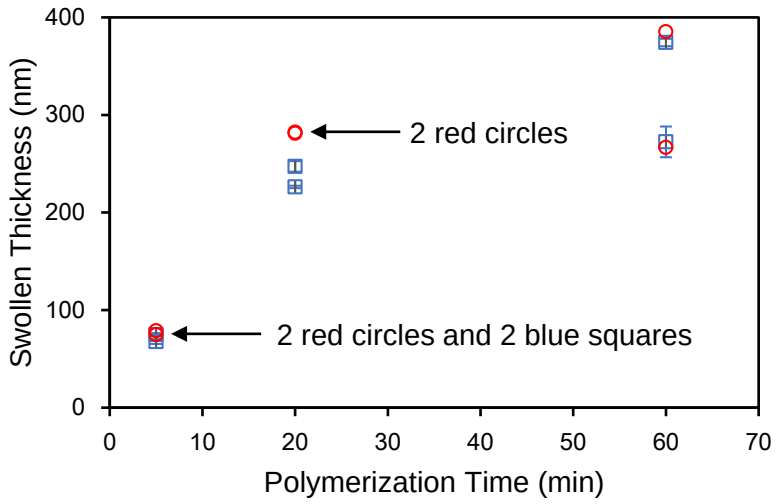

Figure 2.12. The water-swollen thicknesses of PSPMK brushes on Au-coated wafers before (blue squares) and after (red circles) immersion in a 20 mM SDS solution.

Water contact angles also show no change after treatment of films with SDS. The hexadecane contact angle in water was ~180 º, even after exposing the film to 20 mM SDS and briefly rinsing with water. Moreover, the hexadecane contact angle in a 20 mM SDS solution was also ~180º, and the oil easily detaches from the PSPMK-modified surface. Taken together, these results imply that negatively charged brushes resist SDS adsorption and should resist fouling in the filtration of emulsions stabilized with this surfactant. Because surfactant should coat oil droplets in stabilized emulsions, we expect the fouling tendencies of such emulsions to resemble those of the surfactant itself.

2.3.3.2.Cationic Surfactant

2.3.3.2.1. Effect of CTAB Concentration

Unlike SDS, the cationic surfactant CTAB will experience electrostatic attraction to PSPMK brushes. After immersion in a 3 mM CTAB solution and rinsing with water, the absorbances of the CH_2 symmetric and asymmetric stretches at 2925 and 2854 cm^{-1} increase dramatically in the reflectance IR spectra of PSPMK films (Figure 2.13),

indicating CTAB adsorption. The position and intensity of sulfonate absorbances also shift, and the intensity of the C=O peak decreases suggesting a change in the "dry" PSPMK conformation and in the counterions of the sulfonate groups after CTAB exposure.[47-49]

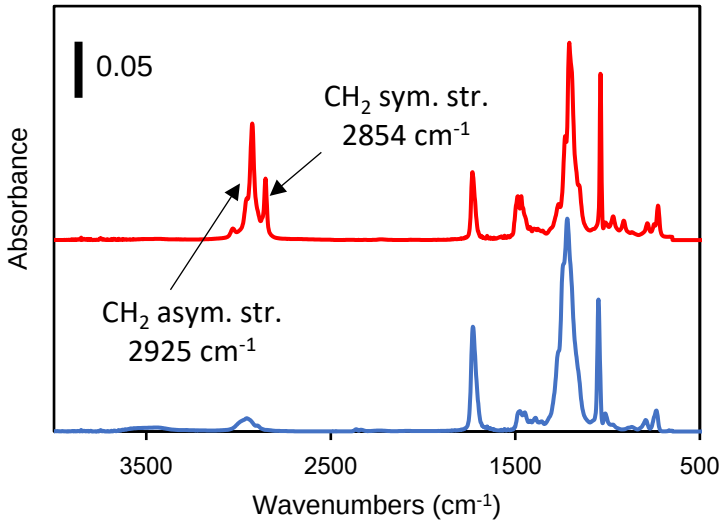

Figure 2.13. Reflectance IR spectra of PSPMK brushes before (bottom) and after (top) immersion in 2 mM CTAB for 12 h and rinsing with water. Growth of the PSPMK brush employed 1-h polymerization.

Figure 2.14 shows the increase in the absorbance at 2925 cm^{-1} as a function of the CTAB concentration in solution (films were rinsed with water prior to obtaining the spectra). At CTAB concentrations from 0.4 to 1.5 mM, the absorbance at 2925 cm^{-1} increases slightly with CTAB concentration, but upon increasing the CTAB concentration from 1.5 to 5 mM, the amount of CTAB adsorption, as quantified by the increase in absorbance at 2925 cm^{-1}, decreases 76%. Nevertheless, the overall swollen film thickness increases continuously with CTAB concentration (Figure 2.14). At the lowest CTAB concentrations, surfactants exist as single molecules (the CMC is 0.9 mM[50]) that should diffuse throughout the film and adsorb to brushes. The surfactants likely replace water in the film, so despite the brush becoming more hydrophobic it does not collapse significantly.

With increasing CTAB concentration, adsorption of micelles may dominate, and their added mass apparently increases the thickness of the swollen film. However, extensive adsorption of micelles at the brush surface may hinder further sorption of CTAB micelles and single molecules (Figure 2.14) despite the increase in swollen thickness. CTAB adsorption likely neutralizes much of the negative charge near the surface of the PSPMK brushes and makes them more oleophilic, as indicated by only a 58º hexadecane contact angle in water (Figure 2.15) after CTAB adsorption.

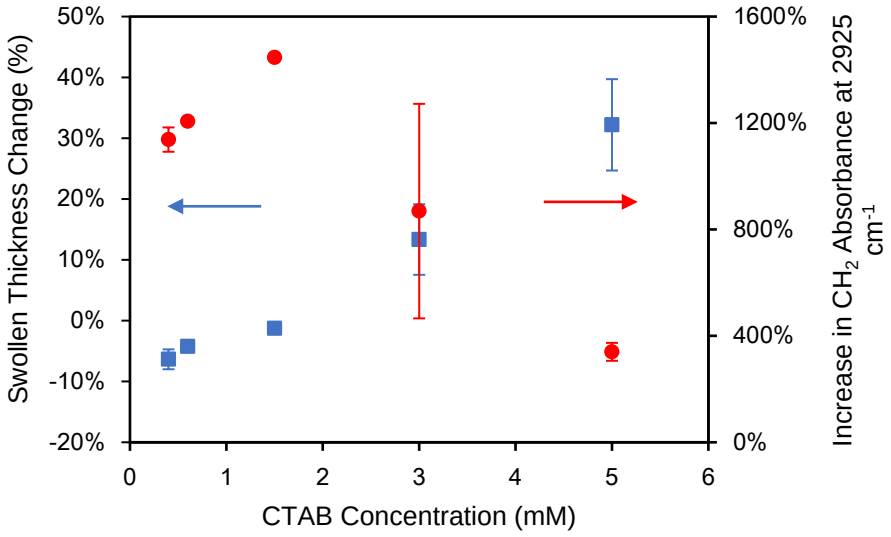

Figure 2.14. Percent change in swollen thickness (blue squares) and percent increase in the CH_2 IR absorbance at 2925 cm^{-1} (red circles) after immersion of brushes in solutions with varying CTAB concentrations. Swelling was determined first in deionized water and subsequently in the CTAB solution, whereas the IR absorbance was determined after immersion in deionized water or CTAB solution and subsequent rinsing with water, and drying with N_2. All films were initially prepared using a 1-h polymerization time. Error bars represent standard deviations (n=12 measurements on 4 wafers).

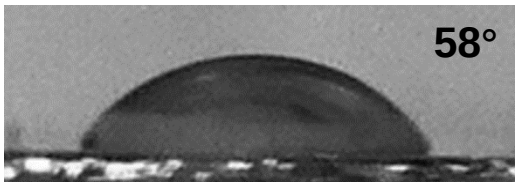

Figure 2.15. Contact angle of hexadecane in deionized water on a PSPMK-modified wafer treated with CTAB. The wafer was exposed to 5 mM CTAB for 12 h and rinsed with water before the contact angle measurement.

2.3.3.2.2. Effect of the Density of PSPMK Brushes on CTAB Adsorption and Changes in Swelling

In early studies, we used some older batches of the disulfide initiator that did not always give similar thicknesses for a given polymerization time, presumably because some of the initiator had decomposed and the densities of chains were not the same on all wafers. However, these films show similar swollen thicknesses, so they offer a chance to examine the effect of brush density on CTAB adsorption. We employ the magnitude of the $–SO_3^-$ absorbance at 1219 cm^{-1} as an indicator of brush density for films with similar swollen thicknesses of 340 nm. Figure 2.16 shows that with higher density (greater $-SO_3^-$ absorbance), PSPMK brushes collapse less and even increase in thickness upon immersion in 3 mM CTAB. However, the $-CH_2$ absorbance due to adsorbed surfactant is similar for all of the films after rinsing with water. As mentioned above, adsorption of CTAB micelles apparently stretches polymer chains for films with a high density. In this case, the micelle does not simply replace water. For the lowest density films, the micelle adsorption causes chain collapse, perhaps as the chains conform to the micelle.

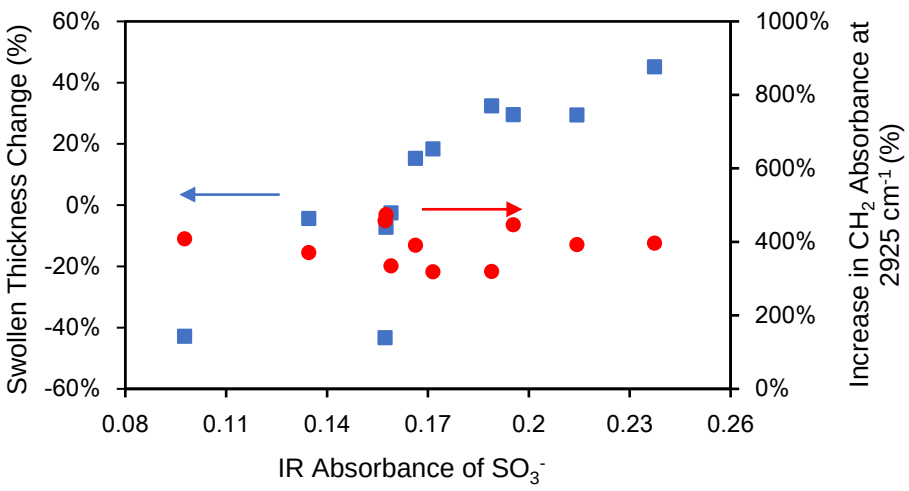

Figure 2.16. The change in the water-swollen thickness of PSPMK brushes in 3 mM CTAB (blue squares) with respect to the thickness in deionized water, and the percent increase in the $–CH_2$ IR absorbance at 2925 cm^{-1} (red circles) as a function of the sulfonate absorbance at 1219 cm^{-1} in the pristine film. IR absorbances were determined after rinsing films with water and drying with N_2. The increase in absorbance at 2925 cm^{-1} stems from surfactant adsorption, and film density should increase with increasing sulfonate absorbance.

2.3.4. Emulsion Filtration with PSPMK-Modified Membranes

2.3.4.1.Filtration of SDS-Stabilized Emulsions

We examined dead-end filtration of hexadecane submicron emulsions stabilized with either SDS or CTAB. Hexadecane serves a representative oil with a low surface energy[10] and is widely used in fundamental research[21, 45, 51]. Light-scattering measurements show that the oil droplet size distributions (Figure 2.17) are similar for emulsions stabilized with SDS and CTAB. In both cases, the droplets have a size range from 40 to 1000 nm, and the diameters of 90% (by volume) of the oil droplets are smaller than 500 nm. The volume-weighted mean diameters are 280 and 229 nm for SDS and CTAB-stabilized oil droplets, respectively. All these data correspond to the definition of a submicron emulsion,[14] and the droplet size distribution was approximately the same at the beginning and end of filtrations. The filtration employs initial oil volume fractions of 0.7%. The oil content in wastewater

from different industries varies from 0.0013% to 25.97% (volume fraction), and most oily wastes contain 0.1-1% oil.[1] During filtrations of SDS-stabilized emulsions with PSPMK-modified and NF270 membranes, the hexadecane concentration in the permeate approaches or is less than the limit of detection (9 x 10^{-6} M). Thus, the oil rejection is usually >99.9% and always >99.8%.

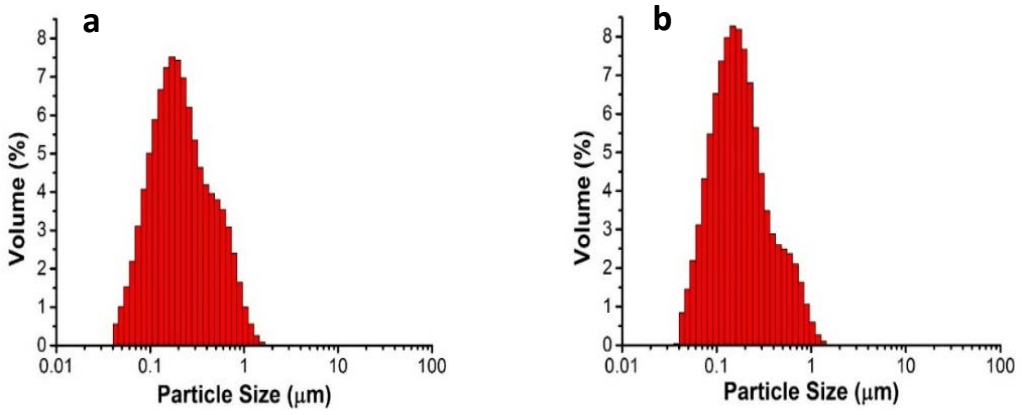

Figure 2.17. Size distributions of hexadecane submicron emulsions stabilized by SDS (a) and CTAB (b).

Figure 2.18a shows the specific flux (flux divided by the transmembrane pressure drop) during filtration of an SDS-stabilized emulsion through a PSPMK-modified (1-h polymerization) membrane. Because the oil rejection is around 100% over the entire filtration, the feed oil concentration is nearly constant. The flux during the filtration (~18 LMH/bar) is about 75% of the pure water flux (~23 LMH/bar), which suggests minimal membrane fouling. More importantly, the flux does not decline over 12 h, further confirming the fouling resistance of the brushes. The pure water flux after filtration was 29.9 LMH/bar (Figure 2.19a), 30% higher than that before filtration. This increase in pure

water flux may result from a change in the brush confirmation, but the high water flux after

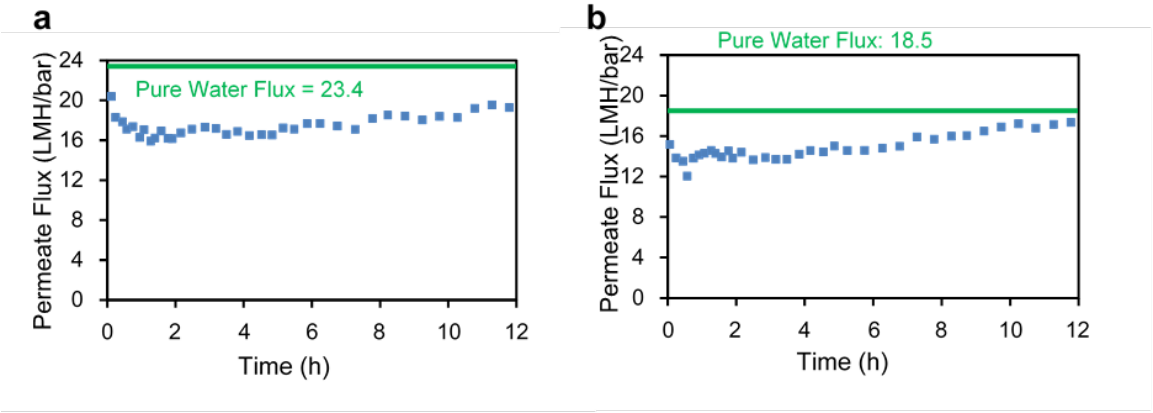

Figure 2.18. Specific fluxes (blue squares) in dead-end filtration of SDS-stabilized hexadecane submicron emulsions through PSPMK-modified membranes. The SPMK polymerization time was 1 h (a) or 45 min (b). The green horizontal lines show the pure water flux before filtration. Initially, the emulsion contained 24.3 mM hexadecane in 0.36 mM SDS.

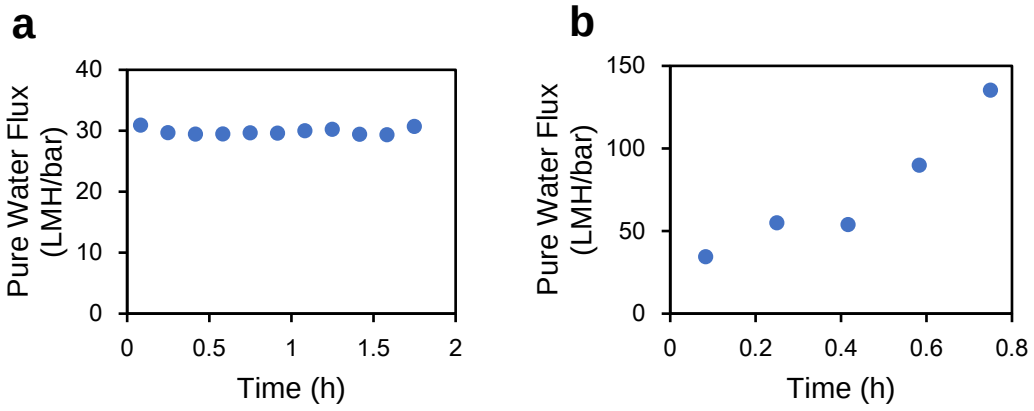

Figure 2.19. Pure water flux (after a 12-h filtration of an SDS-stabilized emulsion) for membranes modified using (a) 1-h and (b) 45-min SI-ATRP of SPMK.

filtration confirms the strong anti-fouling nature of the PSPMK-modified membrane. The highly hydrated, negatively charged brush clearly resists adsorption of oil droplets. We should note that a control nylon membrane with no modification shows much higher flux (2 to 3 orders of magnitude) but little oil rejection due to the large pores (nominally 1.2 μm) (Figure 2.20a, b).

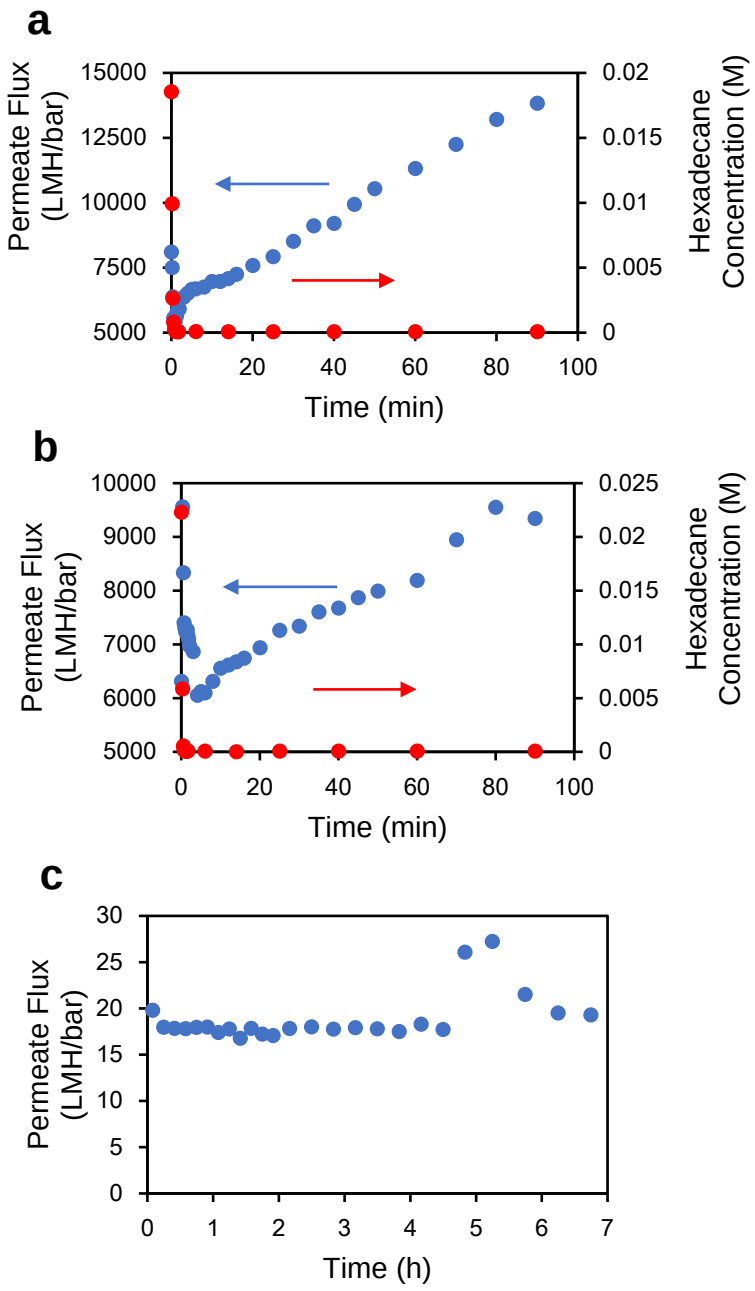

Figure 2.20. Replicate dead-end filtrations. (a), (b): filtration of SDS-stabilized hexadecane emulsions with bare nylon membranes with 1.2 μm pores. The specific flux (blue circles) drops at the beginning due to membrane fouling and increases quickly after the oil permeates through the membrane in 1.5 min. The hexadecane concentration (red circles) falls to zero because deionized water replenishes the feed cell. (c): filtration of an SDS-stabilized hexadecane emulsion with a PSPMK-modified membrane (polymerization time: 45min). The permeate flux (blue circles) increases after 5h of filtration, and visible oil appears in the permeate after that time.

Decreasing the polymerization time from 1 h to 45 min during membrane modification should lead to polymer brushes with a similar swollen thickness (Figure 2.4) but a lower charge density (Figure 2.7). Figure 2.18b shows the permeate flux for a membrane modified with 45 min of SPMK polymerization. Compared to filtration through a membrane modified with 1 h of polymerization, the fluxes and oil rejections are similar. However, for the membrane modified with 45 min of polymerization the flux increases gradually during the experiment, and the pure water flux after filtration increases dramatically (Figure 2.19b), suggesting some collapse of the low-density brushes. A replicate membrane (Figure 2.20c) prepared with 45 min of PSPMK polymerization was not hydrophilic enough to maintain high oil rejection longer than 5 h. Thus, decreasing the polymerization time may increase flux, but the low density of polymer chains will likely lead to eventual brush collapse.

2.3.4.2.Filtration of CTAB-Stabilized Emulsions

In dramatic contrast to SDS, filtration of CTAB-stabilized submicron emulsions through PSPMK-modified membranes leads to oil breakthrough and an initial dramatic increase in flux (Figure 2.21). Because we add the emulsion to the Amicon cell and replenish the cell with deionized water from a feed tank during the filtration, the concentrations of oil and surfactant in the feed rapidly decline when oil rejection is low. Thus, the hexadecane concentration in the permeate first increases with time as the membrane becomes more permeable in the presence of the cationic surfactant and then declines because of less oil in the feed. Permeate flux also initially increases with time as the brush collapses and then becomes constant when there is minimal surfactant in the feed. However, the flux never returns to its initial low value, suggesting the brush remains collapsed.

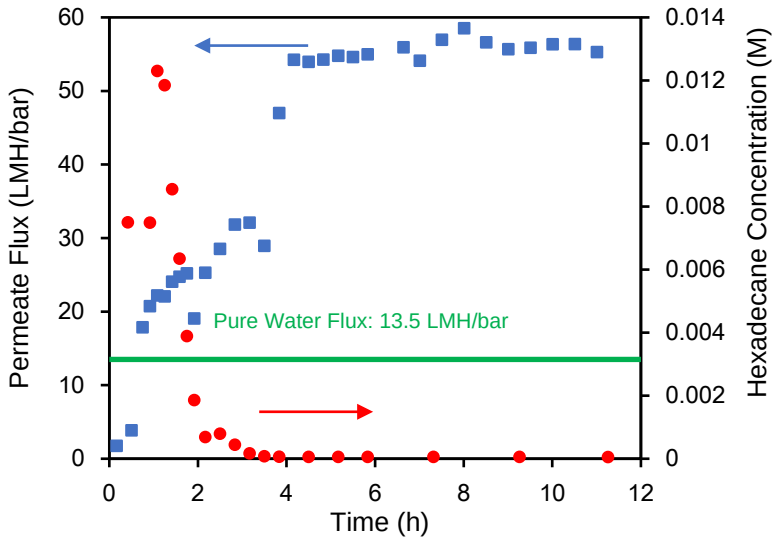

Figure 2.21. Permeate hexadecane concentrations (red circles) and specific fluxes (blue squares) during dead-end filtration of a CTAB-stabilized hexadecane submicron emulsion through a PSPMK-modified membrane. The horizontal green line shows the pure water flux prior to the filtration. The membrane was modified with a 1-h polymerization. The PSPMK-modified membrane showed low oil rejection, and all of the hexadecane permeated through the membrane in 4 h. The initial hexadecane feed concentration was 17.9 mM, but this value declined rapidly during the filtration due to low rejection and cell replenishment with deionized water.

As Figure 2.22 illustrates, we speculate that for low-density chains, polymer brushes likely collapse as they wrap around CTAB-stabilized oil micelles. Even for membranes modified with a 1-h polymerization, brush deswelling is sufficient to give a permeate flux that is 4 times the pure water flux prior to exposure to surfactant. Moreover, the membranes show minimal oil rejection after brush collapse. This mechanism is consistent with the data in Figure 2.16, where brush thickness decreases in the presence of CTAB for films with the lowest density. The relatively low density of functional groups on the nylon surface likely leads to less initiator and significantly less dense brushes than polymerization from a monolayer of initiator on the Au-coated wafer. The concentration

of CTAB in the initial feed solution is also low, 0.36 mM, which tends to lead to brush collapse (Figure 2.14).

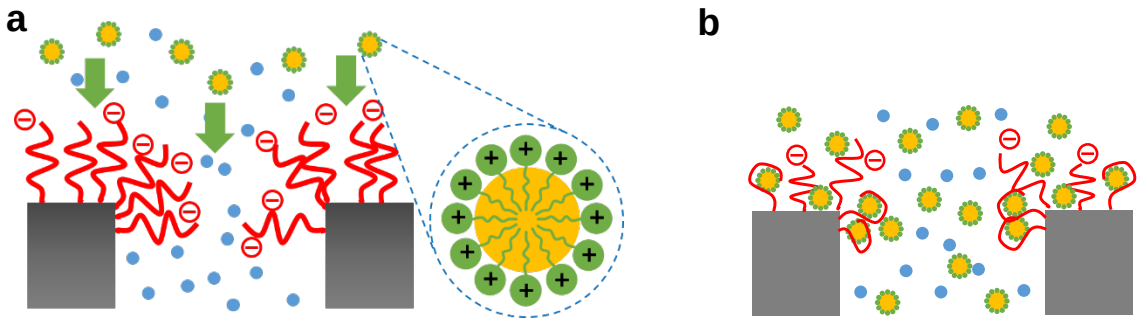

Figure 2.22. Cartoon of filtration of CTAB-stabilized submicron emulsions with PSPMK modified-membranes: (a) polymer brushes swell well in water prior to contact with CTAB and oil droplets stabilized by CTAB; (b) positively charged oil droplets adsorb to the negatively charged PSPMK to cause brush collapse. The blue, yellow and green balls represent water, oil droplets and CTAB molecules, respectively. The brush modification likely extends much farther into the membrane than the figure shows.

2.3.5. Comparison of Filtration with PSPMK-Modified Membranes and NF270 *Nanofiltration Membranes*

We also performed dead-end emulsion filtration through commercial NF270 membranes. We chose these membranes because their pure water specific flux (~19.6 LMH/bar) is similar to that of brush-modified membranes, which enables a fair comparison of fouling tendencies. Moreover, these membranes have a negatively charged surface (zeta potential of -20 mV around neutral pH[34, 52-53]), and their small effective pore size (0.49 nm[54]) should lead to nearly 100% oil rejection. As expected, the NF270 membranes exhibited oil rejections >99.9%, regardless of surfactant. Initially, flux declines most rapidly for solutions containing the cationic surfactant (Figure 2.23), presumably because of favorable electrostatic interactions with the negatively charged surface.[54] Even with an anionic surfactant, however, the negatively charged surface is not sufficient to prevent fouling.

With SDS-stabilized emulsions, the permeate flux declines 98.7% over the course of the 12-h filtration. Given time, micelle adsorption to the membranes occurs regardless of surfactant charge. Interestingly, the flux at the end of the filtration is higher for the CTAB-stabilized emulsion than for the SDS-stabilized system. After formation of an oil coating on the membrane, fouling will likely depend more on the emulsion than on the properties of the underlying brush.

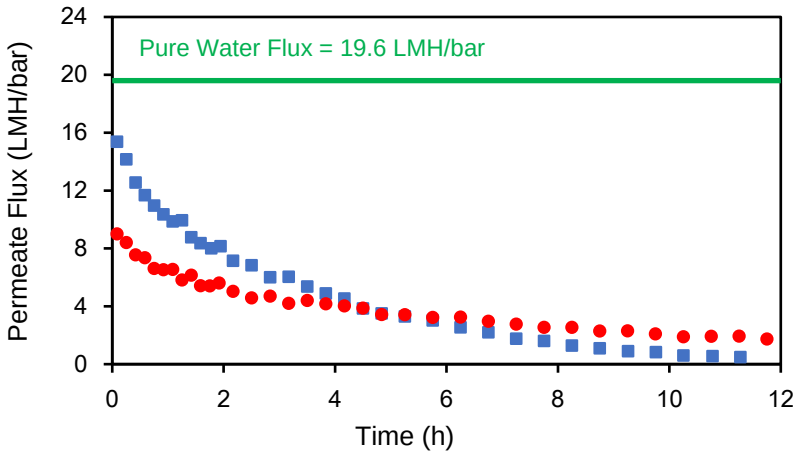

Figure 2.23. Evolution of specific permeate flux with time during filtration of aqueous submicron emulsions through NF270 membranes. Blue squares and red circles represent filtration with an SDS-stabilized and a CTAB-stabilized emulsion, respectively. The horizontal green line shows the average pure water flux.

Compared to the brush-modified membranes prepared with a 1-h polymerization (Figure 2.18a), the NF270 membranes show similar oil rejection (almost 100%), but the brush-modified membranes exhibit no significant permeate flux declines with time. For example, 12 h into filtration of SDS-stabilized emulsions, the permeate flux was ~18 LMH/bar for the PSPMK-modified membrane and only ~0.2 LMH/bar for the NF270 membrane. With CTAB-stabilized emulsions, the NF270 membrane is clearly superior to the brush-modified membrane because of higher rejection. Nevertheless, the NF270

membrane still shows a strong fouling tendency in the cationic surfactant. We should also note that a recent study suggests that growth of zwitterionic polymer brushes only on the surface of membranes may lead to permeate fluxes up to 6000 LMH/bar,[12] which could make such membranes much more attractive for oil-water separations.

2.4. Conclusions

This research investigated the effect of surfactants (a) on the swelling of polyanionic brushes on planar surfaces and (b) on emulsion filtration through porous membranes modified with similar brushes. Anionic surfactants do not alter the aqueous swelling of PSPMK brushes, nor do they significantly decrease flux and rejection during filtration of surfactant-stabilized oil emulsions through brush-modified membranes. In contrast, cationic surfactants adsorb to the polyanionic brushes, presumably due to electrostatic attraction. When polymer chain density and surfactant concentration are low, adsorption of CTAB causes brush collapse, and on microporous membranes this collapse leads to greatly enhanced flux and minimal rejection of oil droplets with diameters <1 μm. On planar surfaces, high-density brushes do not collapse in the presence of CTAB, although they do adsorb the surfactant. Unfortunately, synthesis of high-density brushes on microporous membranes is a challenge due to a low functional group density on the membrane surface. However, knowledge of the surfactants present in a given solution may allow design of specific brushes (polyanionic or polycationic) that resist fouling.

REFERENCES

REFERENCES

1. Cheryan, M.; Rajagopalan, N. Membrane Processing of Oily Streams. Wastewater Treatment and Waste Reduction. *J. Membr. Sci.* **1998,** *151*, 13-28.

2. 40 CFR 435.15, Standards of Performance for New Sources (NSPS), Environmental Protection Agency: Washington, DC, 1994.

3. Duhon, H. Produced Water Treatment: Yesterday, Today, and Tomorrow. *Oil Gas Facil.* **2012**, *1*, 29-31.

4. Frankiewicz, T. In *Understanding the Fundamentals of Water Treatment, the Dirty Dozen — 12 Common Causes of Poor Water Quality*, 11th Produced Water Seminar, Houston, TX, Jan. 17-19; 2001.

5. Duong, P. H. H.; Chung, T. S. Application of Thin Film Composite Membranes with Forward Osmosis Technology for the Separation of Emulsified Oil-Water. *J. Membr. Sci.* **2014,** *452*, 117-126.

6. Hu, X.; Yu, Y.; Zhou, J.; Wang, Y.; Liang, J.; Zhang, X.; Chang, Q.; Song, L. The Improved Oil/Water Separation Performance of Graphene Oxide Modified Al_2O_3 Microfiltration Membrane. *J. Membr. Sci.* **2015,** *476*, 200-204.

7. Kota, A. K.; Kwon, G.; Choi, W.; Mabry, J. M.; Tuteja, A. Hygro-Responsive Membranes for Effective Oil-Water Separation. *Nat. Commun.* **2012,** *3*, 1025-1032.

8. Pan, Y. Q.; Wang, T. T.; Sun, H. M.; Wang, W. Preparation and Application of Titanium Dioxide Dynamic Membranes in Microfiltration of Oil-in-Water Emulsions. *Sep. Purif. Technol.* **2012,** *89*, 78-83.

9. Tuteja, A.; Choi, W.; Mabry, J. M.; McKinley, G. H.; Cohen, R. E. Robust Omniphobic Surfaces. *P. Natl. Acad. Sci. USA* **2008,** *105* (47), 18200-18205.

10. Kwon, G.; Kota, A. K.; Li, Y. X.; Sohani, A.; Mabry, J. M.; Tuteja, A. On-Demand Separation of Oil-Water Mixtures. *Adv. Mater.* **2012,** *24*, 3666-3671.

11. Solomon, B. R.; Hyder, M. N.; Varanasi, K. K. Separating Oil-Water Nanoemulsions Using Flux-Enhanced Hierarchical Membranes. *Sci. Rep.* **2014,** *4*, 5504-5509.

12. Gao, S. J.; Zhu, Y. Z.; Zhang, F.; Jin, J. Superwetting Polymer-Decorated SWCNT Composite Ultrathin Films for Ultrafast Separation of Oil-in-Water Nanoemulsions. *J. Mater. Chem. A* **2015,** *3*, 2895-2902.

13. Lovelyn, C.; Attama, A. A. Current State of Nanoemulsions in Drug Delivery. *J. Biomater. Nanobiotechnol.* **2011,** *2*, 626-639.

14. Benita, S.; Levy, M. Submicron Emulsions as Colloidal Drug Carriers for Intravenous Administration: Comprehensive Physicochemical Characterization. *J. Pharm. Sci.* **1993,** *82*, 1069-1079.

15. Wang, L. J.; Li, X. F.; Zhang, G. Y.; Dong, J. F.; Eastoe, J. Oil-in-Water Nanoemulsions for Pesticide Formulations. *J. Colloid Interf. Sci.* **2007,** *314*, 230-235.

16. Quintanilla-Carvajal, M. X.; Camacho-Diaz, B. H.; Meraz-Torres, L. S.; Chanona-Perez, J. J.; Alamilla-Beltran, L.; Jimenez-Aparicio, A.; Gutierrez-Lopez, G. F. Nanoencapsulation: A New Trend in Food Engineering Processing. *Food Eng. Rev.* **2010,** *2*, 39-50.

17. Bernardi, D.; Pereira, T.; Maciel, N.; Bortoloto, J.; Viera, G.; Oliveira, G.; Rocha-Filho, P. Formation and Stability of Oil-in-Water Nanoemulsions Containing Rice Bran Oil: in vitro and in vivo Assessments. *J. Nanobiotechnol.* **2011,** *9*, 44-52.

18. Talegaonkar, S.; Negi, L. Nanoemulsion in Drug Targeting. In *Targeted Drug Delivery : Concepts and Design*, Devarajan, P. V.; Jain, S., Eds.; Springer International Publishing, 2015, pp 433-459.

19. Asua, J. M. Miniemulsion Polymerization. *Prog. Polym. Sci.* **2002,** *27*, 1283-1346.

20. Bechthold, N.; Tiarks, F.; Willert, M.; Landfester, K.; Antonietti, M. Miniemulsion Polymerization: Applications and New Materials. *Macromol. Symp.* **2000,** *151*, 549-555.

21. Zhu, Y.; Zhang, F.; Wang, D.; Pei, X. F.; Zhang, W.; Jin, J. A Novel Zwitterionic Polyelectrolyte Grafted PVDF Membrane for Thoroughly Separating Oil from Water with Ultrahigh Efficiency. *J. Mater. Chem. A* **2013,** *1*, 5758-5765.

22. Boussu, K.; Kindts, C.; Vandecasteele, C.; Van der Bruggen, B. Surfactant Fouling of Nanofiltration Membranes: Measurements and Mechanisms. *Chemphyschem* **2007,** *8*, 1836-1845.

23. Wandera, D.; Himstedt, H. H.; Marroquin, M.; Wickramasinghe, S. R.; Husson, S. M. Modification of Ultrafiltration Membranes with Block Copolymer Nanolayers for Produced Water Treatment: The Roles of Polymer Chain Density and Polymerization Time on Performance. *J. Membr. Sci.* **2012,** *403*, 250-260.

24. de Vos, W. M.; Biesheuvel, P. M.; de Keizer, A.; Kleijn, J. M.; Stuart, M. A. C. Adsorption of Anionic Surfactants in a Nonionic Polymer Brush: Experiments, Comparison with Mean-Field Theory, and Implications for Brush-Particle Interaction. *Langmuir* **2009,** *25*, 9252-9261.

25. Konradi, R.; Rühe, J. Binding of Oppositely Charged Surfactants to Poly(methacrylic acid) Brushes. *Macromolecules* **2005,** *38*, 6140-6151.

26. Dunlop, I. E.; Thomas, R. K.; Titmus, S.; Osborne, V.; Edmondson, S.; Huck, W. T. S.; Klein, J. Structure and Collapse of a Surface-Grown Strong Polyelectrolyte Brush on Sapphire. *Langmuir* **2012,** *28*, 3187-3193.

27. Cao, Q. Q.; Zuo, C. C.; Li, L. J. Electrostatic Binding of Oppositely Charged Surfactants to Spherical Polyelectrolyte Brushes. *Phys. Chem. Chem. Phys.* **2011,** *13*, 9706-9715.

28. Cao, Q. Q.; Zuo, C. C.; Li, L. J.; Gao, M. F. Interactions of Polyelectrolyte Brushes with Oppositely Charged Surfactants. *Colloid Polym. Sci.* **2011,** *289*, 1089-1102.

29. Döbbelin, M.; Arias, G.; Loinaz, I.; Llarena, I.; Mecerreyes, D.; Moya, S. Tuning Surface Wettability of Poly(3-sulfopropyl methacrylate) Brushes by Cationic Surfactant-Driven Interactions. *Macromol. Rapid Commun.* **2008,** *29*, 871-875.

30. Wang, H.; Zhang, H.; Yuan, S. L.; Liu, C. B.; Xu, Z. Molecular Dynamics Study of the Adsorption of Anionic Surfactant in a Nonionic Polymer Brush. *J. Mol. Model.* **2014,** *20*, 2267-2275.

31. Zhang, R.; Ma, S.; Wei, Q.; Ye, Q.; Yu, B.; van der Gucht, J.; Zhou, F. The Weak Interaction of Surfactants with Polymer Brushes and Its Impact on Lubricating Behavior. *Macromolecules* **2015,** *48*, 6186-6196.

32. IndustryARC. *Oilfield Surfactants Market Analysis.* 2017. http://industryarc.com/-Report/243/oil-field-surfactants-market-analysis.html (accessed Aug 12, 2017).

33. Matyjaszewski, K.; Xia, J. Atom Transfer Radical Polymerization. *Chem. Rev.* **2001,** *101*, 2921-2990.

34. Manttari, M.; Pekuri, T.; Nystrom, M. NF270, a New Membrane Having Promising Characteristics and Being Suitable for Treatment of Dilute Effluents from the Paper Industry. *J. Membr. Sci.* **2004,** *242*, 107-116.

35. Shah, R. R.; Merreceyes, D.; Husemann, M.; Rees, I.; Abbott, N. L.; Hawker, C. J.; Hedrick, J. L. Using Atom Transfer Radical Polymerization to Amplify Monolayers of Initiators Patterned by Microcontact Printing into Polymer Brushes for Pattern Transfer. *Macromolecules* **2000,** *33*, 597-605.

36. Xu, F. J.; Zhao, J. P.; Kang, E. T.; Neoh, K. G.; Li, J. Functionalization of Nylon Membranes via Surface-Initiated Atom-Transfer Radical Polymerization. *Langmuir* **2007,** *23*, 8585-8592.

37. Masci, G.; Bontempo, D.; Tiso, N.; Diociaiuti, M.; Mannina, L.; Capitani, D.; Crescenzi, V. Atom Transfer Radical Polymerization of Potassium 3-sulfopropyl Methacrylate: Direct Synthesis of Amphiphilic Block Copolymers with Methyl Methacrylate. *Macromolecules* **2004,** *37*, 4464-4473.

38. Unsal, E.; Elmas, B.; Caglayan, B.; Tuncel, M.; Patir, S.; Tuncel, A. Preparation of an Ion-Exchange Chromatographic Support by a "Grafting From" Strategy Based on Atom Transfer Radical Polymerization. *Anal. Chem.* **2006,** *78*, 5868-5875.

39. Huang, W.; Baker, G. L.; Bruening, M. L. Controlled Synthesis of Cross-Linked Ultrathin Polymer Films by Using Surface-Initiated Atom Transfer Radical Polymerization. *Angew. Chem.* **2001,** *113*, 1558-1560.

40. Harris, J. J.; Bruening, M. L. Electrochemical and in Situ Ellipsometric Investigation of the Permeability and Stability of Layered Polyelectrolyte Films. *Langmuir* **1999,** *16*, 2006-2013.

41. Jasiewicz, K.; Pietrzak, R. Metals Ions Removal by Polymer Membranes of Different Porosity. *Scientific World J.* **2013**, *2013*, 1-7.

42. Density of Plastics. http://www.dotmar.com.au/density.html (accessed Sep 29 2015).

43. Staples, E.; Penfold, J.; Tucker, I. Adsorption of Mixed Surfactants at the Oil-Water Interface. *J. Phys. Chem. B* **2000,** *104*, 606-614.

44. Palencia, M.; Rivas, B. L.; Pereira, E.; Hernandez, A.; Pradanos, P. Study of Polymer-Metal Ion-Membrane Interactions in Liquid-Phase Polymer-Based Retention (LPR) by Continuous Diafiltration. *J. Membr. Sci.* **2009,** *336*, 128-139.

45. Kobayashi, M.; Terayama, Y.; Yamaguchi, H.; Terada, M.; Murakami, D.; Ishihara, K.; Takahara, A. Wettability and Antifouling Behavior on the Surfaces of Superhydrophilic Polymer Brushes. *Langmuir* **2012,** *28*, 7212-7222.

46. Zhang, X. C.; Jackson, J. K.; Burt, H. M. Determination of Surfactant Critical Micelle Concentration by a Novel Fluorescence Depolarization Technique. *J. Biochem. Bioph. Meth.* **1996,** *31*, 145-150.

47. Meaurio, E.; Zuza, E.; Lopez-Rodriguez, N.; Sarasua, J. R. Conformational Behavior of Poly(L-lactide) Studied by Infrared Spectroscopy. *J. Phys. Chem. B* **2006,** *110*, 5790-5800.

48. Kujawski, W.; Nguyen, Q.; Neel, J. Infrared Investigations of Sulfonated Ionomer Membranes. I. Water–Alcohol Compositions and Counterions Effects. *J. Appl. Polym. Sci.* **1992,** *44*, 951-958.

49. Leyte, J. C.; Zuiderwe.Lh; Vledder, H. J. An IR Investigation of Polyion-Counterion Interactions. *Spectrochim. Acta, Part A* **1967,** *A 23*, 1397-1407.

50. Li, W.; Zhang, M.; Zhang, J.; Han, Y. Self-Assembly of Cetyl Trimethylammonium Bromide in Ethanol-Water Mixtures. *Front. Chem. China* **2006,** *1*, 438-442.

51. Solomon, B. R.; Hyder, N.; Varanasi, K. K. Separating Oil-Water Nanoemulsions Using Flux-Enhanced Hierarchical Membranes. *Sci. Rep.* **2014,** *4*, 1-6.

52. Nghiem, L. Removal of Emerging Trace Organic Contaminants by Nanofiltration and Reverse Osmosis. Ph.D. Thesis [Online], University of Wollongong, Australia, **2005**. http://ro.uow.edu.au/theses/377/ (accessed Aug 12, 2017)

53. Malaisamy, R.; Talla-Nwafo, A.; Jones, K. L. Polyelectrolyte Modification of Nanofiltration Membrane for Selective Removal of Monovalent Anions. *Sep. Purif. Technol.* **2011,** *77*, 367-374.

54. Lee, J. H.; Chung, J. Y.; Chan, E. P.; Stafford, C. M. Correlating Chlorine-Induced Changes in Mechanical Properties to Performance in Polyamide-Based Thin Film Composite Membranes. *J. Membr. Sci.* **2013,** *433*, 72-79.

Chapter 3. Aqueous Swelling of Zwitterionic Poly(Sulfobetaine Methacrylate) Brushes in the Presence of Ionic Surfactants

Portions of this chapter are being submitted to *Macromolecules* (Yang, Z., Tarabara, V. V., and Bruening, M. L.).

3.1. Introduction

Polyelectrolyte brushes, dense assemblies of charged polymers attached through one end to a surface,[1] can be extremely hydrophilic and provide both enthalpic and entropic barriers to nonspecific adsorption of a wide range of analytes.[2-4] Thus, a number of studies employed such coatings as anti-biofouling materials,[5-10] and these brushes may also serve as lubricating films with extremely low friction coefficients in water.[11-14] Additionally, several groups derivatized polyelectrolyte brushes with affinity reagents to capture specific proteins.[15-18] In certain cases, the properties of specific brushes can change in response to temperature,[19, 20] pH[21-23] and solvent,[24-27] creating "smart" surfaces.

However, small ions may diffuse into polyelectrolyte brushes and change their swelling and anti-fouling properties. For example, polyanionic and polycationic brushes collapse in solutions with increasing ionic strength due to charge screening and a decrease in electrostatic repulsion.[28-30] This work focuses on the impact of ionic surfactants on brush swelling in aqueous solutions. Due to their amphiphilic nature that results from both hydrophilic and hydrophobic moieties, surfactants are vital in a wide range of applications such as protein solubilization,[31, 32] emulsification,[33-35] cleaning,[36-38] and fabric softening.[39-41] Even low concentrations of surfactants may dramatically change the anti-fouling properties of polyelectrolyte films. Our previous work showed that polyanionic brushes resist adsorption of anionic surfactants,[42] and polyanionic brush-coated membranes

completely repel emulsified oil droplets stabilized with these surfactants. However, surfactants and surfactant-stabilized oil droplets with a charge opposite to that of the polyelectrolyte brushes adsorb strongly to these coatings because of electrostatic attraction.[42, 43] As a result, in the presence of oppositely charged surfactants, polyelectrolyte brushes become hydrophobic and collapse in polar solvents.

Polyzwitterionic brushes contain both positive and negative charges, and as with polyanionic or polycationic brushes, the strong affinity of these charged groups for water leads to a superhydrophilic film.[9, 44-48] Nevertheless, the strong inter- and intra-molecular associations between opposite charges in polyzwitterionic brushes lead to unusual trends in swelling. For example, in contrast to polyanionic or polycationic brushes, poly(sulfobetaine methacrylate) (PSBMA) brushes show enhanced swelling in aqueous solutions with increasing ionic strength.[29, 49-51] Thus, the presence of both cationic and anionic groups in the polyzwitterions may lead to a different response to ionic surfactants than in simple polyelectrolyte brushes. Although some studies examined surfactant interactions with zwitterionic groups,[52-58] very few of them focused on surfactant-polyzwitterionic brush interactions,[53, 56] especially for brushes with varying thicknesses. Zhou and co-workers recently showed no effect of surfactants on the lubrication behavior of polyzwitterionic brushes, suggesting no surfactant uptake.[58] However, here we show that surfactant sorption is a function of surfactant charge and concentration, as well as brush thickness.

This research examines the swelling of zwitterionic PSBMA brushes in the presence of both anionic and cationic surfactants. We chose PSBMA because among the common zwitterionic polymers poly(sulfobetaine methacrylate), poly(carboxybetaine

methacrylate) and poly(phosphobetaine methacrylate), the swelling behavior of PSBMA in both water and salt solutions is better understood,[29, 50] which may prove helpful in explaining PSBMA swelling in the presence of ionic surfactants. We employ surface-initiated atom transfer radical polymerization (SI-ATRP) to grow poly[2-(methacryloyloxy)ethyl dimethyl-(3-sulfopropyl)ammonium hydroxide] (PMEDSAH) brushes on both Au-coated Si wafers and porous nylon membranes (Scheme 3.1). Films on Au-coated wafers facilitate characterization of brush thickness, swelling, and surfactant adsorption, whereas membranes enable examination of the effect of swelling on filtration.

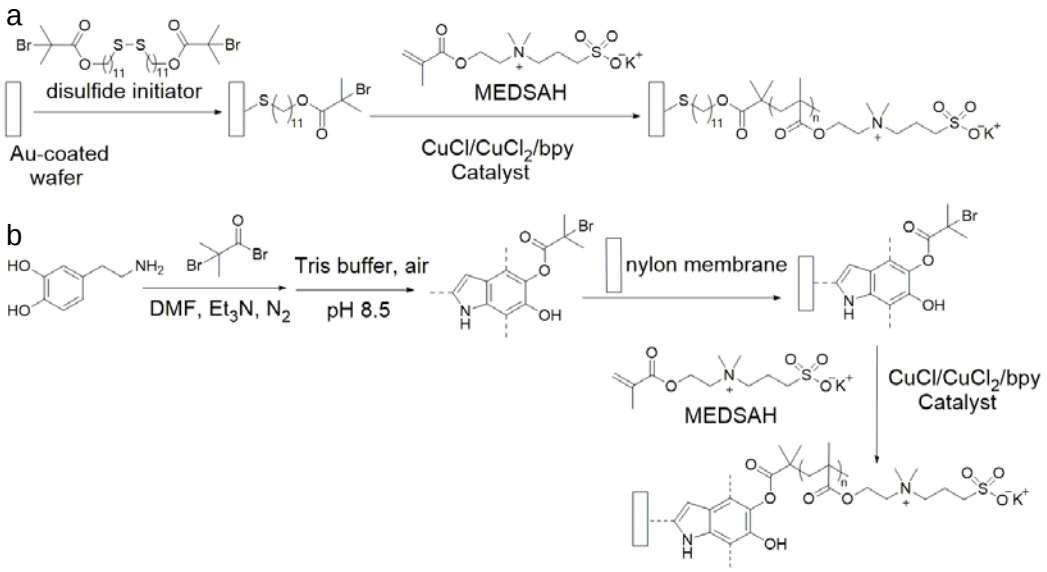

Scheme 3.1. Surface-initiated atom transfer radical polymerization of MEDSAH on (a) Au-coated wafers and (b) nylon membranes.

3.2. Experimental

3.2.1. Materials

Hydrophilic nylon membranes with nominal 0.45 μm diameter pores were obtained from Sterlitech (25 mm diameter, NY4525100). Si (111) wafers were purchased from University Wafer (Boston, MA) and coated with Au at LGA Thin Films (Santa Clara, CA) by

sputtering 200 nm of gold on 20 nm of Cr on Si wafers. [2-(Methacryloyloxy) ethyl] dimethyl-(3-sulfopropyl) ammonium hydroxide (97%, MEDSAH), dopamine hydrochloride (98%), 11-mercapto-1-undecanol (97%), ammonium chloride (≥99.5%), α-bromoisobutyryl bromide (98%, BIBB), 2,2'-bipyridine (≥99%, bpy) and sodium dodecyl sulfate (98.5%, SDS) were obtained from Sigma-Aldrich. Tris(hydroxymethyl)aminomethane hydrochloride (≥99%, Tris hydrochloride) was purchased from Invitrogen, and dodecyltrimethylammonium bromide (99%, DTAB) was acquired from Acros Organics. Bromine (100%) and triethylamine (100%) were purchased from J.T. Baker, whereas copper (I) chloride (≥99.995%), copper (II) chloride dihydrate (≥99.0%) and dimethylformamide (≥99.8%, DMF) were acquired from Jade Scientific. Acetone (99.7%) and ethyl acetate were purchased from Fisher Scientific and anhydrous dichloromethane, hexane (analytical reagent grade, AR) and chloroform (AR) were obtained from Macron Fine Chemicals. Dichloromethane was used as received, and chloroform, toluene and triethylamine were dried with molecular sieves (3 Å, Sigma-Aldrich) before use. Aqueous solutions were prepared using deionized water (Milli-Q, 18.2 MΩ·cm). The disulfide initiator, $(BrC(CH_3)_2COO(CH_2)_{11}S)_2$ was synthesized according to literature procedures.[59]

3.2.2. Preparation of PMEDSAH Brushes on Au-Coated Wafers and Nylon Membranes

3.2.2.1.Initiator Immobilization

Immobilization of the disulfide initiator on Au-coated wafers included cleaning the substrate with ethanol, drying with N_2, cleaning with UV/ozone for 15 min, immersion in a 1 mM ethanolic solution of $(BrC(CH_3)_2COO(CH_2)_{11}S)_2$ for 24 h, rinsing with ethanol and drying under a stream of N_2. The protocol for immobilizing the initiator on nylon

membranes combined two literature procedures.[60, 61] Nylon membranes were extracted with acetone for 12 h and then dried with N_2. Dopamine hydrochloride (2.1 mmol) was dissolved in DMF (20 mL), and this mixture was degassed via three freeze-pump-thaw cycles before transfer into a glove bag and mixing with triethylamine (1.1 mmol). BIBB (1.1 mmol) was then added dropwise to the mixture with gentle stirring, followed by stirring for 3 h. The solution was subsequently well mixed with 100 mL of Tris hydrochloride solution (2.8 M), and the pH was adjusted to 8.5 using NaOH. Clean nylon membranes were immersed in this dopamine solution for 48 h, removed from the glove bag and the solution, and rinsed with ~100 mL of water and dried with N_2, forming polydopamine initiators (PDA-BIBB) on the surface.

3.2.2.2.Polymerization of MEDSAH

PMEDSAH brushes on Au-coated wafers were prepared using the parameters of a procedure for the synthesis of polyanionic brushes.[42] MEDSAH (35 mmol) was dissolved in a DMF/water mixture (1/1 v/v, 30 mL) in a round-bottom flask. The mixture was degassed via four freeze-pump-thaw cycles. The catalyst was prepared by dissolving CuCl (0.016 mmol), $CuCl_2$ (0.016 mmol) and bpy (0.08 mmol) in a DMF/water mixture (1/1 v/v, 40 mL) and degassing via four freeze-pump-thaw cycles. Then 5 mL of the Cu-bpy solution was mixed with the monomer solution in a N_2-filled glove bag. The polymerization solution was injected into vials, and wafers or membranes modified with initiators were submerged in these solutions. After various polymerization times, the wafers or membranes were removed from the glove bag, rinsed with ~100 mL of water and dried with N_2. All membrane samples in this work were prepared with a polymerization time of 24 h. Polymerization times on Au-coated wafers ranged from 0.5 to 8 h.

3.2.3. Characterization of Modified Au-Coated Wafers and Nylon Membranes

3.2.3.1.Fourier Transform Infrared Spectroscopy (FTIR)

Au-coated wafers modified with disulfide initiator and PMEDSAH brushes were characterized by reflectance FTIR spectroscopy (Nicolet 6700 FT-IR spectrometer, Thermo Scientific, with a Pike grazing angle (80°) attachment and p-polarization). A UV/ozone-cleaned Au-coated wafer served as a background. To examine surfactant adsorption to swollen brushes, brush-modified wafers were transferred directly from water to surfactant solutions without drying. After a 12-h immersion in the surfactant solution, the wafer was rinsed with ~100 mL of water from a wash bottle for ~2 min prior to drying with N_2 and obtaining a reflectance FTIR spectrum. To determine whether surfactant adsorbs to brushes in solution and can be removed by water rinsing, wafers were not rinsed by water after removal from the surfactant solutions. Instead, the solution on wafers was wiped off with a KimWipe to remove surfactants in solutions, followed by IR characterization. A bare Au-coated wafer treated in the same way served as a control. IR data are reported as a pseudo absorbance, which is the logarithm of the ratio of the reflected intensities from the bare wafer and from the film-coated wafer.

3.2.3.2.Ellipsometry

Both dry and swollen thicknesses and refractive indices of the polymer brushes on Au-coated wafers were determined using a rotating analyzer ellipsometer (model M-44, J.A. Woollam) at an incident angle of 75°. For determining the swollen thickness, brush-coated wafers were immersed in solution in a homemade trapezoidal cell with glass windows.[62, 63] To determine brush thickness and optical constants, the refractive index of the brush was

fit using an effective medium approximation (EMA) model, as shown in Figure 3.1. For samples in air, the EMA model contains a Cauchy material for PMEDSAH brushes along with air-filled voids. The Cauchy material employed Eq. 3.1 to fit its refractive indices,

$$n(\lambda) = A + \frac{B}{\lambda^2} \qquad \text{Eq. 3.1}$$

where n is the refractive index, λ is the wavelength of incident light in μm, and A and B are constants. To characterize brushes, initial estimate values of A and B were set as 1.5 and 0.01, respectively. Initial guesses for the fractions of both polymers and air were 50%. When samples were immersed in solutions, an ambient layer representing the solution was set as the top material above the EMA layer (Figure 3.1b). The refractive index of the ambient layer was determined as a Cauchy material in an experiment with reflection from a Si wafer covered by a 25-nm thick SiO_2 layer (Figure 3.1c). Since all solutions are aqueous, the initial estimates of the parameters A and B in the Cauchy equation for the ambient layer were set as 1.33 and 0.01, respectively. In the EMA model, initial guesses for the fractions of polymers and solutions were 50%. The actual values of all parameters were determined by fitting calculated data to experimental data. Ellipsometric measurements were performed on three spots on each wafer.

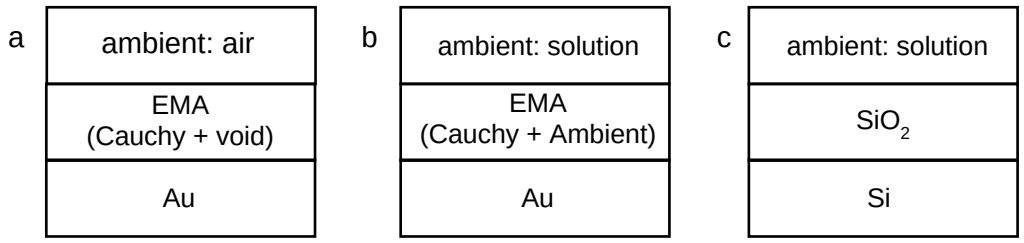

Figure 3.1. Optical models for PMEDSAH brushes in (a) air and (b) solutions. Image (c) shows the model we used to determine optical constants of surfactant solutions.

3.2.3.3.X-Ray Photoelectron Spectroscopy (XPS)

XPS was carried out with a Perkin-Elmer PHI 5600 ESCA system with an Al Kα X-ray source (1486.6 eV) running at a power of 350 W at a take-off angle of 45°.

3.2.3.4.Scanning Electron Microscopy (SEM)

The surface morphology of membranes was observed with field-emission SEM (JSM-7500F, JEOL). The membranes were mounted on the sample studs with double-sided conductive adhesive tape. A thin layer of osmium (8 nm) was coated on the sample surface prior to the SEM imaging, which was performed at an accelerating voltage of 5 kV. To characterize their cross-sections, membranes were frozen in liquid nitrogen and after removal from the nitrogen, they were quickly cracked with a razor blade to create a sharp edge with minimal membrane deformation.

3.2.3.5.Contact Angle Measurements

Contact angles of water or hexadecane on surfaces were determined using a phone camera and contact angle calculation software (VCA2000, AST Products). Contact angles of water in air were determined by placing a drop of water on dry samples. To determine the surface hydrophilicity in water and surfactant solutions, the samples were first immersed in these solutions for 12 h. Then the samples were placed facing downward in a funnel capped with a rubber stopper and filled with water or surfactant solutions. A drop of hexadecane was released from beneath the samples using a syringe (Figure 3.2). We employed this method because hexadecane droplets tend to float away from needles and surfaces in these solutions.

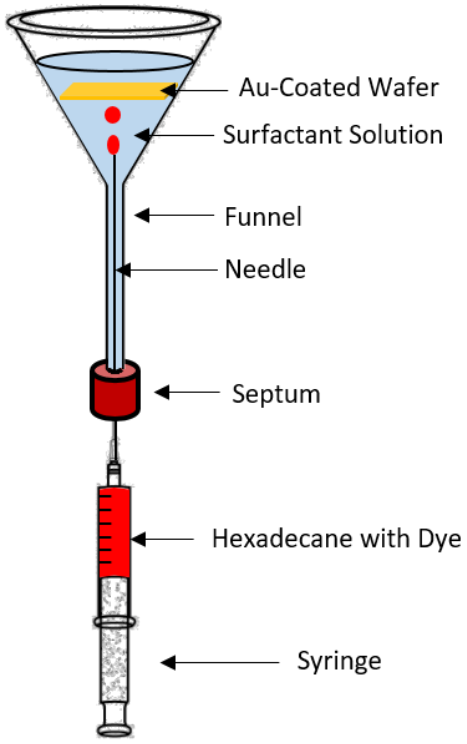

Figure 3.2. Apparatus for the measurement of hexadecane contact angles on wafers in surfactant solutions.

3.2.4. Determination of Membrane Permeability and Brush Swelling on Membranes

The specific fluxes through membranes (L/(m^2·h·bar)), LMH/bar) were determined in dead-end filtration using a 15-mL Amicon cell (Model 8010, Millipore) with a suspended stir bar rotating at 45 rpm. The cell was connected to a stainless steel feed tank (standard 2 gallon pressure vessel, Pope Scientific) (Figure 3.3), and the applied pressure was constant at 0.7 bar. Pure water permeability was determined using deionized water as the feed, whereas the permeability in surfactant and salt solutions was measured by filling the feed tank with those solutions. Changes in the swelling of PMEDSAH brushes on membranes were estimated via the Hagen-Poiseuille equation (Eq. 3.2),[64]

$$\frac{J}{\Delta P} = \frac{n\pi r^4}{8\eta\tau\Delta x} \qquad \text{Eq. 3.2}$$

where J is the permeate flux (L/(m^2·h)), r is the radius of membrane pores, n is the number of pores per unit area, ΔP is the transmembrane pressure (0.7 bar), η is the dynamic viscosity, which is almost the same for water and the solutions examined in this work,[65-67] Δx is the membrane thickness (~100 μm) and τ is the pore tortuosity. Thus, by comparing water permeabilities of modified membranes and bare nylon membranes and assuming constant τ and n, the pore size of modified membranes can be calculated using Eq. 3.3 and a value for the radii of pores in the unmodified membrane.

$$\frac{J_1}{J_2} = \left(\frac{r_1}{r_2}\right)^4 \qquad \text{Eq. 3.3}$$

The swollen thickness of brushes is equal to the difference between the pore radius of bare membranes and brush-modified membranes. (This is a crude approximation given the spongy nature of these membranes.) All of the filtration experiments were repeated with 2 or 3 membranes.

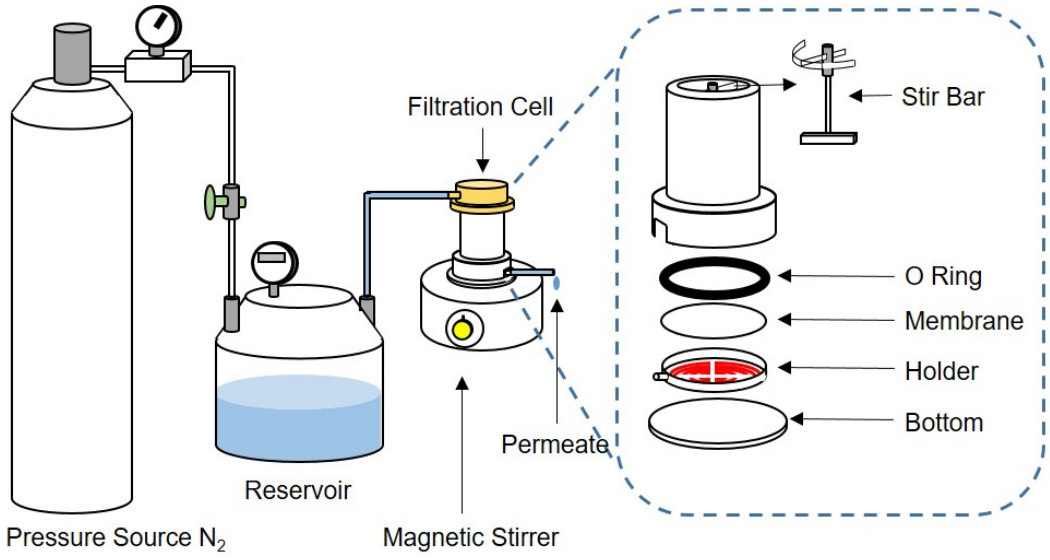

Figure 3.3. Diagram of the apparatus for dead-end filtration.

3.3. Results and Discussion

3.3.1. Brush Synthesis on Au-Coated Wafers and Nylon Membranes

Scheme 3.1 shows the SI-ATRP strategy we employ to grow polyzwitterionic brushes on Au-coated wafers. The reflective Au surface enables brush characterization with reflectance IR spectroscopy and ellipsometry. IR spectra confirm both the disulfide initiator adsorption (Figure 3.4a) and PMEDSAH brush growth (Figure 3.4b). In particular, the presence of sulfonate stretches at 1218 and 1041 cm^{-1}, a C=O stretch at 1731 cm^{-1} and a C-N stretch at 1486 cm^{-1} are consistent with the presence of brushes on the surface. Figure 3.5 shows that both the peak height for the sulfonate stretch at 1218 cm^{-1} and the dry thickness of PMEDSAH brushes increase with polymerization time, indicating continuous brush growth. With the exception of the longest polymerization time, the sulfonate stretching peak height and thickness increase proportionally, giving confidence in the characterization techniques. The relatively large standard deviations in Figure 3.5 and disagreement in IR and ellipsometry data at the longest polymerization time may suggest a rough surface and some uncontrolled polymerization. This could stem in part from the insolubility of PMEDSAH in common organic solvents (such as DMF) despite full dissolution of the monomer MEDSAH. Thus, polymerization may proceed in a heterogeneous system that gives rise to a broad molecular weight distribution and large thickness variations.[68]

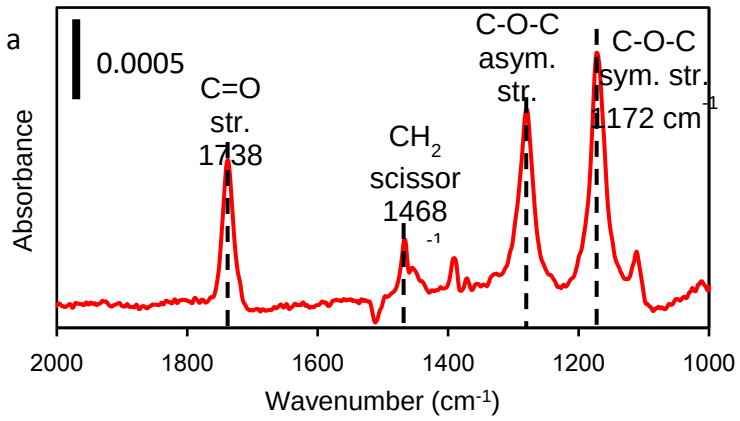

Figure 3.4 (cont'd)

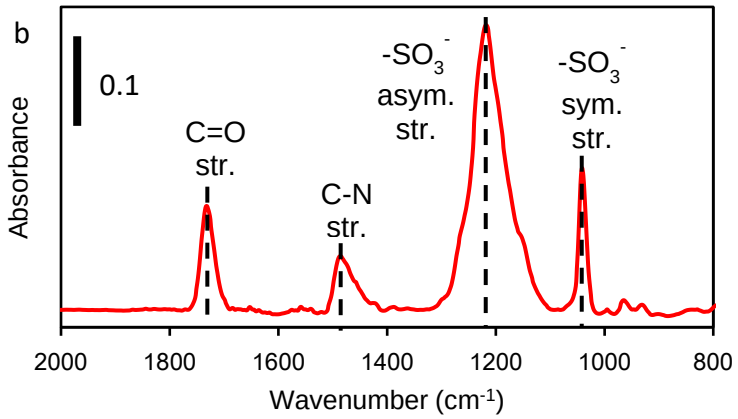

Figure 3.4. Reflectance FTIR spectrum of (a) the disulfide initiator ($(BrC(CH_3)_2COO(CH_2)_{11}S)_2$) and (b) PMEDSAH brushes on a Au-coated Si wafer. The brush dry thickness was 412 nm.

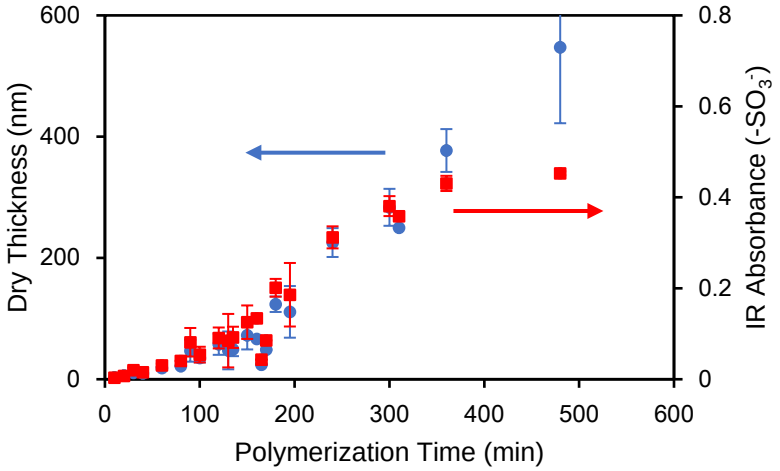

Figure 3.5. Dry brush thickness (blue circles) and IR absorbances of sulfonate groups at 1218 cm^{-1} (red squares) as a function of polymerization time for PMEDSAH brushes grown on Au wafers. Error bars represent the standard deviation of measurements on three different films.

We employed XPS to characterize the growth of the PDA-BIBB initiator and zwitterionic PMEDSAH brushes on non-reflective nylon membranes. Figure 3.6 shows XPS wide scan spectra of the surfaces of a bare nylon membrane, a PDA-BIBB-coated nylon membrane, and a PMEDSAH-coated nylon membrane. After the polymerization of dopamine-BIBB on the membrane, signals representing Br 3d (76 eV), Br 3p (188 eV) and

Br 3s (261.1 eV) appear, which is consistent with the presence of initiating groups on the PDA-BIBB coated surface (Figure 3.6b). The strong S 2p (172 eV) and S 2s (236 eV) signals only detected on PMEDSAH-coated membranes (Figure 3.6c) confirm the growth of PMEDSAH brushes. Signals from Br remain after polymerization, suggesting that some initiators are unreacted or some of the chain ends remain active after 24 h of polymerization.

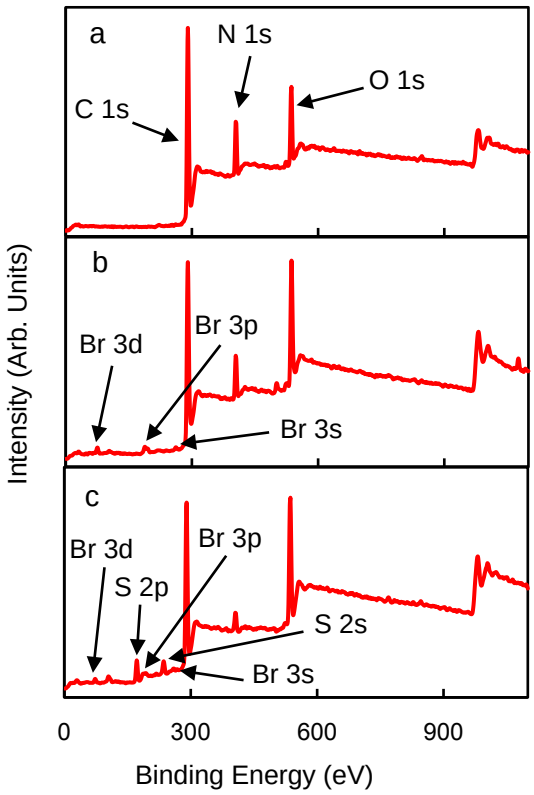

Figure 3.6. XPS wide scan spectra of (a) bare nylon membranes and membranes modified with (b) PDA-BIBB initiator and (c) PMEDSAH brushes.

SEM images show the differences in morphology for bare, PDA-BIBB- and PMEDSAH-modified nylon membranes. Top-view SEM images (Figure 3.7a, b, c) suggest a decreasing porosity and pore size after coating with PDA-BIBB and PMEDSAH. Cross-sectional images (Figure 3.7d, e, f) show that the membrane remains porous throughout the

modification steps, but due to the spongy structure, we cannot tell from these images (Figure 3.7d, e, f) whether the pore size decreases in the membrane interior after coating.

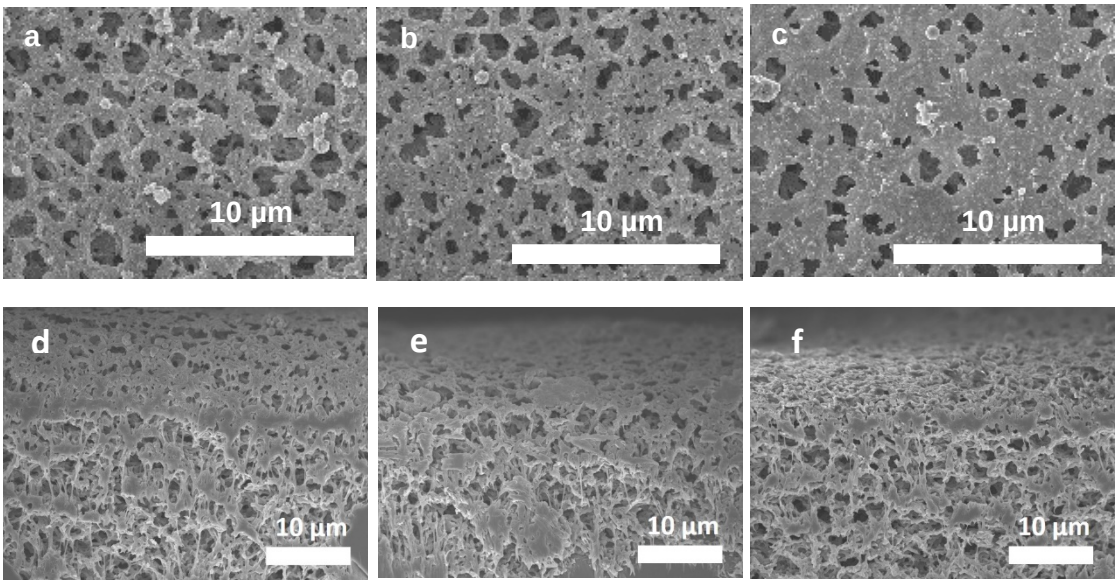

Figure 3.7. SEM images of (a,d) bare nylon membranes and membranes modified with (b,e) PDA-BIBB initiator and (c, f) PMEDSAH brushes. Figures a, b, c are the top-view images while Figures d, e, f are the cross-sectional images. Modification employed 48 h of PDA-BIBB deposition and 24 h of polymerization.

3.3.2. Brush Swelling and Wettability

Figure 3.8 shows the swollen thicknesses of PMEDSAH brushes on Au-coated wafers in deionized water along with their percent swelling (compared to a dry film in air) as a function of the dry brush thickness. In the plot, the swollen thickness appears to be a linear function of the dry thickness, with ~150% swelling. However, the thinnest brushes (dry thickness <20 nm) tend to swell more (~250%). This agrees with another measure of the brush density, the ratio of the sulfonate group IR absorbance (1218 cm^{-1}) to the swollen brush thickness.[69, 70] This ratio has its lowest values in films with dry thicknesses <20 nm (Figure 3.9). Previous research shows that the formation of intra-group, inter-chain, and intra-chain associations in polyzwitterionic brushes yields crosslinked networks.[29, 68] Very

thin brushes with short polymer chains and low chain densities likely possess fewer inter- and intra-chain associations, leading to higher swelling in water. As brushes grow thicker, longer chains give more chances for crosslinking and formation of denser networks. After the dry brush thickness surpasses 20 nm, the brush density in water is relatively constant. However, we should note that determination of swollen thickness is more prone to error for thinner films.

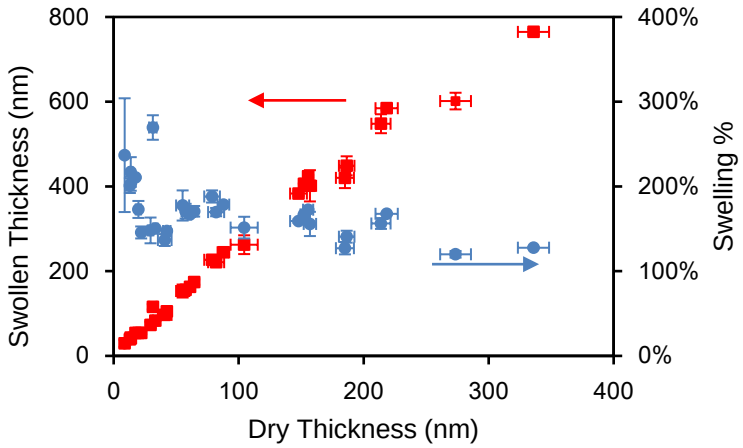

Figure 3.8. Water-swollen thicknesses (red squares) and percent swelling (blue circles) of PMEDSAH brushes as a function of their dry thickness. Error bars represent standard deviations of measurements on three films. Error bars are not always visible due to their small values. Swollen thicknesses were determined in water after a 12-h immersion.

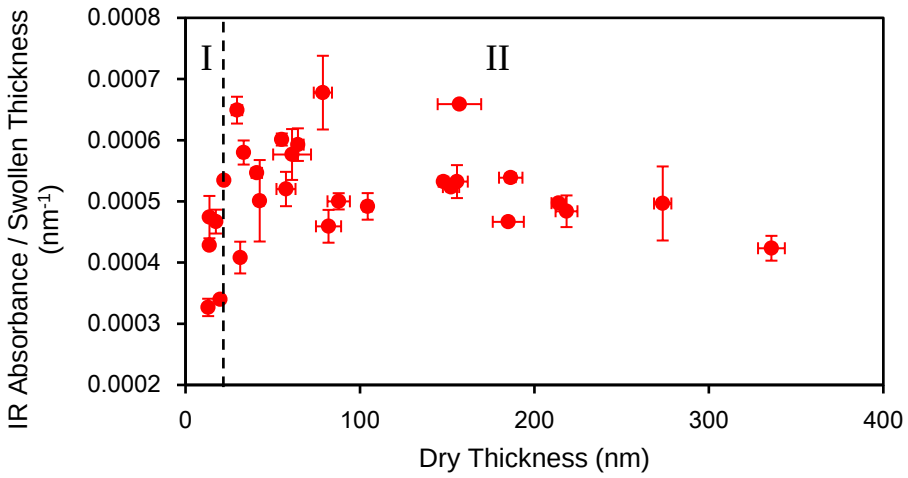

Figure 3.9. (cont'd) Reflectance IR absorbance at 1218 cm^{-1} (dry films) divided by the swollen PMEDSAH brush thickness in water as a function of the dry film thickness. The ratio of IR absorbance to swollen film thickness provides a measure of density. The plot is divided into two regions according to dry brush thickness: I (< 20 nm), II (> 20 nm). Error bars represent standard deviations of measurements on three films.

We characterized surface wettability by measuring hexadecane contact angles in both air and water. As Figure 3.10 shows, on PMEDSAH-coated wafers and membranes, the contact angle of hexadecane increases from ~10° to 150-170° after changing the ambient region from air to water. In most cases, hexadecane will bead up and eventually detach from the surface on both wafers and membranes. In control experiments, bare Au-coated wafers show hexadecane contact angles smaller than 20° in both air and water. These results show that PMEDSAH brushes on both gold and modified nylon become superoleophobic underwater, consistent with previous research.[30, 61]

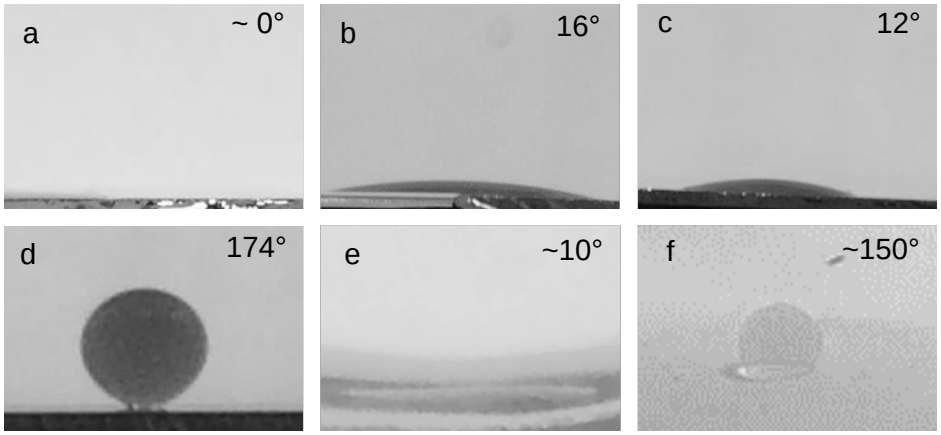

Figure 3.10. Contact angles of hexadecane on bare Au-coated wafers (a, b), PMEDSAH-modified wafers (c, d) and PMEDSAH-modified membranes (e, f). The images were obtained in air (a, c, e) and water (b, d, f). Images in water are rotated 180°.

3.3.3. Interactions between Ionic Surfactants and PMEDSAH Brushes

PSBMA brushes are well known as anti-biofouling materials,[71-73] and they also show significant adsorption of inorganic salts, which increases brush swelling.[29, 50] Ionic

surfactants contain both charged groups and alkyl backbones and possess properties of both ions and hydrophobic molecules. Thus, surfactants may affect swelling very differently than simple salts, so this section examines interactions between PSBMA brushes and ionic surfactants, as well as the resulting brush swelling.

3.3.3.1.Anionic Surfactant (SDS)

3.3.3.1.1. Effect of PMEDSAH Brush Thickness on Swelling

To study SDS adsorption as a function of PMEDSAH brush thickness, we prepared an extensive series of films with dry thicknesses varying from 2 to 700 nm. As Figure 3.11

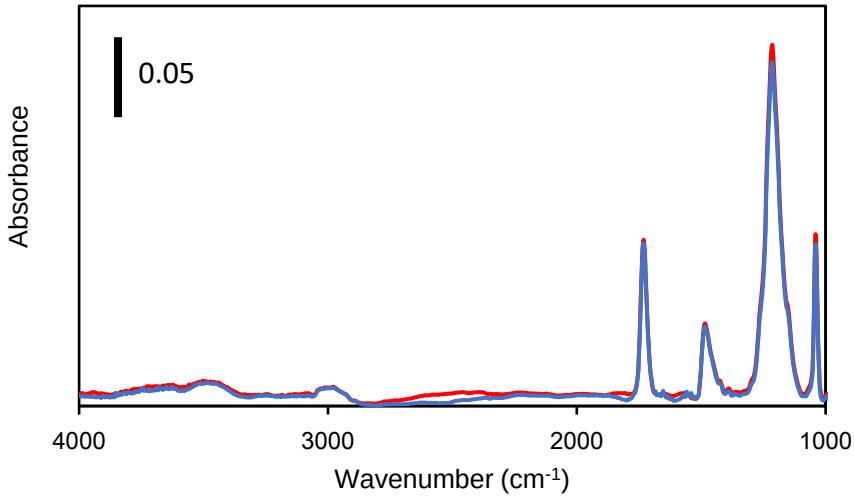

Figure 3.11. Reflectance IR spectra of a PMEDSAH brush before (red) and after (blue) immersion in a 6 mM SDS solution and rinsing with water. The brush dry thickness was 340 nm.

shows, the IR spectra of PMEDSAH-coated wafers before and after immersion in SDS solutions are essentially identical. The only difference is that the peak heights after immersion in SDS solutions decrease by about 5%, which may indicate a small amount of polymer degradation.[74, 75] In addition, the swollen thickness in pure water is the same before and after immersion in SDS solutions (see Figure 3.13 below), indicating that any SDS adsorption on PMEDSAH brushes and its effect on brush swelling disappear after

water rinsing. To characterize surfactant adsorption for films while immersed in surfactant solutions, we dried brush-coated wafers with a KimWipe to remove surfactant solutions prior to IR characterization but did not rinse with water. The spectra of films treated in this way show a clear increase in the intensities of the CH_2 symmetric and asymmetric stretches at 2854 and 2927 cm^{-1} (Figure 3.12), indicating SDS adsorption. To demonstrate that this adsorption stems from the SDS in PMEDSAH brush layers, rather than the SDS in residual solution left on the surface, we performed the same experiment with a bare Au-coated wafer. As Figure 3.12 shows, this control experiment showed no absorbance from CH_2 stretches, suggesting that the new CH_2 peaks in SDS-exposed PMEDSAH films stem from SDS adsorbed to PMEDSAH brushes. This result is consistent with previous research where quartz crystal microbalance with dissipation monitoring (QCM-D) showed SDS adsorption in PMEDSAH brushes.[58]

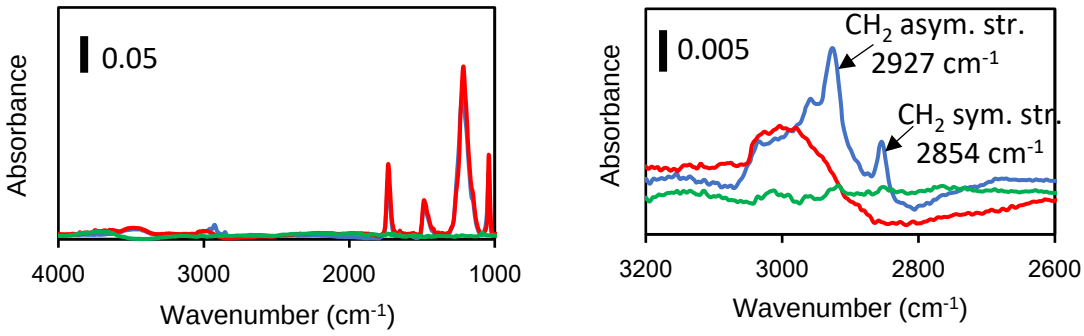

Figure 3.12. Reflectance IR spectra of a PMEDSAH brush after immersion in 6 mM SDS followed by a water rinse (red), and after immersion in the same SDS solution without a water rinse (blue). In the latter case, the film was dried with a Kimwipe to remove residual solution. A bare Au-coated surface after immersion in 6 mM SDS without water rinsing (dried with a Kimwipe) served as a control (green). The figure on the right expands the region of the spectrum where CH_2 stretches appear. The brush dry thickness was 340 nm.

Figure 3.13 shows the swelling of PMEDSAH brushes in both water and 6 mM SDS solutions. We divide the data into three regions according to their dry thickness: I (<20 nm), II (20-150 nm) and III (>150 nm). For PMEDSAH brushes in region I, a significant thickness increase occurs upon transfer of brushes from water into 6 mM SDS. As discussed above, crosslinked networks are likely present in the PMEDSAH brush, and SDS may diffuse into the brush and screen charges on polymer chains, interrupting the crosslinks and allowing polymer chains to stretch. Weaker polymer networks in thinner films probably lead to a lower brush density in SDS solution than in water (Figure 3.14).

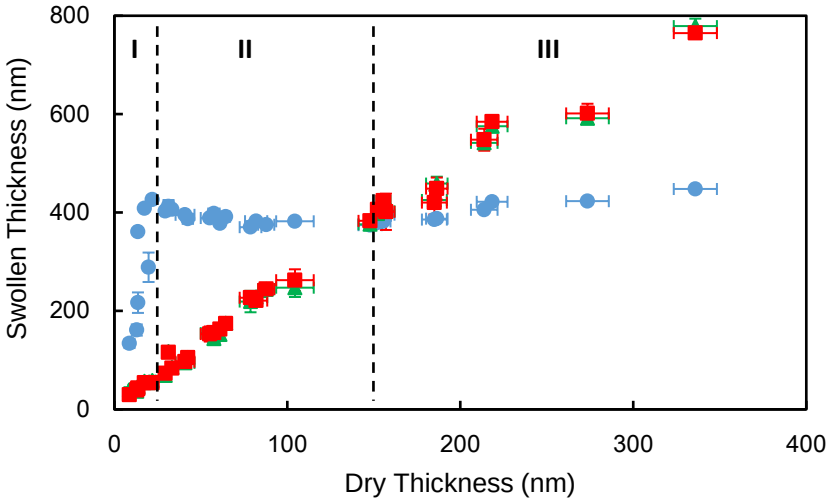

Figure 3.13. Ellipsometric thicknesses of swollen PMEDSAH brushes in 6 mM SDS (blue circles), as well as in deionized water before (red squares) and after (green triangles) immersion in SDS solution and rinsing. Thicknesses are plotted as a function of dry brush thickness in ambient air, and dashed vertical lines depict dry thicknesses of 20 and 150 nm. Error bars represent standard deviations of measurements on three films. The error bars are often not obvious due to their small values, and red and green symbols typically overlap.

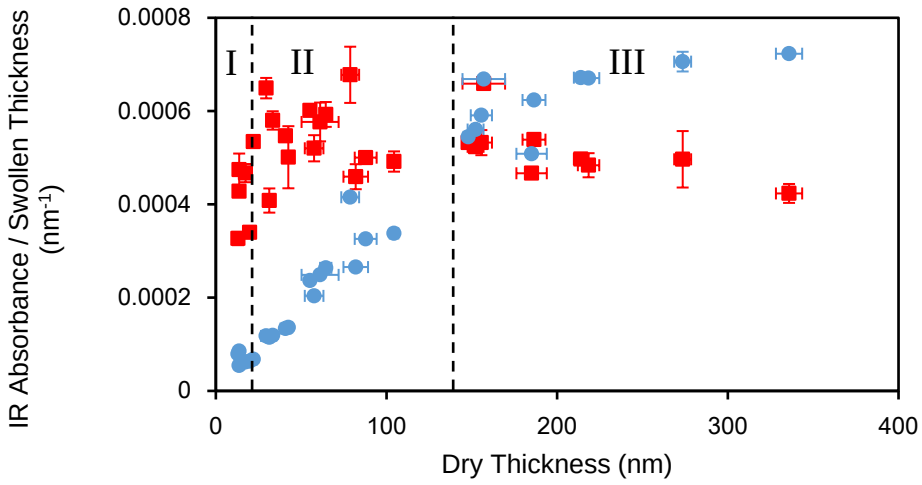

Figure 3.14. PMEDSAH brush density, as indicated by IR absorbance (1218 cm^{-1} in dry films) divided by the brush thickness in water (red squares) or by the brush thickness in 6 mM SDS (blue circles) as a function of dry brush thickness. The plot is divided into three regions according to dry brush thickness: I (< 20 nm), II (20-150 nm), III (> 150 nm). Error bars represent standard deviations of measurements on three films. Some of the error bars are not visible due to their small values.

In region II, where the dry thickness of PMEDSAH brushes is between 20 and 150 nm, the swollen brush thickness in SDS is essentially constant at around 400 nm (Figure 3.13), so the brush density in 6 mM SDS increases with brush dry thickness (Figure 3.14) and the percent thickness difference between PMEDSAH films in 6 mM SDS and in water declines (Figure 3.15). Remarkably, even in region III in Figure 3.13, the brush swollen thickness in 6 mM SDS still remains constant, so the film density becomes greater than in deionized water (Figure 3.14) and the percent thickness difference between brushes in deionized water and in 6 mM SDS becomes negative (Figure 3.15). Chen and co-workers reported that binding of salts like NaCl disturbs the ordering of strongly hydrogen-bonded water molecules in the zwitterionic brush layer to disrupt superhydrophilicity.[76] We think SDS has the same effect as high concentrations of salts. In addition, the hydrophobic tail

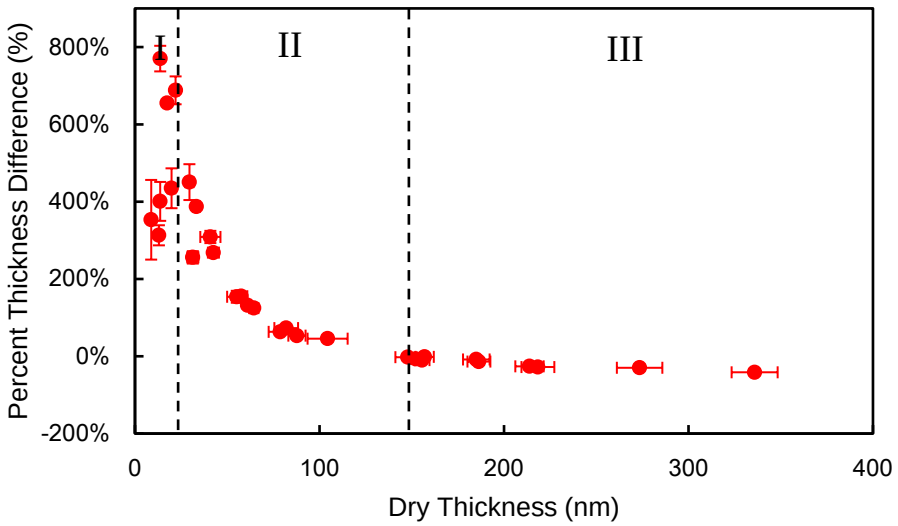

Figure 3.15. Percent thickness difference between PMEDSAH films in 6 mM SDS and in water as a function of the dry brush thickness. The plot is divided into three regions according to dry brush thickness: I (< 20 nm), II (20-150 nm) and III (> 150 nm). Error bars represent standard deviations of measurements on three films. Some of the error bars are not visible due to their small values.

of SDS will reduce the hydrophilicity of PMEDSAH brushes. Unlike thin brushes with short polymer chains that tend to swell upon breaking of crosslinks, thick brushes consist of longer and more extended chains. Therefore, as brushes grow thicker, the disordered water binding and increased hydrophobicity after SDS adsorption will lead to less brush swelling despite disruption of crosslinking. However, even for thick films hexadecane cannot attach to these brush-coated surfaces in 6 mM SDS, whereas a control experiment shows that hexadecane quickly sticks to a bare Au-coated wafer (Figure 3.16). As the contact angle only reflects the wettability of the exposedsurface,[77-79] this result indicates that the outermost brush layer is still superhydrophilic, although the brush swells less than in deionized water.

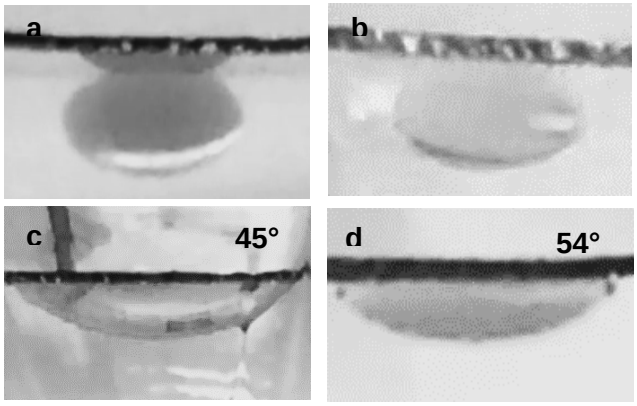

Figure 3.16. Contact angles of hexadecane on (a) PMEDSAH brush-modified Au-wafer in 1 mM SDS, (b) PMEDSAH brush-modified Au-wafer in 6 mM SDS, (c) bare Au-wafer in 1 mM SDS and (d) bare Au-wafer in 6 mM SDS. PMEDSAH brushes in (a) and (b) have a dry thickness of 260 nm.

3.3.3.1.2. Swelling as a Function of SDS Concentration

Figure 3.17 shows the percent thicknesses difference of PMEDSAH brushes in SDS solutions (compared to in water) as a function of SDS concentrations. To examine the effect of concentrations both above and below the SDS critical micelle concentration (8 mM),[80] we set the surfactant concentration range from 0.5 to 20 mM. As Figure 3.17 reveals, for thin brushes (dry thickness < 150 nm) increasing the SDS concentration from 0.5 to 6 mM leads to higher brush swelling, presumably due to more charge screening. With a brush dry thickness >150 nm, increasing the SDS concentration leads to a thickness decrease. In this case due to the more flexible and extended chains, the disordering of water molecules and the hydrophobicity of SDS may dominate thickness changes, and thus the increase in SDS concentration will lead to more SDS adsorption and a less swollen polymer network. Above 6 mM, further increasing the SDS concentration has minimal effect on the swelling of PMEDSAH brushes, probably because SDS adsorption in brush layers reaches its upper limit near the critical micelle concentration (8 mM). Figure 3.18 shows additional data on the swollen thicknesses and percent swelling differences (relative to in deionized water) of

PMEDSAH brushes in 0.5, 1, 2, 4, 12, 16, 20 mM SDS. These data follow the trends in Figure 3.17.

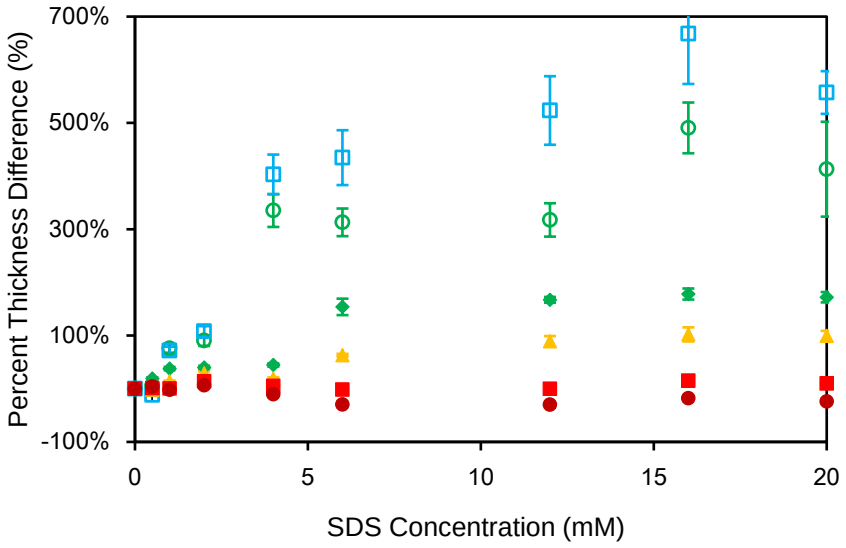

Figure 3.17. Percent thickness difference of PMEDSAH brushes in SDS solutions (compared to in water) as a function of SDS concentration and dry thickness. Symbols in different colors and shapes represent brushes with dry thickness of 33 nm (blue empty squares), 24 nm (green empty circles), 33 nm (blue empty squares), 67 nm (green solid diamonds), 136 nm (yellow solid triangles), 200 nm (red solid squares), and 267 nm (brown solid circles). Error bars represent standard deviations of measurements on three films. The Y error bars are not obvious due to their small values.

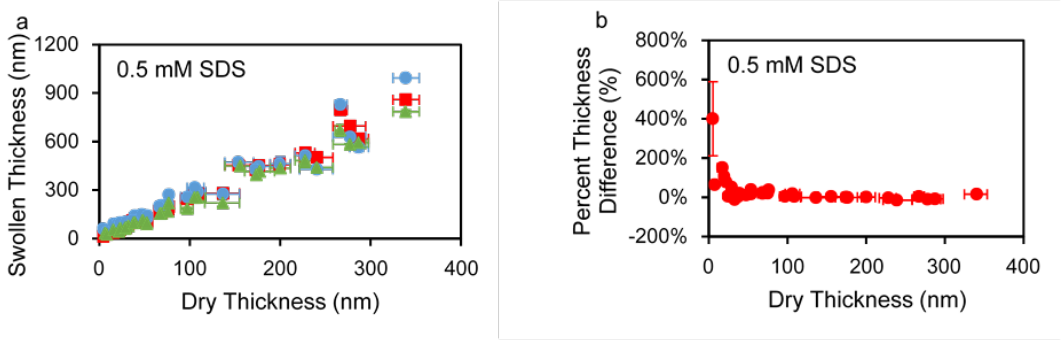

Figure 3.18 (cont'd)

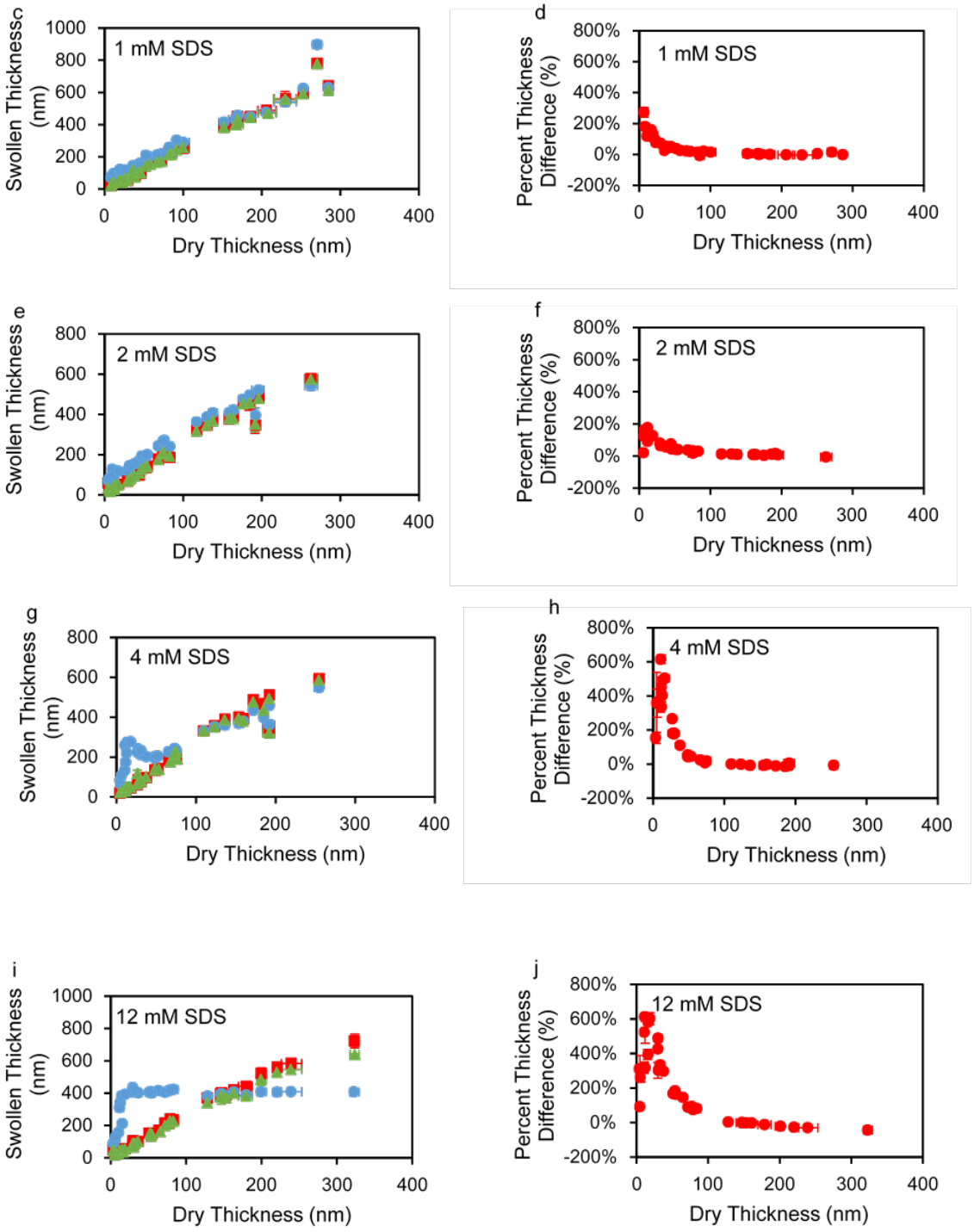

Figure 3.18 (cont'd)

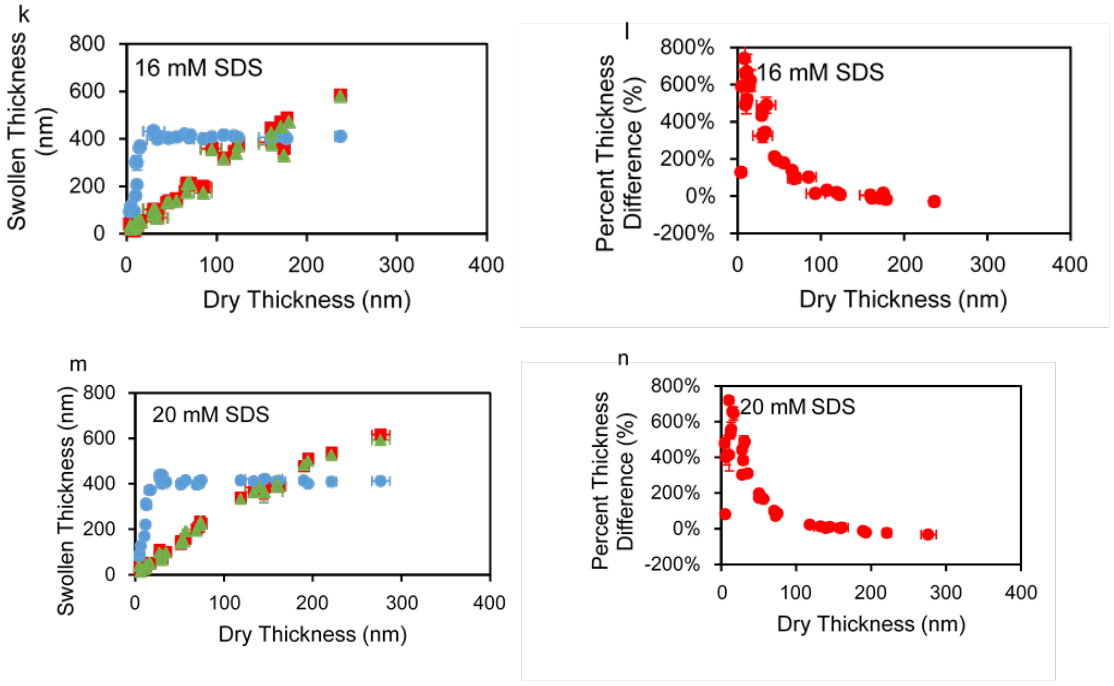

Figure 3.18. Ellipsometric thicknesses (a, c, e, g, i, k, m) and percent thickness differences relative to in deionized water (b, d, f, h, j, l, n) of swollen PMEDSAH brushes in 0.5, 1, 2, 4, 12, 16, 20 mM SDS as a function of dry brush thickness. In the figures on the left, thicknesses of swollen PMEDSAH brushes in SDS, as well as in deionized water before and after immersion in SDS solution and rinsing are plotted as blue circles, red squares and green triangles, respectively. Error bars represent standard deviations of measurements on three films. Some error bars are not visible due to their small values. All the data in Figure 3.18 was measured using the same batch of samples in the following order: 0.5, 1, 6, 12, 20, 4, 2, 16 mM SDS.

3.3.3.1.3. Swelling in Salt Solutions

To examine if the changes in brush swelling upon SDS addition are simple charge-screening effects, we also characterized the swelling behavior of PMEDSAH brushes in NaCl solutions. As Figures 3.19 and 3.20 show, low NaCl concentrations (5 mM) lead to small increases in brush swelling below 50% (compared to swelling in deionized water), whereas brushes in 500 mM NaCl show a swelling trend similar to that in 6 mM SDS (compare Figure 3.13 and Figure 3.21). This suggests that disordering of water molecules in thick PMEDSAH films decreases brush thickness in both SDS and 500 mM NaCl

solutions. Compared with NaCl, SDS starts to induce the unusual brush swelling trends from a much lower concentration, presumably because the hydrophobic tail of SDS favors partitioning into the film.

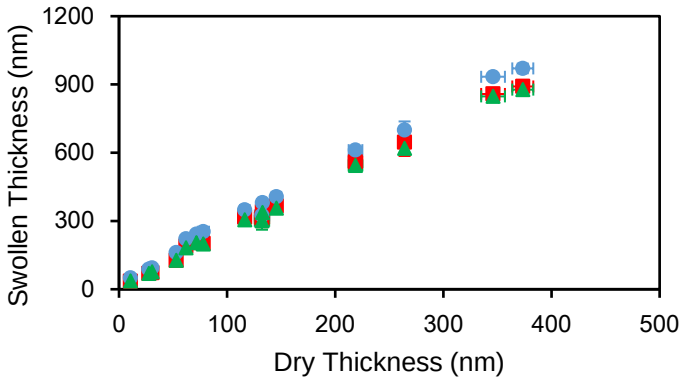

Figure 3.19. Swollen thicknesses of PMEDSAH brushes in 5 mM NaCl (blue circles), and the deionized water-swollen thicknesses before (red squares) and after (green triangles) immersion in NaCl (and rinsing) as a function of dry brush thickness. Error bars represent standard deviations of measurements on three films. Some error bars are not visible due to their small values.

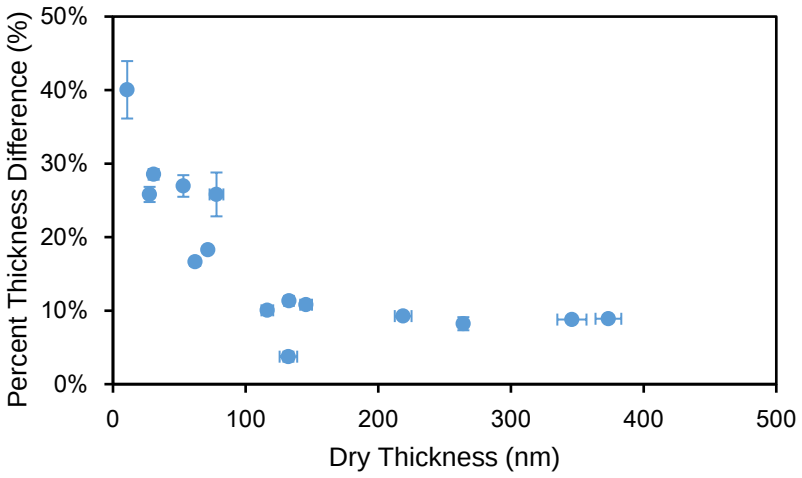

Figure 3.20. Percent thickness difference between PMEDSAH films in 5 mM NaCl and in water as a function of the dry brush thickness. Error bars represent standard deviations of measurements on three films.

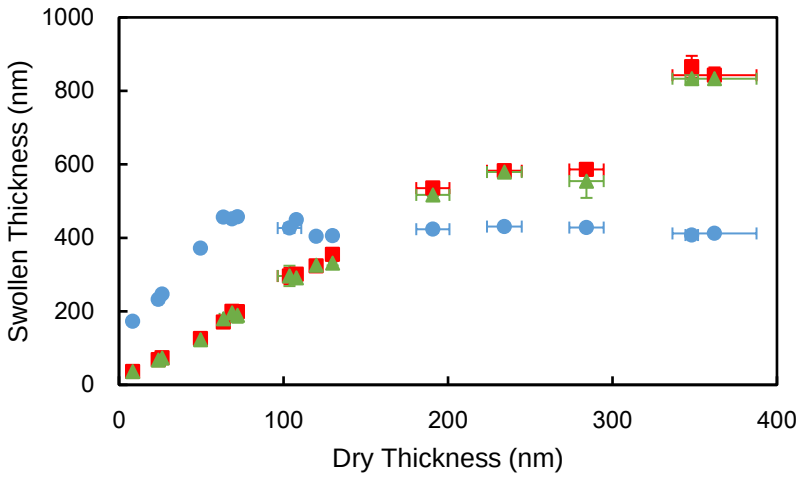

Figure 3.21. Swollen thicknesses of PMEDSAH brushes in 500 mM NaCl (blue circles), and the water-swollen thickness before (red squares) and after (green triangles) immersion in NaCl (and rinsing) as a function of dry brush thickness. Error bars represent standard deviations of measurements on three films. Some error bars are not visible due to their small values.

3.3.3.2.Cationic Surfactant (DTAB)

To examine the effect of surfactant charge on zwitterionic brushes, we selected DTAB as a cationic surfactant because it has the same hydrophobic tail as SDS. Similar to experiments with SDS, IR spectra show that DTAB adsorbs to PMEDSAH brushes immersed in surfactant solution (Figure 3.22), but rinsing readily removes the surfactant (Figure 3.23).

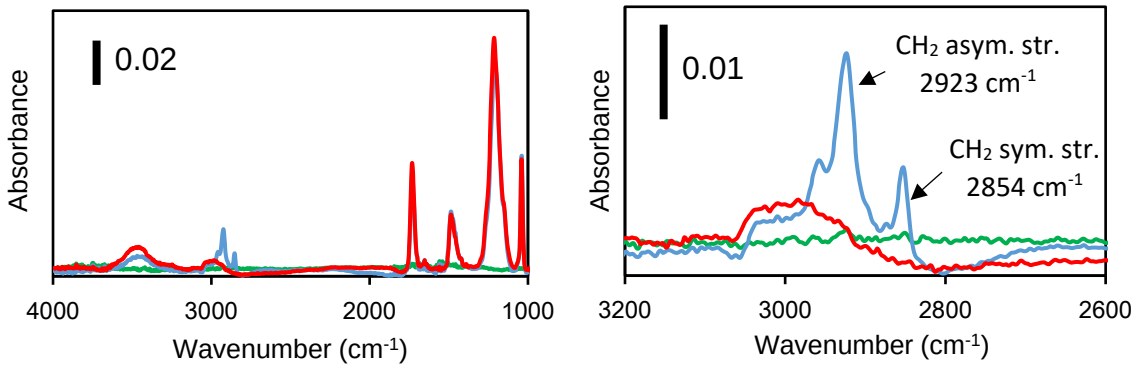

Figure 3.22. Reflectance IR spectra of a PMEDSAH brush after immersion in 10 mM DTAB and a water rinse (red), and after immersion in 10 mM DTAB without a water rinse (blue). In the latter case, the film was dried with a Kimwipe to remove residual solution. A bare Au-coated surface after immersion in 10 mM DTAB without water rinsing (dried with a Kimwipe) served as a control (green). The brush dry thickness was 340 nm.

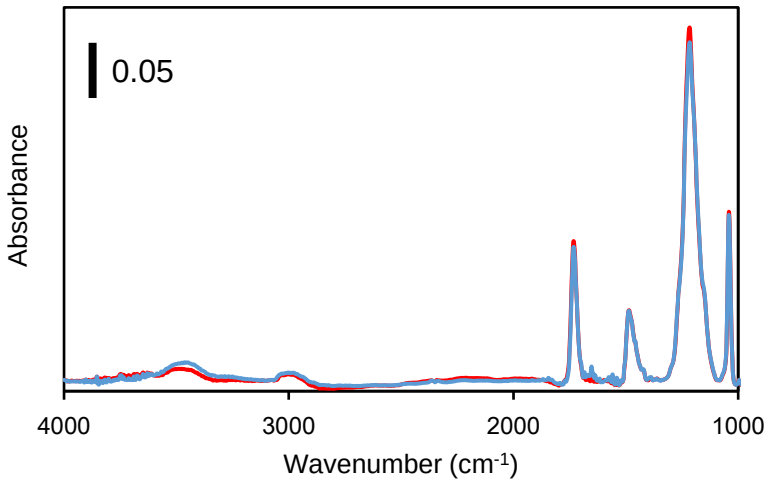

Figure 3.23. Reflectance IR spectra of a PMEDSAH brush before (red) and after (blue) immersion in 10 mM DTAB solution and rinsing. The brush dry thickness was 340 nm.

3.3.3.2.1. Effect of Brush Thickness

As Figure 3.24 shows, when dry PMEDSAH brushes are thinner than 200 nm, their swelling in 5 mM DTAB is slightly higher than that in water (from a 70% to 0% increase in swollen thickness as brushes grow thicker), presumably due to charge screening and breaking of crosslinks. However, for these films the percent increase in swelling (compared to in water) is around 10-fold lower than with 6 mM SDS. This low swelling in the solution of cationic surfactant may occur because the quaternary ammonium cation of DTAB has hydrophobic methyl groups that decrease partitioning into the superhydrophilic brush layer or make films more hydrophobic. The HLB (hydrophilic-lipophilic balance) values calculated by the Davies method for SDS and DTAB are 40 and 23.3, respectively.[81, 82] For PMEDSAH brushes with dry thicknesses around 300 nm, immersion in 5 mM DTAB results in collapsed brushes (compared to in deionized water) with a water-swollen thickness around 400 nm, which is the same swelling behavior as in concentrated SDS

solutions. This probably results from the disordering of water molecules and the hydrophobic tail of surfactants.

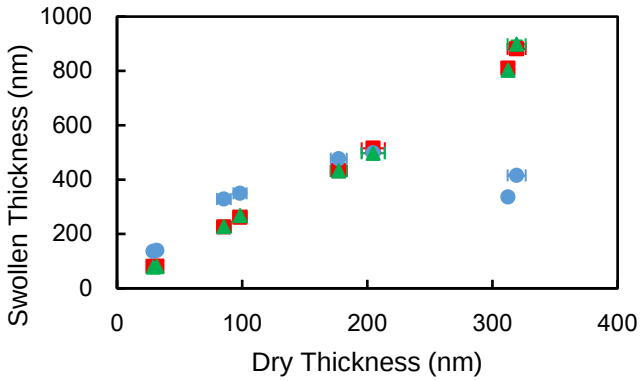

Figure 3.24. Swollen thickness of PMEDSAH brushes in 5 mM DTAB solution (blue circles), and the water-swollen thickness before (red squares) and after (green triangles) immersion in DTAB solutions and rinsing as a function of dry brush thickness. Error bars represent standard deviations of measurements on three films. Some error bars are not obvious due to their small values.

3.3.3.2.2. Effect of DTAB Concentration

In solutions with DTAB concentrations of 1 and 2 mM, the swelling of PMEDASH brushes is similar with that shown in Figure 3.24 (see Figure 3.25). When the DTAB concentration is 10 or 20 mM, however, no decrease in PMEDSAH brush swelling (relative to in deionized water) occurs regardless of brush thickness. Instead, there is a steady brush swelling 50% higher than in water, except for very thin films which show swelling >50% higher than in water (Figure 3.25). Instead of moving freely on PMEDSAH brush surfaces in 6 mM SDS and in 5 mM DTAB, hexadecane droplets attach to the brush surface in 10 mM DTAB, indicating reduced hydrophilicity of the outermost brush layers. As DTAB molecules diffuse into PMEDSAH brushes, some of them will form ion pairs with zwitterions, but the binding is not strong due to the hydrophobicity of DTAB. Thus, we suppose when DTAB concentration is close to its critical micelle concentration, which is 14 mM,[83] the bonded DTAB molecules may form micelles with free DTAB molecules in

the outermost brush region, decreasing the brush superhydrophilicity and perhaps preventing further DTAB diffusion into the brushes.

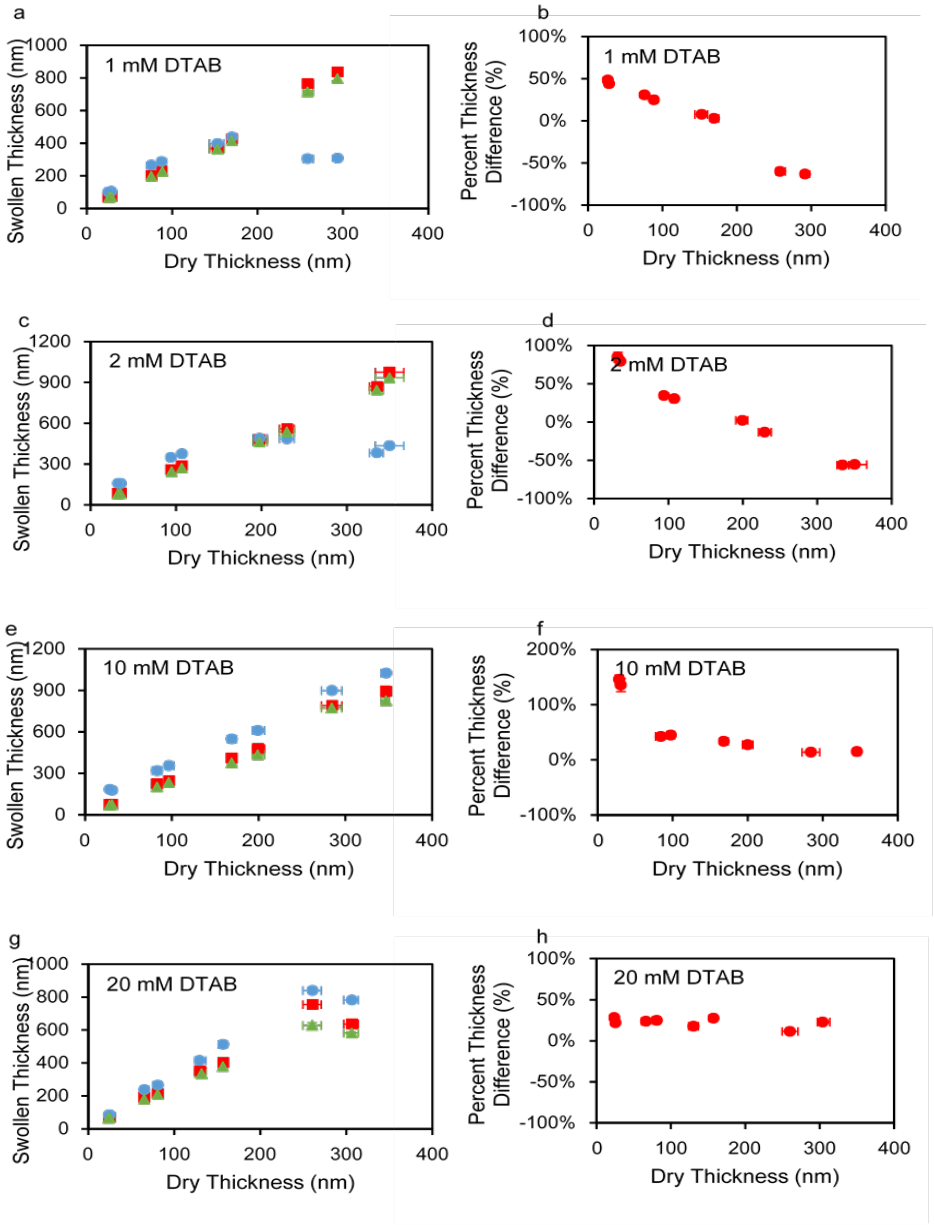

Figure 3.25. Ellipsometric thicknesses (a, c, e, g) and percent thickness differences relative to in deionized water (b, d, f, h) of swollen PMEDSAH brushes in 1, 2, 10, and 20 mM DTAB as a function of dry brush thickness. Thicknesses of swollen PMEDSAH brushes in DTAB, as well as in deionized water before and after immersion in DTAB and rinsing are plotted as blue circles, red squares and green triangles, respectively. Error bars represent standard deviations of measurements on three films. Some error bars are not visible due to their small values.

3.3.3.3.Dead-End Filtration of Surfactant Solutions with PMEDSAH-Modified Membranes

To examine the implications of ionic surfactant adsorption to PSBMA brushes, we performed dead-end filtrations of surfactant solutions through PMEDSAH-modified membranes. As discussed above, thick PMEDSAH brushes decrease in thickness only in

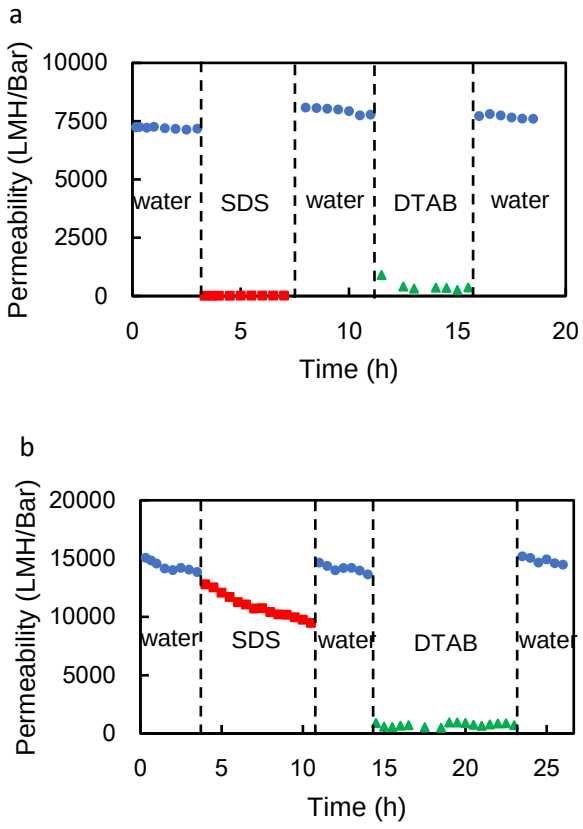

Figure 3.26. Dead-end filtrations of 6 mM SDS (red squares) and 2 mM DTAB (green triangles) through (a) PMEDSAH-coated nylon membranes and (b) bare nylon membranes. Pure water permeability (blue circles) was determined between surfactant filtrations.

SDS solutions with surfactant concentrations of 6 mM and above or in DTAB solutions with surfactant concentrations of 5 mM and below. Thus, we prepared 6 mM SDS and 2 mM DTAB to examine the swelling of brushes on membranes. Figure 3.26 shows that pure water permeabilities of the PMEDSAH-modified membrane and the bare nylon membrane with a pore size of 0.45 µm are ~7500 and ~13000 LMH/Bar, respectively. With the crude

assumption of a uniform distribution of cylindrical pores with a diameter of 0.45 μm, and using Equation 3, these filtration data suggest a swollen brush thickness of ~30 nm in deionized water. This low thickness implies that PMEDSAH brushes are much thinner than brushes on Au-coated wafers. Based on the permeabilities of PMEDSAH-modified membranes in surfactant solutions, the calculated swollen brush thicknesses in 6 mM SDS and 2 mM DTAB are 180 and 130 nm, respectively. This is consistent with the high swelling of thin brushes in 6 mM SDS (Figure 3.13) and relatively low swelling in 2 mM DTAB (Figure 3.25). The adsorption of SDS to PMEDSAH brushes on nylon induces charge screening and brush swelling, leading to blockage of membrane pores and extremely low permeability. Less adsorption of DTAB, presumably due to the hydrophobicity of its head group, induces lower brush swelling and a higher permeability. As discussed above, rinsing with water removes SDS and DTAB from polymer brushes. Thus, the membrane permeability returns to its original value after rinsing with water, as Figure 26 shows. Figure 3.26b also suggests significant adsorption of multilayers of DTAB in bare nylon membranes, probably due to the hydrophobicity of DTAB. Given the small length of DTAB (< 2 nm) compared with the membrane pore size (0.45 μm), the low fluxes imply multilayer adsorption. In contrast, SDS decreases flux through nylon membranes by only 30%. Figure 3.27 shows replicate data for filtrations.

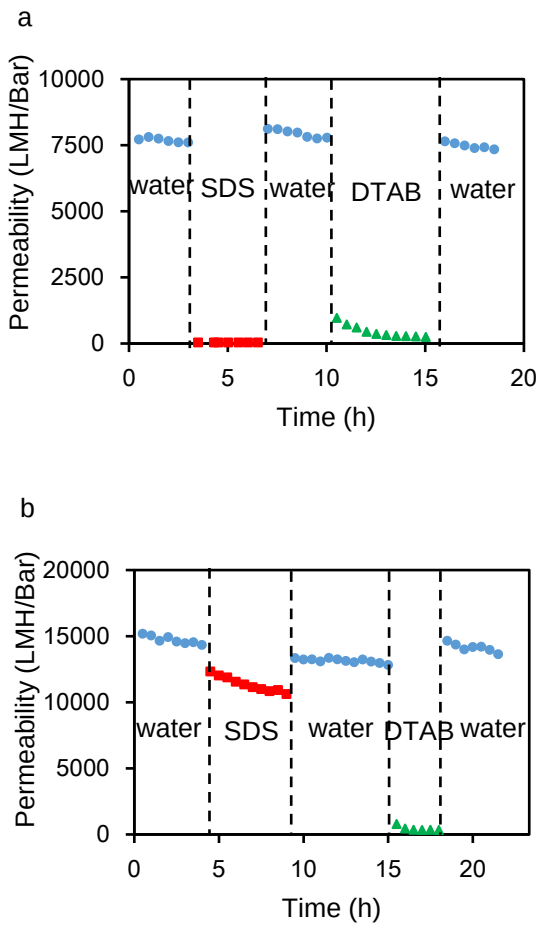

Figure 3.27. Replicate dead-end filtrations of 6 mM SDS (red squares) and 2 mM DTAB (green triangles) through (a) PMEDSAH-coated nylon membranes and (b) bare nylon membranes. Pure water permeability (blue circles) was determined before and after surfactant filtrations. These experiments were performed with a different set of membranes than Figure 3.26.

3.4. Conclusions

This research investigated the sorption of ionic surfactants in zwitterionic PSBMA brushes along with the resulting brush swelling. For thin brushes with dry thicknesses <20 nm, the presence of SDS leads to a swelling increase of about 400% with respect to swelling in water. Presumably the surfactant diffuses into the brush layer and screens charges to disrupt ionic crosslinks and enhance aqueous swelling. In contrast, for thicker films the surfactant decreases aqueous swelling, probably because of the hydrophobicity of the surfactant tail

and the disordering of water molecules around zwitterions. Similar trends in swelling as a function of dry film thickness occur in 500 mM NaCl. The more hydrophobic cationic surfactant DTAB has less effect on brush swelling than SDS for thin brushes. However, with low surfactant concentrations (≤ 5 mM) and thick (>200 nm) brushes DTAB has the same effect as SDS: a decrease in aqueous swelling. Filtration data with brush-modified membranes are consistent with high swelling of thin brushes in SDS, as permeability decreases by 99.8% in 6 mM SDS. Meanwhile, the membrane permeability in 2 mM DTAB is more than 20 times higher than that in 6 mM SDS, consistent with lower swelling of PMEDSAH brushes in the cationic surfactant.

REFERENCES

REFERENCES

1. Barbey, R.; Lavanant, L.; Paripovic, D.; Schuwer, N.; Sugnaux, C.; Tugulu, S.; Klok, H. A. Polymer Brushes Via Surface-Initiated Controlled Radical Polymerization: Synthesis, Characterization, Properties, and Applications. *Chem. Rev.* **2009**, *109*, 5437-5527.

2. Li, L. Y.; Chen, S. F.; Zheng, J.; Ratner, B. D.; Jiang, S. Y. Protein Adsorption on Oligo(Ethylene Glycol)-Terminated Alkanethiolate Self-Assembled Monolayers: The Molecular Basis for Nonfouling Behavior. *J. Phys. Chem. B* **2005**, *109*, 2934-2941.

3. Chen, S. F.; Li, L. Y.; Zhao, C.; Zheng, J. Surface Hydration: Principles and Applications toward Low-Fouling/Nonfouling Biomaterials. *Polymer* **2010**, *51*, 5283-5293.

4. Jeon, S.; Lee, J.; Andrade, J.; De Gennes, P. Protein—Surface Interactions in the Presence of Polyethylene Oxide: I. Simplified Theory. *J. Colloid Interface Sci.* **1991**, *142*, 149-158.

5. Bernards, M. T.; Cheng, G.; Zhang, Z.; Chen, S. F.; Jiang, S. Y. Nonfouling Polymer Brushes Via Surface-Initiated, Two-Component Atom Transfer Radical Polymerization. *Macromolecules* **2008**, *41*, 4216-4219.

6. Chang, Y.; Liao, S. C.; Higuchi, A.; Ruaan, R. C.; Chu, C. W.; Chen, W. Y. A Highly Stable Nonbiofouling Surface with Well-Packed Grafted Zwitterionic Polysulfobetaine for Plasma Protein Repulsion. *Langmuir* **2008**, *24*, 5453-5458.

7. Feng, W.; Brash, J. L.; Zhu, S. P. Non-Biofouling Materials Prepared by Atom Transfer Radical Polymerization Grafting of 2-Methacryloloxyethyl Phosphorylcholine: Separate Effects of Graft Density and Chain Length on Protein Repulsion. *Biomaterials* **2006**, *27*, 847-855.

8. Feng, W.; Zhu, S. P.; Ishihara, K.; Brash, J. L. Adsorption of Fibrinogen and Lysozyme on Silicon Grafted with Poly(2-Methacryloyloxyethyl Phosphorylcholine) Via Surface-Initiated Atom Transfer Radical Polymerization. *Langmuir* **2005**, *21*, 5980-5987.

9. Zhang, Z.; Chen, S. F.; Jiang, S. Y. Dual-Functional Biomimetic Materials: Nonfouling Poly(Carboxybetaine) with Active Functional Groups for Protein Immobilization. *Biomacromolecules* **2006**, *7*, 3311-3315.

10. Higaki, Y.; Kobayashi, M.; Murakami, D.; Takahara, A. Anti-Fouling Behavior of Polymer Brush Immobilized Surfaces. *Polymer Journal* **2016**, *48*, 325-331.

11. Kobayashi, M.; Takahara, A. Synthesis and Frictional Properties of Poly(2,3-Dihydroxypropyl Methacrylate) Brush Prepared by Surface-Initiated Atom Transfer Radical Polymerization. *Chem. Lett.* **2005**, *34*, 1582-1583.

12. Kobayashi, M.; Terayama, Y.; Hosaka, N.; Kaido, M.; Suzuki, A.; Yamada, N.; Torikai, N.; Ishihara, K.; Takahara, A. Friction Behavior of High-Density Poly(2-Methacryloyloxyethyl Phosphorylcholine) Brush in Aqueous Media. *Soft Matter* **2007**, *3*, 740-746.

13. Sakata, H.; Kobayashi, M.; Otsuka, H.; Takahara, A. Tribological Properties of Poly(Methyl Methacrylate) Brushes Prepared by Surface-Initiated Atom Transfer Radical Polymerization. *Polymer Journal* **2005**, *37*, 767-775.

14. Wei, Q. B.; Cai, M. R.; Zhou, F.; Liu, W. M. Dramatically Tuning Friction Using Responsive Polyelectrolyte Brushes. *Macromolecules* **2013**, *46*, 9368-9379.

15. Wang, W.; Li, L.; Henzler, K.; Lu, Y.; Wang, J.; Han, H.; Tian, Y.; Wang, Y.; Zhou, Z.; Lotze, G. Protein Immobilization onto Cationic Spherical Polyelectrolyte Brushes Studied by Small Angle X-Ray Scattering. *Biomacromolecules* **2017**, *18*, 1574-1581.

16. Levin, A.; Czeslik, C. Effect of High Pressure on Protein Binding to Poly (Acrylic Acid) Brushes. *Biophys. J.* **2017**, *112*, 590a.

17. Khalaf, R.; de Neuville, B. C.; Morbidelli, M. Protein Adsorption in Polyelectrolyte Brush Type Cation-Exchangers. *J. Chromatogr. A* **2016**, *1471*, 126-137.

18. Iwasaki, Y.; Omichi, Y.; Iwata, R. Site-Specific Dense Immobilization of Antibody Fragments on Polymer Brushes Supported by Silicone Nanofilaments. *Langmuir* **2008**, *24*, 8427-8430.

19. Xia, F.; Feng, L.; Wang, S.; Sun, T.; Song, W.; Jiang, W.; Jiang, L. Dual‐Responsive Surfaces That Switch between Superhydrophilicity and Superhydrophobicity. *Adv. Mater.* **2006**, *18*, 432-436.

20. Azzaroni, O.; Brown, A. A.; Huck, W. T. S. UCST Wetting Transitions of Polyzwitterionic Brushes Driven by Self-Association. *Angew. Chem. Int. Ed.* **2006**, *45*, 1770-1774.

21. Zhang, J.; Kou, R.; Liu, G. Effect of Salt Concentration on the pH Responses of Strong and Weak Polyelectrolyte Brushes. *Langmuir* **2017**.

22. Liu, G. M.; Zhang, G. Z. Periodic Swelling and Collapse of Polyelectrolyte Brushes Driven by Chemical Oscillation. *J. Phys. Chem. B* **2008**, *112*, 10137-10141.

23. Zhou, F.; Shu, W. M.; Welland, M. E.; Huck, W. T. S. Highly Reversible and Multi-Stage Cantilever Actuation Driven by Polyelectrolyte Brushes. *J. Am. Chem. Soc.* **2006**, *128*, 5326-5327.

24. Gao, K.; Kearney, L. T.; Howarter, J. A. Planar Phase Separation of Weak Polyelectrolyte Brushes in Poor Solvent. *J.Polymer Sci. Part B: Polymer Phys.* **2017**, *55*, 370-377.

25. Li, L.; Li, J.; Lukehart, C. M. Graphitic Carbon Nanofiber-Poly(Acrylate) Polymer Brushes as Gas Sensors. *Sensor Actuat. B-Chem* **2008**, *130*, 783-788.

26. Santer, S.; Kopyshev, A.; Donges, J.; Yang, H. K.; Rühe, J. Dynamically Reconfigurable Polymer Films: Impact on Nanomotion. *Adv. Mater.* **2006**, *18*, 2359-2362.

27. Li, D. J.; Sheng, X.; Zhao, B. Environmentally Responsive "Hairy" Nanoparticles: Mixed Homopolymer Brushes on Silica Nanoparticles Synthesized by Living Radical Polymerization Techniques. *J. Am. Chem. Soc.* **2005**, *127*, 6248-6256.

28. Terayama, Y.; Arita, H.; Ishikawa, T.; Kikuchi, M.; Mitamura, K.; Kobayashi, M.; Yamada, N.; Takahara, A. In Chain Dimensions in Free and Immobilized Brush States of Polysulfobetaine in Aqueous Solution at Various Salt Concentrations, *J. Phys. Conf. Ser.*, 2011; IOP Publishing: 2011; p 012010.

29. Hoshino, T.; Tanaka, Y.; Jinnai, H.; Takahara, A. Surface and Interface Analyses of Polymer Brushes by Synchrotron Radiation. *J. Phys. Soc. Jpn.* **2013**, *82*.

30. Kobayashi, M.; Terayama, Y.; Yamaguchi, H.; Terada, M.; Murakami, D.; Ishihara, K.; Takahara, A. Wettability and Antifouling Behavior on the Surfaces of Superhydrophilic Polymer Brushes. *Langmuir* **2012**, *28*, 7212-7222.

31. Moore, P. N.; Puvvada, S.; Blankschtein, D. Role of the Surfactant Polar Head Structure in Protein-Surfactant Complexation: Zein Protein Solubilization by SDS and by SDS/$C_{12}E_n$ Surfactant Solutions. *Langmuir* **2003**, *19*, 1009-1016.

32. Deo, N.; Jockusch, S.; Turro, N. J.; Somasundaran, P. Surfactant Interactions with Zein Protein. *Langmuir* **2003**, *19*, 5083-5088.

33. Rosen, M. J., Emulsification by Surfactants. In *Surfactants and Interfacial Phenomena*, John Wiley & Sons, Inc., 2004; p 303-331.

34. Bouchemal, K.; Briancon, S.; Perrier, E.; Fessi, H. Nano-Emulsion Formulation Using Spontaneous Emulsification: Solvent, Oil and Surfactant Optimisation. *Int. J. Pharm.* **2004**, *280*, 241-251.

35. Walstra, P. Principles of Emulsion Formation. *Chem. Eng. Sci.* **1993**, *48*, 333-349.

36. Franklin, V. J. Cleaning Efficacy of Single-Purpose Surfactant Cleaners and Multi-Purpose Solutions. *Contact Lens and Anterior Eye* **1997**, *20*, 63-68.

37. Kaplan, M. C.; Jegou, A.; Chaufer, B.; Rabiller-Baudry, M.; Michalsky, M. C. Adsorption of Lysozyme on Membrane Material and Cleaning with Non-Ionic Surfactant Characterized through Contact Angle Measurements. *Desalination* **2002**, *146*, 149-154.

38. Jurado, E.; Bravo, V.; Luzon, G.; Fernandez-Serrano, M.; Garcia-Roman, M.; Altmajer-Vaz, D.; Vicaria, J. M. Hard-Surface Cleaning Using Lipases: Enzyme-Surfactant Interactions and Washing Tests. *J. Surfactants Deterg.* **2007**, *10*, 61-70.

39. Giolando, S. T.; Rapaport, R. A.; Larson, R. J.; Federle, T. W.; Stalmans, M.; Masscheleyn, P. Environmental Fate and Effects of Deedmac - a New Rapidly Biodegradable Cationic Surfactant for Use in Fabric Softeners. *Chemosphere* **1995**, *30*, 1067-1083.

40. Miao, Z. C.; Yang, J. Z.; Wang, L.; Liu, Y.; Zhang, L.; Li, X. L.; Peng, L. Synthesis of Biodegradable Lauric Acid Ester Quaternary Ammonium Salt Cationic Surfactant and Its Utilization as Calico Softener. *Mater. Lett.* **2008**, *62*, 3450-3452.

41. Saraiva, S. A.; Abdeinur, P. V.; Catharino, R. R.; Nunes, G.; Eberlin, M. N. Fabric Softeners: Nearly Instantaneous Characterization and Quality Control of Cationic Surfactants by Easy Ambient Sonic-Spray Ionization Mass Spectrometry. *Rapid Commun. Mass Spec.* **2009**, *23*, 357-362.

42. Yang, Z. F.; Tarabara, V. V.; Bruening, M. L. Adsorption of Anionic or Cationic Surfactants in Polyanionic Brushes and Its Effect on Brush Swelling and Fouling Resistance During Emulsion Filtration. *Langmuir* **2015**, *31*, 11790-11799.

43. Dunlop, I. E.; Thomas, R. K.; Titmus, S.; Osborne, V.; Edmondson, S.; Huck, W. T. S.; Klein, J. Structure and Collapse of a Surface-Grown Strong Polyelectrolyte Brush on Sapphire. *Langmuir* **2012**, *28*, 3187-3193.

44. Li, X.; Hu, X.; Cai, T. Construction of Hierarchical Fouling Resistance Surfaces onto Poly (Vinylidene Fluoride) Membranes for Combating Membrane Biofouling. *Langmuir* **2017**, *33*, 4477-4489.

45. Higaki, Y.; Fröhlich, B.; Yamamoto, A.; Murakami, R.; Kaneko, M.; Takahara, A.; Tanaka, M. Ion-Specific Modulation of Interfacial Interaction Potentials between Solid Substrates and Cell-Sized Particles Mediated Via Zwitterionic, Super-Hydrophilic Poly (Sulfobetaine) Brushes. *J. Phys. Chem. B* **2017**, *121*, 1396-1404.

46. Ezzat, M.; Huang, C. J. Zwitterionic Polymer Brush Coatings with Excellent Anti-Fog and Anti-Frost Properties. *RSC. Adv.* **2016**, *6*, 61695-61702.

47. Kobayashi, M.; Terayama, Y.; Kikuchi, M.; Takahara, A. Chain Dimensions and Surface Characterization of Superhydrophilic Polymer Brushes with Zwitterion Side Groups. *Soft Matter,* **2014**, *9, 5138-5148*.

48. Sun, Y.; Chen, C.; Xu, H.; Lei, K.; Xu, G.; Zhao, L.; Lang, M. Surface Modification of Silicon Wafer by Grafting Zwitterionic Polymers to Improve Its Antifouling Property. *Appl. Surf. Sci.* **2017**, *419*, 642-649.

49. Polzer, F.; Heigl, J.; Schneider, C.; Ballauff, M.; Borisov, O. V. Synthesis and Analysis of Zwitterionic Spherical Polyelectrolyte Brushes in Aqueous Solution. *Macromolecules* **2011**, *44*, 1654-1660.

50. Kobayashi, M.; Ishihara, K.; Takahara, A. Neutron Reflectivity Study of the Swollen Structure of Polyzwitterion and Polyeletrolyte Brushes in Aqueous Solution. *J. Biomat. Sci.-Polym. E* **2014**, *25*, 1673-1686.

51. Xiang, T.; Luo, C. D.; Wang, R.; Han, Z. Y.; Sun, S. D.; Zhao, C. S. Ionic-Strength-Sensitive Polyethersulfone Membrane with Improved Anti-Fouling Property Modified by Zwitterionic Polymer Via in Situ Cross-Linked Polymerization. *J. Membr. Sci.* **2015**, *476*, 234-242.

52. Che, Y.-J.; Tan, Y.; Ren, X.; Xin, H.; Meng, F. Solution Properties of Hydrophobically Modified Acrylamide-Based Polysulfobetaines in the Presence of Surfactants. *Colloid Polym. Sci.* **2012**, *290*, 1237-1245.

53. Chen, H.; Kelley, M.; Guo, C.; Yarger, J. L.; Dai, L. L. Adsorption and Release of Surfactant into and from Multifunctional Zwitterionic Poly(NIPAm-*co*-DMAPMA-*co*-AAc) Microgel Particles. *J. Colloid Interface Sci.* **2015**, *449*, 332-340.

54. Costa, T.; de Azevedo, D.; Stewart, B.; Knaapila, M.; Valente, A. J. M.; Kraft, M.; Scherf, U.; Burrows, H. D. Interactions of a Zwitterionic Thiophene-Based Conjugated Polymer with Surfactants. *Polym. Chem.* **2015**, *6*, 8036-8046.

55. Johnson, K. M.; Fevola, M. J.; Lochhead, R. Y.; McCormick, C. L. Hydrophobically Modified Acrylamide-Based Polybetaines. II. Interaction with Surfactants in Aqueous Solution. *J. Appl. Polym. Sci.* **2004**, *92*, 658-671.

56. Johnson, K. M.; Poe, G. D.; Lochhead, R. Y.; McCormick, C. L. The Synthesis of Hydrophobically Modified Water‐Soluble Polyzwitterionic Copolymers and Responsiveness to Surfactants in Aqueous Solution. *J. Macromol. Sci., Part A* **2004**, *41*, 587-611.

57. Kudaibergenov, S.; Jaeger, W.; Laschewsky, A. In *Supramolecular Polymers Polymeric Betains Oligomers*; Abe, A., Kobayashi., S., Eds.; Springer, 2006; pp 157-224.

58. Zhang, R.; Ma, S.; Wei, Q.; Ye, Q.; Yu, B.; van der Gucht, J.; Zhou, F. The Weak Interaction of Surfactants with Polymer Brushes and Its Impact on Lubricating Behavior. *Macromolecules* **2015**, *48*, 6186-6196.

59. Shah, R. R.; Merreceyes, D.; Husemann, M.; Rees, I.; Abbott, N. L.; Hawker, C. J.; Hedrick, J. L. Using Atom Transfer Radical Polymerization to Amplify Monolayers of Initiators Patterned by Microcontact Printing into Polymer Brushes for Pattern Transfer. *Macromolecules* **2000**, *33*, 597-605.

60. Li, C. Y.; Wang, W. C.; Xu, F. J.; Zhang, L. Q.; Yang, W. T. Preparation of pH-Sensitive Membranes Via Dopamine-Initiated Atom Transfer Radical Polymerization. *J. Membr. Sci.* **2011**, *367*, 7-13.

61. Ye, G.; Lee, J.; Perreault, F.; Elimelech, M. Controlled Architecture of Dual-Functional Block Copolymer Brushes on Thin-Film Composite Membranes for Integrated

"Defending" and "Attacking" Strategies against Biofouling. *ACS Appl. Mater. Inter.* **2015**, *7*, 23069-23079.

62. Harris, J. J.; Bruening, M. L. Electrochemical and in Situ Ellipsometric Investigation of the Permeability and Stability of Layered Polyelectrolyte Films. *Langmuir* **2000**, *16*, 2006-2013.

63. Huang, W.; Baker, G. L.; Bruening, M. L. Controlled Synthesis of Cross-Linked Ultrathin Polymer Films by Using Surface-Initiated Atom Transfer Radical Polymerization. *Angew. Chem. Int. Ed.* **2001**, *40*, 1510-1512.

64. Mulder, J., *Basic Principles of Membrane Technology*, 2nd Ed.; Springer, 1996; Vol. 4, p 170.

65. Hossain, M. F.; Biswas, T. K.; Islam, M.; Huque, M. E. Volumetric and Viscometric Studies on Dodecyltrimethylammonium Bromide in Aqueous and in Aqueous Amino Acid Solutions in Premicellar Region. *Monatsh. Chem. Chem. Mon.* **2010**, *141*, 1297-1308.

66. Ito, T.; Mizutani, H. The Viscosity of Aqueous Sodium Dodecyl Sulfate Solution and the Effect of Inorganic Electrolytes on It. *J. Japan Oil Chemists' Soc.* **1968**, *17*, 246-248.

67. Kestin, J.; Khalifa, H. E.; Correia, R. J. Tables of the Dynamic and Kinematic Viscosity of Aqueous NaCl Solutions in the Temperature Range 20–150 C and the Pressure Range 0.1–35 Mpa. *J. Phys. Chem. Ref. Data* **1981**, *10*, 71-88.

68. Terayama, Y.; Kikuchi, M.; Kobayashi, M.; Takahara, A. Well-Defined Poly (Sulfobetaine) Brushes Prepared by Surface-Initiated ATRP Using a Fluoroalcohol and Ionic Liquids as the Solvents. *Macromolecules* **2010**, *44*, 104-111.

69. Crompton, T. R., *Practical Polymer Analysis*. Springer Science & Business Media: 2012.

70. Milosevic, M.; King, S. W. Validation of a Correction Procedure for Removing the Optical Effects from Transmission Spectra of Thin Films on Substrates. *J. Appl. Phys.* **2012**, *112*, 093514.

71. Bengani, P.; Kou, Y.; Asatekin, A. Zwitterionic Copolymer Self-Assembly for Fouling Resistant, High Flux Membranes with Size-Based Small Molecule Selectivity. *J. Membr. Sci.* **2015**, *493*, 755-765.

72. Li, Q.; Bi, Q.-Y.; Liu, T.-Y.; Wang, X.-L. Resistance to Protein and Oil Fouling of Sulfobetaine-Grafted Poly (Vinylidene Fluoride) Hollow Fiber Membrane and the Electrolyte-Responsive Behavior in NaCl Solution. *Appl. Surf. Sci.* **2012**, *258*, 7480-7489.

73. Xiang, T.; Luo, C.-D.; Wang, R.; Han, Z.-Y.; Sun, S.-D.; Zhao, C.-S. Ionic-Strength-Sensitive Polyethersulfone Membrane with Improved Anti-Fouling Property

Modified by Zwitterionic Polymer Via in Situ Cross-Linked Polymerization. *J. Membr. Sci.* **2015**, *476*, 234-242.

74. Tugulu, S.; Klok, H.-A. Stability and Nonfouling Properties of Poly (Poly (Ethylene Glycol) Methacrylate) Brushes under Cell Culture Conditions. *Biomacromolecules* **2008**, *9*, 906-912.

75. Sheiko, S. S.; Sun, F. C.; Randall, A.; Shirvanyants, D.; Rubinstein, M.; Lee, H.-i.; Matyjaszewski, K. Adsorption-Induced Scission of Carbon-Carbon Bonds. *Nature* **2006**, *440*, 191.

76. Leng, C.; Han, X.; Shao, Q.; Zhu, Y.; Li, Y.; Jiang, S.; Chen, Z. In Situ Probing of the Surface Hydration of Zwitterionic Polymer Brushes: Structural and Environmental Effects. *J. Phys. Chem. C* **2014**, *118*, 15840-15845.

77. Hänni-Ciunel, K.; Findenegg, G. H.; von Klitzing, R. Water Contact Angle on Polyelectrolyte-Coated Surfaces: Effects of Film Swelling and Droplet Evaporation. *Soft Mater*. **2007**, *5*, 61-73.

78. Park, I. J.; Lee, S.-B.; Choi, C. K.; Kim, K.-J. Surface Properties and Structure of Poly (Perfluoroalkylethyl Methacrylate). *J. Colloid Interface Sci.* **1996**, *181*, 284-288.

79. Zisman, W. A. In *Contact Angle, Wettability, and Adhesion*, Fowkes. M. F., Ed.; ACS, 1964; Vol. 1, p 22.

80. Khan, A. M.; Shah, S. S. Determination of Critical Micelle Concentration (CMC) of Sodium Dodecyl Sulfate (SDS) and the Effect of Low Concentration of Pyrene on Its CMC Using Origin Software. *J. Chem. Soc. Pakistan* **2008**, *30*, 186.

81. Davies, J. A Quantitative Kinetic Theory of Emulsion Type, I. Physical Chemistry of the Emulsifying Agent. *Proc. 2nd Intern. Congr. Surface Activity, Butterworths Scientific Publication, London* **1957**, *426*.

82. Proverbio, Z.; Bardavid, S.; Arancibia, E.; Schulz, P. Hydrophile–Lipophile Balance and Solubility Parameter of Cationic Surfactants. *Colloids Surf. A: Physicochem. Eng. Asp.* **2003**, *214*, 167-171.

83. Bahri, M. A.; Hoebeke, M.; Grammenos, A.; Delanaye, L.; Vandewalle, N.; Seret, A. Investigation of SDS, DTAB and CTAB Micelle Microviscosities by Electron Spin Resonance. *Colloids Surf. A: Physicochem. Eng. Asp.* **2006**, *290*, 206-212.

Chapter 4. Oil Coalescence on Superoleophobic Membrane Surfaces during Dead-End and Cross-Flow Filtrations

4.1. Introduction

Membrane filtration plays an important role in oil-water separations, especially for removal of submicron and surfactant-stabilized oil droplets from water.[1-4] However, fouling presents a major challenge in these and other membrane applications.[5-7] Foulants attach to the surface and block membrane pores during filtration to greatly reduce membrane permeability. As a result, frequent membrane cleaning or replacement may make filtration unacceptably expensive.

To solve this problem, research groups around the world are creating new membranes with excellent fouling resistance. For example, Yan and co-workers modified ultrafiltration membranes with nano-sized alumina to resist fouling in wastewater from an oil field.[8] Chang produced a poly(ethylene glycol)-coated poly (vinylidene fluoride) membrane that resists fouling by bovine serum albumin (BSA).[9] Rahimpour and co-workers prepared anti-fouling nano-porous PVDF membranes using UV photo-grafting to coat these substrates with both acrylate and amino monomers.[10] However, these modified membranes will most likely show fouling resistance only with diluted solutions or in the initial filtration stage.[11] In addition, the complex or expensive protocols for membrane modification are probably not suitable for large-scale applications.[1]

An equally viable separation strategy could aim to use membranes not as filters but as substrates that catalyze the coalescence of oil droplets. Coalescence has been part of effective oil-removal methods for years,[12] because tiny oil droplets do not readily separate from water. Over time many improvements to coalescence have appeared. For example,

plate separators employ parallel plates to prompt oil contact and coalescence.[13] Induced gas flotation relies on oil coalescing with injected air bubbles to form large and light oil-air bubbles that float to the surface.[14-16] Nevertheless, these traditional techniques can only separate relatively large oil droplets (> 50 μm).[17]

In 2001, Nitsch and co-workers reported membrane-induced oil coalescence and proposed a mechanism for this process.[17] Many subsequent studies aimed to improve this technique. Huck's research group coated surfaces with polymer brushes to capture oil droplets and release them after they coalescence.[18] Yang and co-workers designed nonwoven filter mats for the coalescence of emulsified oil droplets,[19] and Agarwal and co-workers investigated several factors that affect membrane-induced oil coalescence, including surface roughness and orientation.[20, 21] The Fane group also studied factors that affect oil coalescence on membranes, especially the pore size and imposed in-pore shear rate.[22]

Most studies employ hydrophobic membranes for oil coalescence, but this chapter describes my attempts to use a superoleophobic membrane to induce droplet aggregation.[20] As reported previously, hydrophobic membranes may lose their functionality after adsorption of a large amount of oil.[19] Thus, even for membranes that act as coalescers, too much oil adsorption is not productive for droplet coalescence. I hypothesized that a balance between oleophobicity and hydrophobicity may create a surface that induces oil coalescence and simultaneously resists oil adsorption. To initially examine this hypothesis, I prepared zwitterionic poly(sulfobetaine methacrylate) (PSBMA) brushes on different membranes and examined whether oil will coalesce on these substrates. Although PSBMA

brushes are superoleophobic in water,[23, 24] their net uncharged surface may permit weak adsorption of charged oil droplets and subsequent coalescence.

4.2. Experimental

4.2.1. Materials

Hydrophilic nylon membranes with nominal 0.45 μm diameter pores (25 mm diameter, NY4525100) was obtained from Sterlitech. Hydrophilic track-etched polycarbonate membranes with 0.2 μm diameter pores were purchased from Sigma-Aldrich (25 mm diameter, WHA110606). Si (111) wafers were obtained from University Wafer (Boston, MA) and coated with Au at LGA Thin Films (Santa Clara, CA) by sputtering 200 nm of gold on 20 nm of Cr on Si wafers. [2-(Methacryloyloxy) ethyl] dimethyl-(3-sulfopropyl) ammonium hydroxide (97%, MEDSAH), 3-sulfopropyl methacrylate potassium salt (98%, SPMK), dopamine hydrochloride (98%), 11-mercapto-1-undecanol (97%), ammonium chloride (≥99.5%), α-bromoisobutyryl bromide (98%, BIBB), 2,2'-bipyridine (≥99%, bpy) and sodium dodecyl sulfate (98.5%, SDS) were purchased from Sigma-Aldrich. Tris(hydroxymethyl)aminomethane hydrochloride (≥99%, Tris hydrochloride) was obtained from Invitrogen, and dodecyltrimethylammonium bromide (99%, DTAB) was acquired from Acros Organics. Bromine (100%) and triethylamine (100%) were purchased from J.T. Baker, whereas copper (I) chloride (≥99.995%), copper (II) chloride dihydrate (≥99.0%) and dimethylformamide (≥99.8%, DMF) were acquired from Jade Scientific. Acetone (99.7%) and ethyl acetate were purchased from Fisher Scientific. Anhydrous dichloromethane, hexane (analytical reagent grade, AR) and chloroform (AR) were obtained from Macron Fine Chemicals. Dichloromethane was used as received, and chloroform, toluene and triethylamine were dried with molecular sieves (3 Å, Sigma-

Aldrich) before use. Araldite 2020 two-component epoxy adhesive system was obtained from Huntsman. Aqueous solutions were prepared using deionized water (Milli-Q, 18.2 MΩ·cm), and the disulfide initiator, $(BrC(CH_3)_2COO(CH_2)_{11}S)_2$ was synthesized according to literature procedures.[25]

4.2.2. Preparation of Polyelectrolyte Brushes on Membranes

The initiator employed in this chapter is polydopamine modified by α-bromoisobutyryl bromide (PDA-BIBB). The protocols of initiator immobilization and polymerization of both SPMK and MEDSAH on membranes are the same as those described in Chapter 3.

4.2.3. Contact Angle Measurement

Contact angles of water or hexadecane on membrane surfaces were determined using a phone camera and contact angle calculation software (VCA2000, AST Products). Contact angles in air were determined by placing a drop of water or hexadecane on dry membranes. To determine the surface hydrophilicity in water, a drop of hexadecane was first placed on dry membranes, followed by immersing membranes in water.

4.2.4. Emulsion Preparation and Characterization

Hexadecane submicron emulsions stabilized with SDS or CTAB were prepared and characterized as described in Chapter 2. These emulsions were used in dead-end filtrations. As submicron oil droplets are invisible in the direct observation though the membrane (DOTM) system, another emulsion was prepared with a protocol described in the literature.[26] Briefly, 0.1 mmol of surfactant (SDS or CTAB) was dissolved in 1 L of water, followed by addition of 1 mL of hexadecane. Then the mixture was stirred for 20 min at 1000 rpm with a digital stand mixer (RW20 digital dual-range mixer, IKA).

4.2.5. Dead-End Filtration

The specific flux (L/(m^2·h·bar)), referred to as LMH/bar) and observed oil rejection (R, %) of the membranes were determined in the same apparatus using the same method as described in Chapter 2 except for a few changes. Because of the differences in mechanical strengths of different membranes, the applied pressure was 0.7 bar, which is half of the pressure applied in Chapter 2, to avoid breaking or deforming membranes. To achieve more precise control of the concentration of feed solutions, 0.68 mL of the 10% hexadecane emulsion was added to the Amicon cell, followed by the addition of 9.32 mL of water to keep the total volume of the feed solution at 10 mL.

Oil rejection was calculated based on the calibration curve in Figure 4.1. Several blank solutions without hexadecane were analyzed to determine the minimum detectable signal (average of the blank signal plus three times the standard deviation of this signal.) Based on this minimum detectable signal and the calibration curve, the detection limit of these analyses is 8.3 ×10^{-6} M hexadecane. Hexadecane concentration in the feed solution was measured before every filtration and compare with the calculated value to ensure the accuracy of calibration curve.

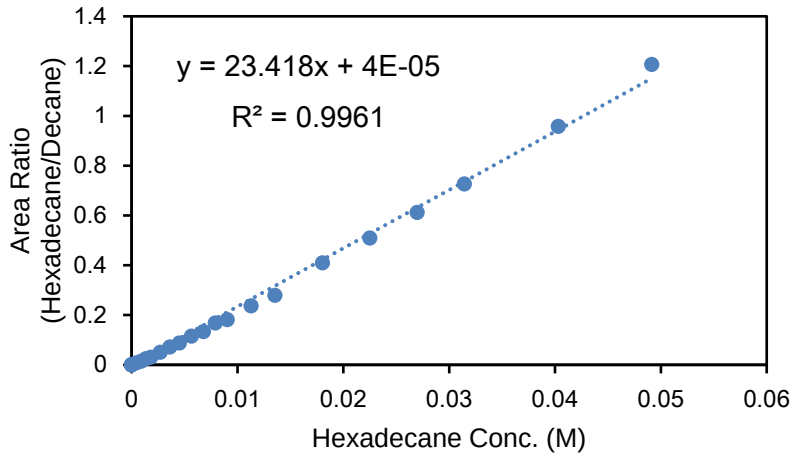

Figure 4.1. GC calibration curve showing a linear relationship between the ratio of GC peak area (hexadecane/decane) and the concentration of hexadecane at high hexadecane concentration.

All of the filtration experiments were repeated with 2 or 3 membranes. Preliminary data only include filtration through modified nylon and track-etched membranes.

4.2.6. Visualization of Oil Coalescence on Membranes during Filtration

Oil coalescence was observed with the DOTM system shown in Figure 4.2.[26] The hydrophilic track-etched polycarbonate membrane with 0.2 µm diameter pores was used

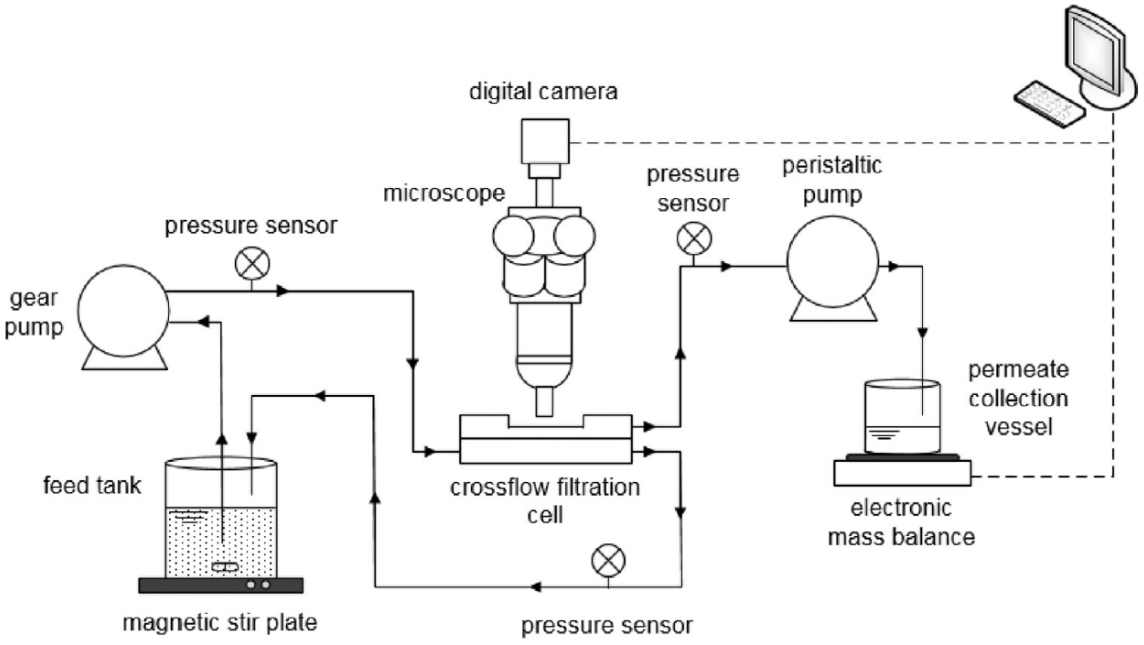

Figure 4.2. Apparatus for DOTM system. Reprinted from reference 26 with permission from Elsevier.

for DOTM because it is sufficiently transparent when wet. Using Araldite 2020 adhesive, the membrane disk with a diameter of 25 mm was framed between two pieces of printing paper. A 2.4 cm^2 square cutout was created on both printing papers for optical observation. Then the framed membrane was placed in the cross-flow filtration cell and secured on the microscope stage with the permeate side facing upwards. Flow rates of the feed and permeate were controlled using a gear pump (drive model 75211-15, Cole-Parmer) and a peristaltic pump (Minipuls 3, Gilson), respectively. The pressures of the feed, retentate and permeate streams were monitored by pressure transducers (Cole-Parmer) interfaced with a

computer. The permeate solution was collected in a beaker on a balance to record the mass and calculate the permeate flux. During the whole filtration and observation, both pumps were maintained at a constant setting to keep uniform flow rates.

4.3. Results and Discussion

4.3.1. Wettability of Membranes

Membrane modification includes two steps: initiator (PDA-BIBB) immobilization and PMEDSAH brush growth, and the reaction times of both steps may affect the wettability. Figure 4.3 shows contact angles of hexadecane on nylon membranes modified with PMEDSAH brushes. To examine the effect of PDA-BIBB deposition on wettability, I kept the PMEDSAH polymerization time constant at 4 h. As Figure 4.3 shows, longer PDA-BIBB deposition times lead to higher hexadecane contact angles, indicating more oleophobic surfaces. We suppose this is due to higher PDA-BIBB coverage on the membrane, which results in thicker PMEDSAH brushes or higher brush coverage. Lee reported that PDA coverage reaches a maximum after immersing surfaces in dopamine solution for about 24 h.[27] Thus, all modified membranes for emulsion filtration employed a 48-h deposition of PDA-BIBB. Figure 4.4 shows that with 4-h PDA-BIBB deposition, membrane surfaces with PMEDSAH brushes polymerized for over 2 h become superoleophobic when immersed in water, leading to oil detachment from membrane, as shown in Figure 4.4a, b and c. To ensure the surface superoleophobicity, we employed a 24 h-polymerization to obtain preliminary filtration results. Future filtrations could examine the fouling resistance of PMEDSAH brush-modified membranes prepared with shorter polymerization times. As a control, the bare nylon membrane shows an underwater

contact angle of hexadecane around 80° (Figure 4.4d), indicating relatively poor fouling resistance to oil adsorption.

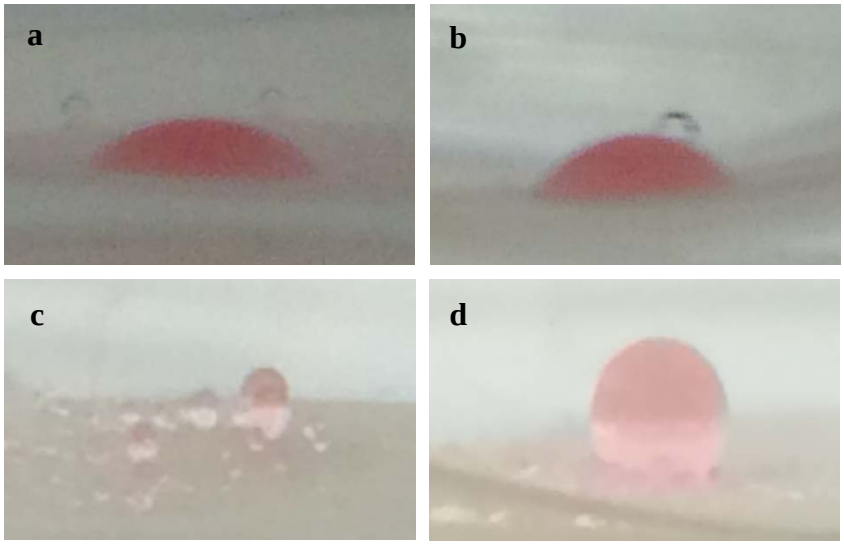

Figure 4.3. Contact angles of hexadecane (with red dye) in water on nylon membranes with a pore size of 0.45 µm after coating with PDA-BIBB and PMEDSAH brushes. The PMEDSAH polymerization time was 4 h, and the PDA-BIBB deposition times were (a) 1 h, (b) 2 h, (c) 3.5 h and (d) 5.5 h.

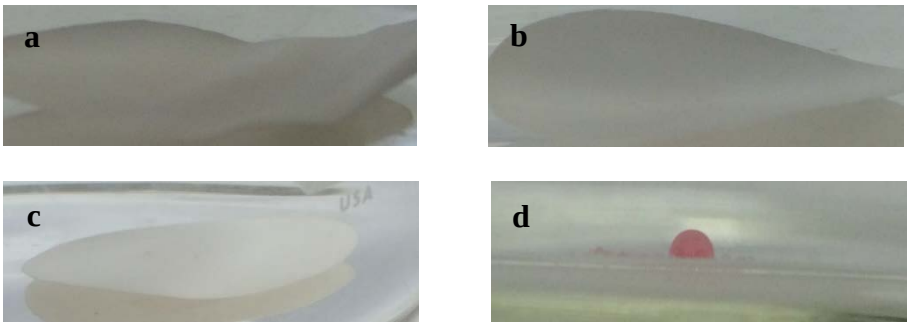

Figure 4.4. Contact angles of hexadecane (with red dye) in water on nylon membranes with a pore size of 0.45 µm after coating with PDA-BIBB and PMEDSAH brushes. The deposition time of PDA-BIBB is 4 h. Polymerization time for PMEDSAH brushes is (a) 2 h, (b) 4 h and (c) 6 h. A bare nylon membrane (d) served as a control. In Figures (a), (b), and (c), the droplet is not visible because it detaches from the membrane.

4.3.2. Dead-End Filtrations of O/W Submicron Emulsions

4.3.2.1.Track-Etched Membrane

4.3.2.1.1. Bare Track-Etched Membrane

As Figure 4.5 shows, during the filtration of an SDS-stabilized submicron emulsion through bare track-etched membranes, the permeate flux is around 60 LMH/Bar, which is only 2% of the pure water flux before filtration. This implies that many membrane pores are at least partially blocked by the oil droplets. On the other hand, the hexadecane concentration in the permeate is always lower than the limit of detection, indicating nearly 100% oil rejection. However, the bare track-etched membrane has a pore size of 0.2 µm, whereas only about half of the oil droplets (volume fraction) have a diameter greater than 0.2 µm (see Figure 4.6a). The very high oil rejection may result from excluded volume, a decrease in the pore size due to oil fouling, adsorption of small droplets, or droplet coalescence. Comparison of the oil droplet diameters in the feed (Figure 4.6a) and retentate (Figure 4.6b) solutions shows some oil coalescence, and the median droplet diameter, termed as D50,[28] increases from 0.196 to 0.325 µm. Nevertheless, this small increase in droplet size does not change the milky look of the emulsion (Figure 4.7).

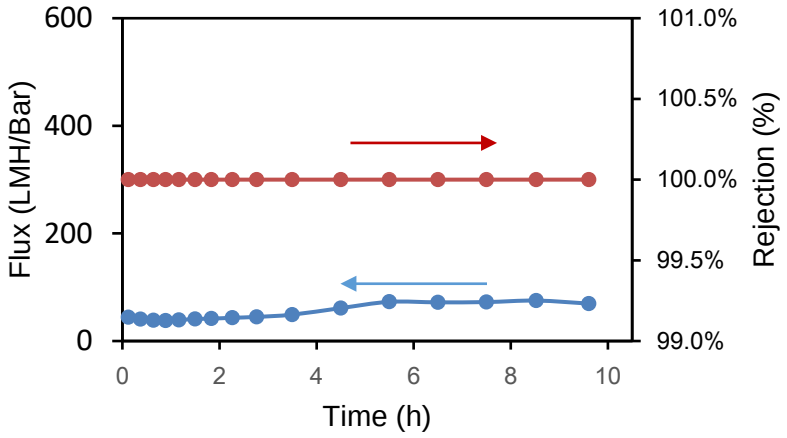

Figure 4.5. (cont'd) Permeate flux and oil rejection during dead-end filtration of an SDS-stabilized emulsion through a bare track-etched membrane.

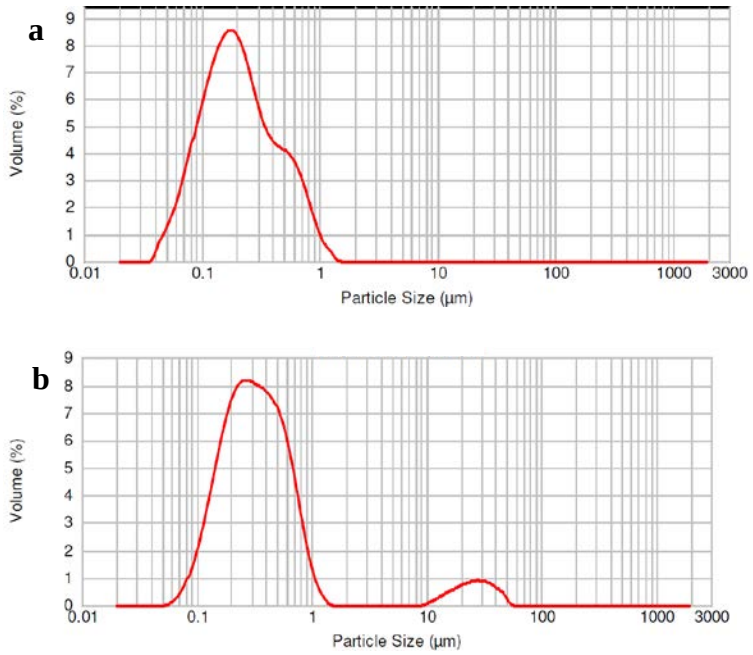

Figure 4.6. Oil droplet size before (a) and after (b) dead-end filtration of an SDS-stabilized emulsion through a bare track-etched membrane.

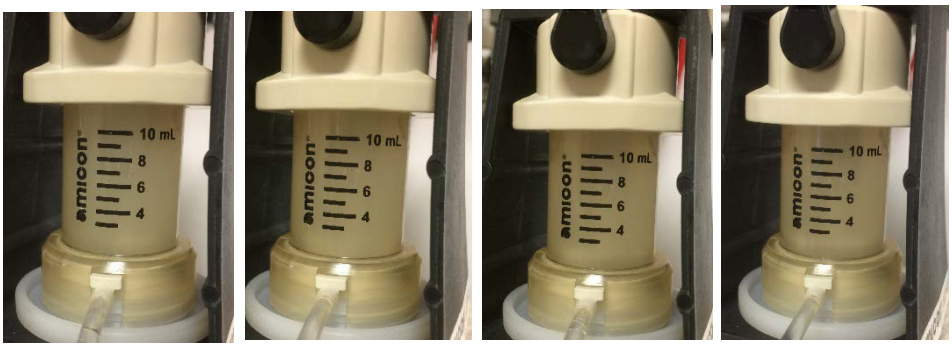

1 h 3 h 6 h 10 h

Figure 4.7. Images of an SDS-stabilized O/W submicron emulsion at different times during filtration through a bare track-etched membrane with 0.2 µm pores.

When we employed the bare track-etched membrane for the filtration of CTAB-stabilized emulsions, the oil rejection is still almost 100%. (Figure 4.8) However, demulsification begins from the start of filtration, making the emulsion gradually look like

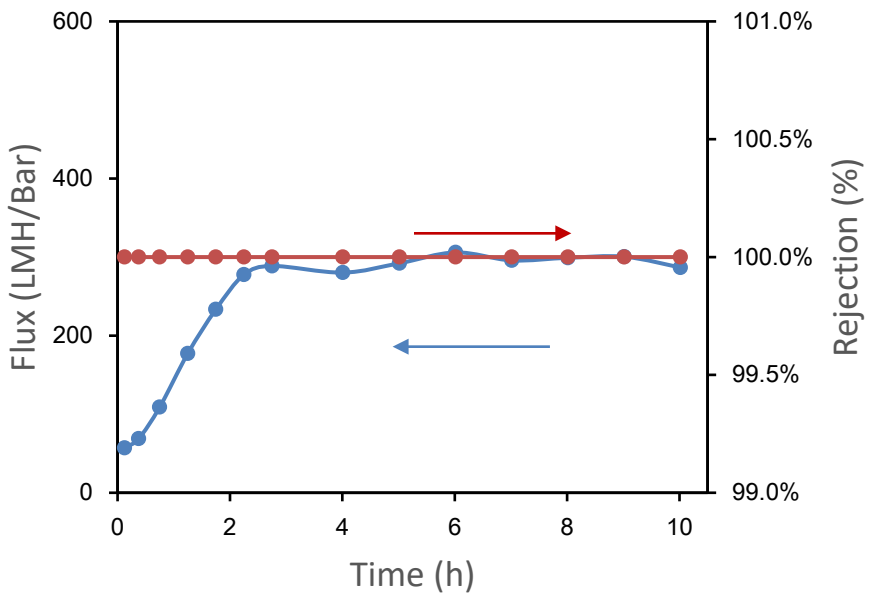

Figure 4.8. Permeate flux and oil rejection during dead-end filtration of a CTAB-stabilized emulsion through a bare track-etched membrane.

milky and finally clear after 3 h of filtration (Figure 4.9). Meanwhile, the permeate flux gradually increased during the first 3 h of filtration and then remained constant. The low

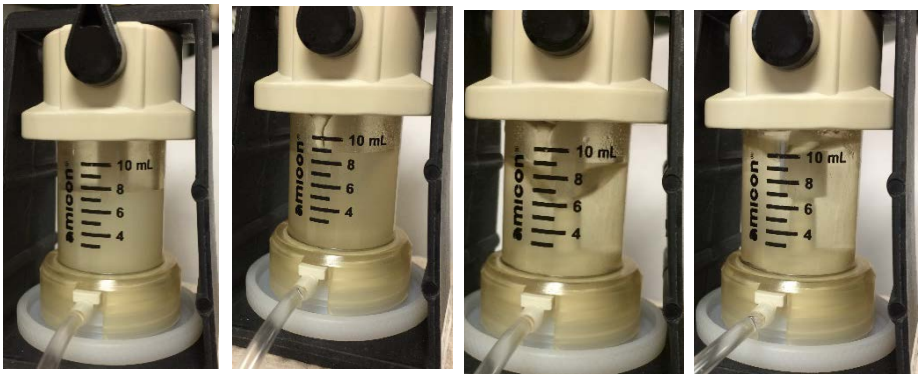

Figure 4.9. Images of a CTAB-stabilized O/W submicron emulsion at different times during filtration through a track-etched membrane with 0.2 μm pores.

initial permeate flux may stem from membrane fouling. The combination of the flux increase and the emulsion clarification suggest that oil droplets attached to the membrane eventually coalesce with other incoming droplets. Larger droplets likely float away from

the membrane to the top of the solution. Stoke's equation (Eq. 1), describes the droplet vertical velocity, V,

$$V = \frac{d^2 g(\rho_w - \rho_o)}{18\mu_w} \quad \text{Eq. 1}$$

where d is the diameter of oil droplet, ρ_w and ρ_o are the densities of water and oil, respectively, and μ_w is the dynamic viscosity of water. (The variable g represents the acceleration due to gravity.). Larger droplets will experience stronger buoyant forces and detach from membrane and float to the surface with relatively high velocities. Alternatively, Nitsch and co-workers reported that as oil droplets become large enough to block membrane pores, water occlusions may create W/O droplets, which can also float to the surface.[17] The detachment of oil from the membrane leads to less pore blocking and an increasing permeate flux, as Figure 4.8 shows. Because we keep adding water from the feed tank into the filtration cell, there is no new oil entering the system. After oil coalesces and floats to the solution surface, the permeate flux remains constant around 300 LMH/Bar. This flux is much lower than the pure water flux before emulsion filtration (2500 LMH/Bar), indicating that oil on or in the membrane still partially blocks the pores.

4.3.2.1.2. Track-Etched Membranes Modified with PDA-BIBB

As Figures 4.10 and 4.11 imply, after coating a track-etched membrane with PDA-BIBB, the ATRP initiator, the modified track-etched membrane induces coalescence of droplets

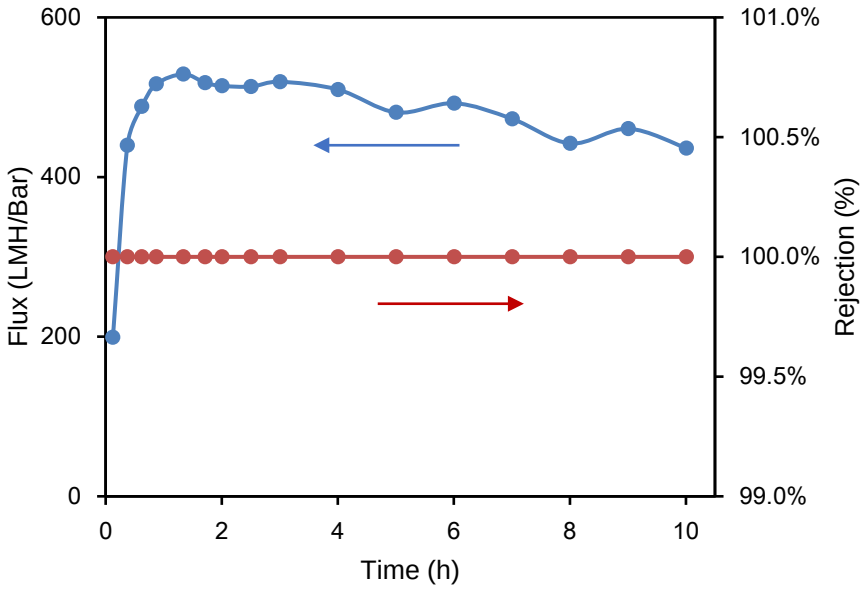

Figure 4.10. Permeate flux (blue) and oil rejection (red) during the dead-end filtration of an SDS-stabilized emulsion through a track-etched membrane modified with PDA-BIBB (the PDA-BIBB deposition time is 48 h).

stabilized by SDS, leading to a flux increase from 200 to 500 LMH/Bar and demulsification within 1-h of filtration. This may stem from the increased roughness after the attachment of PDA-BIBB. As Agarwal reported, higher surface roughness prompts oil coalescence by providing strong adhesion with oil and increasing coalescence efficiency.[20] However, this coating seems to prevent the coalescence of oil droplets stabilized by CTAB, as the flux

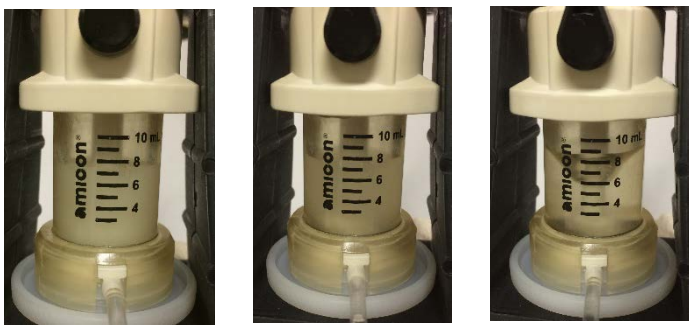

0 h 0.25 h 0.5 h

Figure 4.11. Images of an SDS-stabilized O/W submicron emulsion at different times during dead-end filtration through a track-etched membrane modified with PDA-BIBB (the deposition time is 48 h).

does not greatly increase over 9 h or filtration (Figure 4.12). Additionally, there is only a small difference in oil droplet sizes before (D50 = 0.176 μm) and after filtration (D50 = 0.205 μm) of the CTAB-stabilized emulsion, as Figure 4.13 shows.

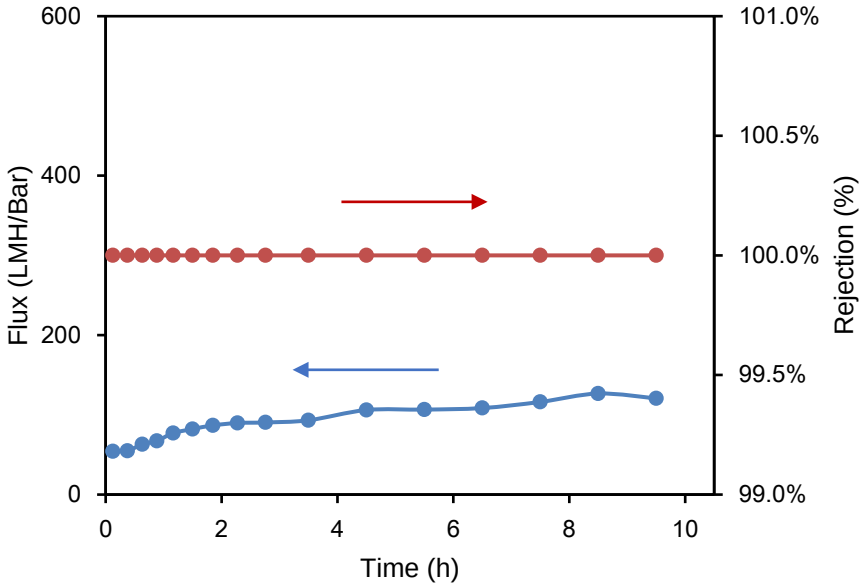

Figure 4.12. Permeate flux (blue) and oil rejection (red) during the dead-end filtration of CTAB-stabilized emulsion using a track-etched membrane modified with PDA-BIBB (the deposition time is 48 h).

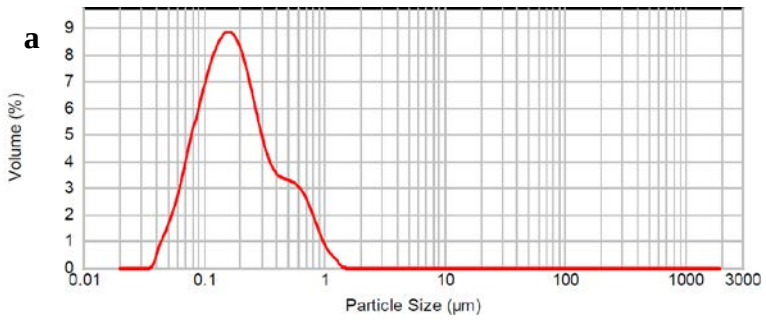

Figure 4.13 (cont'd)

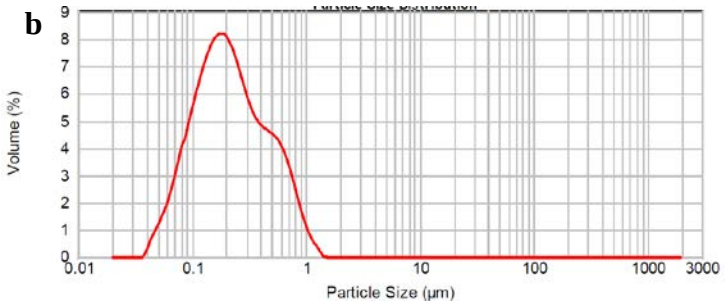

Figure 4.13. Oil droplet size distribution before (a) and after (b) dead-end filtration of a CTAB-stabilized emulsion through a track-etched membrane modified with PDA-BIBB (deposition time: 48 h).

4.3.2.1.3. Track-Etched Membrane Modified with PMEDSAH Brushes

The data in Figures 4.14 and 4.15 indicate that track-etched membranes modified with

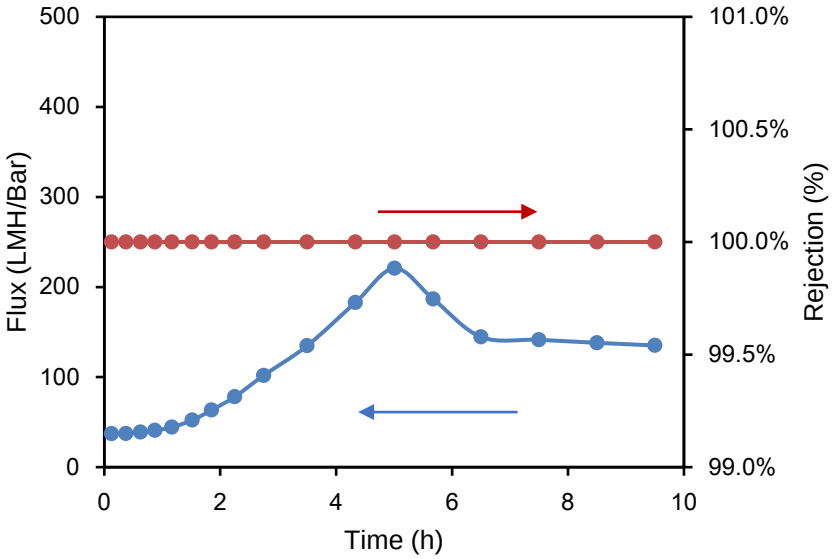

Figure 4.14. Permeate flux (blue) and oil rejection (red) during the dead-end filtration of an SDS-stabilized emulsion through a track-etched membrane modified with PMEDSAH brushes (the polymerization time was 12 h).

superoleophobic PMEDSAH brushes do not induce rapid demulsification of submicron emulsions stabilized by SDS. However, the permeate flux initially increases with time and oil droplets also become marginally larger (D50 increase from 0.213 to 0.268 µm) after

10-h filtration. This is probably because the superoleophobicity of PMEDSAH brushes resists oil adsorption, which is the first step for membrane-induced oil coalescence.[17]

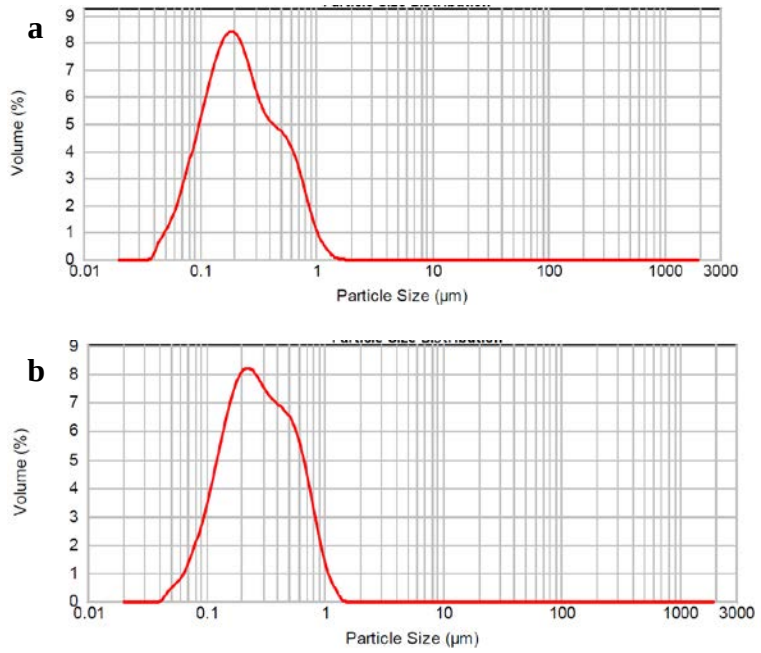

Figure 4.15. Oil droplet size before (a) and after (b) dead-end filtration (10 h) of an SDS-stabilized emulsion through a track-etched membrane modified with PMEDSAH brushes (polymerization time: 12 h).

4.3.2.2.Nylon Membranes

4.3.2.2.1. Bare Nylon Membrane

Demulsification occurs for both SDS- (Figure 4.16) and CTAB-stabilized emulsions (Figure 4.17) during filtration through bare nylon membranes. Since the pore size (0.45 µm) of bare nylon membranes is larger than around 80% of the oil droplets, much of the oil should pass through unfouled membranes. However, the negligible oil concentration in the permeate, which is lower than the detection limit, suggesting that oil adsorbs to the membrane and decreases pore sizes. Increases in flux at long times and solution clarification indicate eventual oil droplet coalescence. The pure water flux through a bare nylon membrane was ~13000 LMH/Bar.

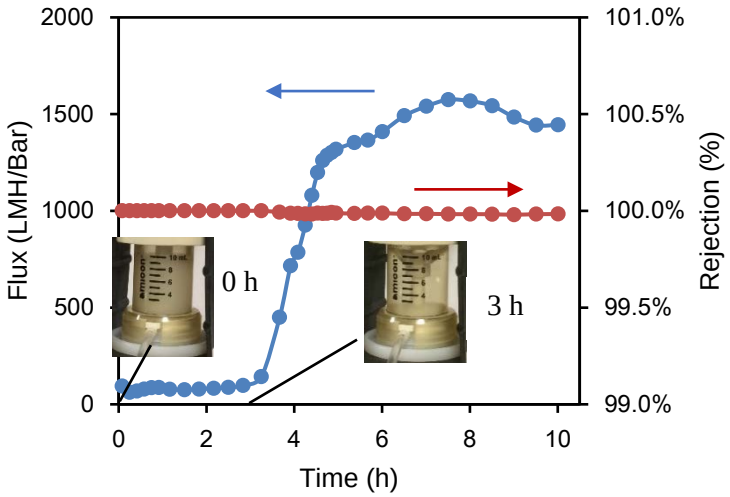

Figure 4.16. Permeate flux (blue) and oil rejection (red) during dead-end filtration of an SDS-stabilized emulsion through a bare nylon membrane with a pore size of 0.45 µm. The photos show the O/W submicron emulsion at different times during the filtration.

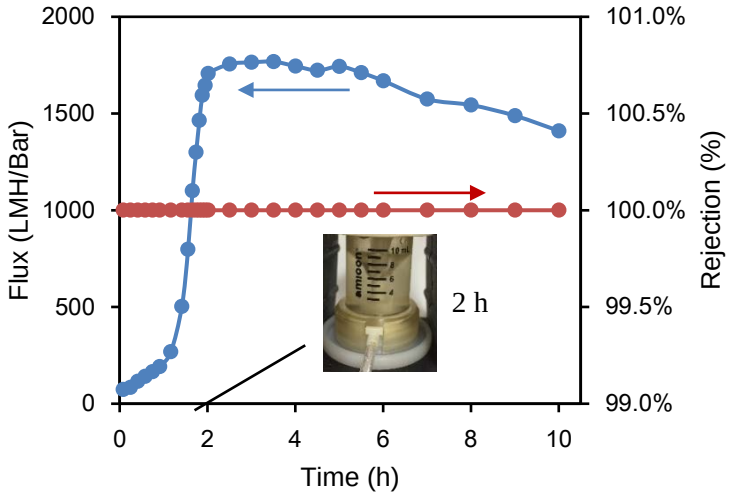

Figure 4.17. Permeate flux (blue) and oil rejection (red) during the dead-end filtration of a CTAB-stabilized emulsion through a bare nylon membrane with a pore size of 0.45 µm. The photo shows the O/W submicron emulsion after 2 h of filtration.

4.3.2.2.2. Nylon Membranes Modified with PMEDSAH Brushes

For emulsions stabilized with SDS, oil coalescence occurs during the filtration with nylon membranes modified with PMEDSAH Brushes and leads to demulsification after 5 h

(Figure 4.18). As discussed above, oil coalescence leads to less pore blocking and a resulting increase in permeate flux. The bare nylon membrane shows a drastic flux increase

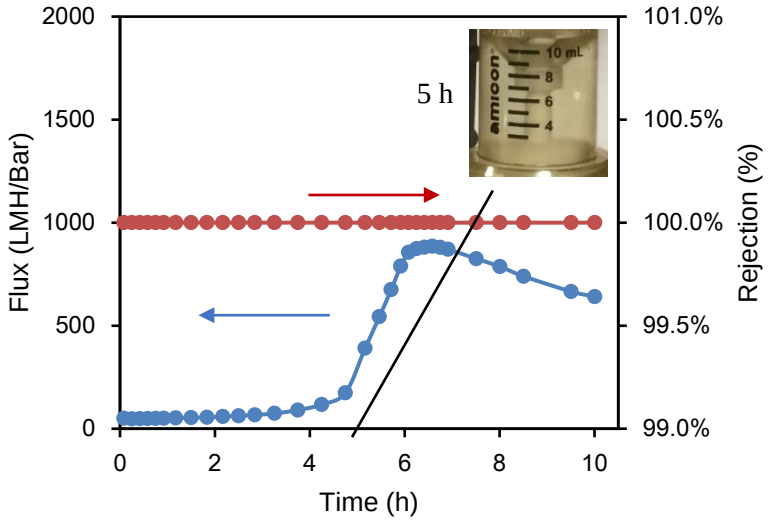

Figure 4.18. Permeate flux (blue) and oil rejection (red) during dead-end filtration of an SDS-stabilized emulsion through a nylon membrane modified with PMEDSAH brushes (24 h polymerization time). The photo shows the O/W submicron emulsion after 2 h-filtration. The pure water flux through the modified membrane was 2600 LMH/Bar.

after 3 h of filtration, but after modification with PMEDSAH brushes, the permeate flux starts to increase dramatically after 5 h of filtration. The superoleophobic coating likely resists some oil attachment in the beginning and delays the demulsification process. As a comparison, the filtration of an SDS-stabilized emulsion using PSPMK-modified membranes (Figure 4.19) leads to a constant permeate flux. As discussed in Chapter 2, this is due to the electrostatic repulsion between negatively charged oil and polyanionic brushes. Thus, we suppose that although the zwitterionic PMEDSAH brushes are superoleophobic, without the strong electrostatic repulsion between oil droplets and the surface, these brushes cannot resist all oil adsorption in dead-end filtration.

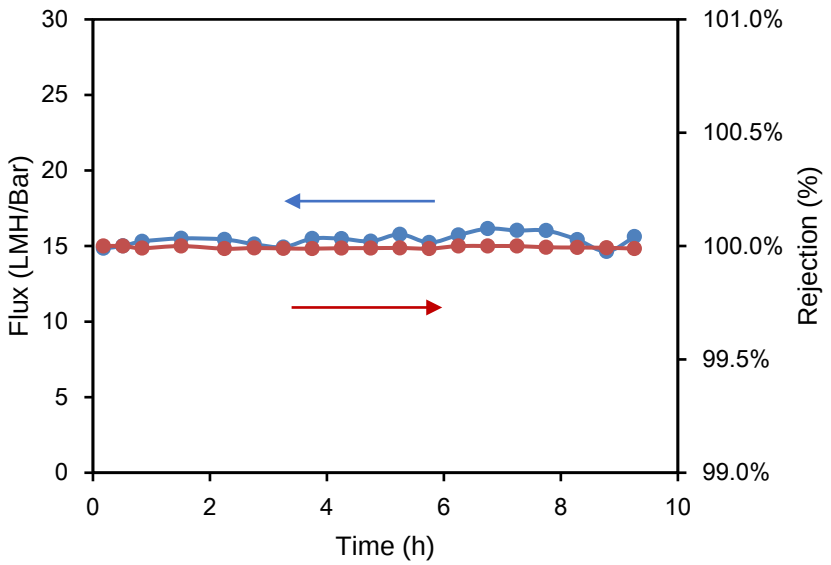

Figure 4.19. Permeate flux (blue) and oil rejection (red) during dead-end filtration of an SDS-stabilized emulsion through a nylon membrane modified with PSPMK brushes (the polymerization time was 24 h).

For CTAB-stabilized emulsions, we did not observe obvious oil coalescence and demulsification during filtration through the PMEDSAH-modified membranes. Figure 4.20 shows the permeate flux and oil rejection during filtration. The small flux increase may stem from either brush collapse after fouling or the coalescence of a small part of oil. The latter may be more convincing since brush collapse may induce a much higher flux increase. According to the Hagen-Poiseuille equation, which I described in Chapter 2, a small change in pore radius will make a significant change in permeate flux. However, this needs to be confirmed by comparing droplet sizes before and after filtration.

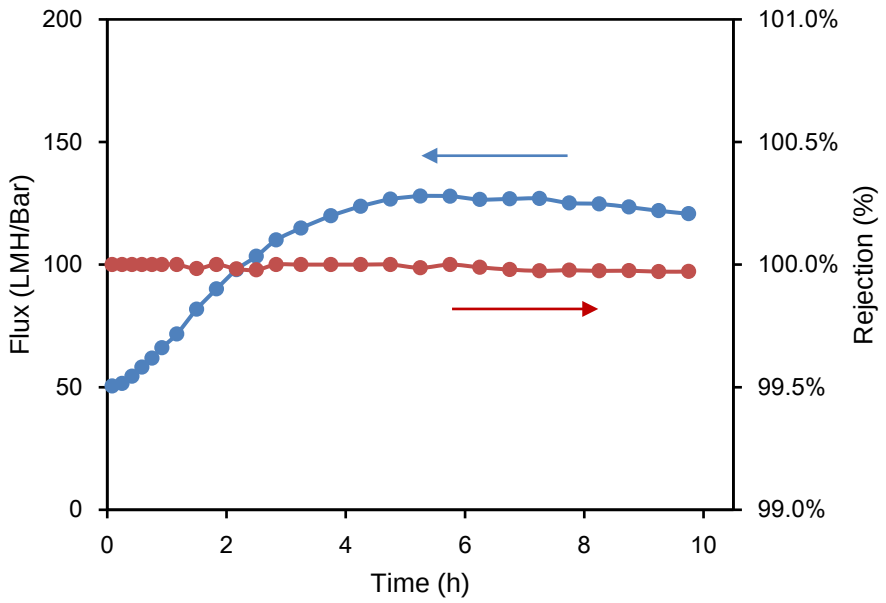

Figure 4.20. Permeate flux (blue) and oil rejection (red) during dead-end filtration of a CTAB-stabilized emulsion through a nylon membrane modification with PMEDSAH brushes (24-h polymerization time).

4.3.3. DOTM

As Figure 4.2 shows, the DOTM system employs cross-flow filtration, and the flow tangential to the membrane may result in less chances for oil contact and coalescence than in dead-end filtration. Because the DOTM pressure and flux data are still not available, I only show qualitatively whether droplet coalescence was visible and compare these results with the dead-end filtration data (Table 4.1). For some types of membranes, the disagreement in oil coalescence between cross-flow and dead-end filtration may result from the different emulsions used in the two system or types of filtration (dead-end and cross-flow). The particle size in the emulsions employed in cross-flow was generally over 10 µm to permit visualization.

Table 4.1. Results of oil coalescence in dead-end filtration and crossflow (DOTM) through bare and modified track-etched membranes. "Y" represents clear oil coalescence and demulsification,

(cont'd) whereas "N" indicates no obvious oil coalescence, even if a small increase in oil droplet size appeared.

	SDS-emulsion		CTAB-emulsion	
	dead-end filtration	DOTM	dead-end filtration	DOTM
bare track-etched	N	N	Y	Y
PDA-BIBB-modified track-etched	Y	N	N	Y
PMEDSAH-modified track-etched	N	N	N	N

4.4. Conclusions

Despite its wide use as an anti-fouling material, the zwitterionic PSBMA brush does not show strong resistance to fouling with submicron oil droplets in dead-end filtrations. For emulsions stabilized with either SDS or CTAB, oil droplets adsorb on this brush surface and block pores, leading to a low permeate flux. However, this oil adsorption may induce oil coalescence, which can break the emulsion and increase the permeate flux. Previous studies about membrane coalescence mainly focused on hydrophobic membranes since oil can attach and coalesce more on these surfaces. Our work shows that a less anti-fouling coating such as the PSBMA brush can also induce oil coalescence, but it does not foul and saturate with oil as easily as hydrophobic membranes. However, more experiments are needed to better understand oil coalescence on PSBMA-modified membranes and design a membrane that can better induce oil coalescence and resist fouling.

REFERENCES

REFERENCES

1. Cheryan, M.; Rajagopalan, N. Membrane Processing of Oily Streams. Wastewater Treatment and Waste Reduction. *J. Membr. Sci.* **1998**, *151*, 13-28.

2. Eriksson, P. Nanofiltration Extends the Range of Membrane Filtration. *Environ. Prog. Sustain. Energy* **1988**, *7*, 58-62.

3. Gupta, A. K. S. Process for Refining Crude Glyceride Oils by Membrane Filtration. U.S. Patent 4,062,882, December 13, 1977.

4. Kajitvichyanukul, P.; Hung, Y.-T.; Wang, L. K. Membrane Technologies for Oil–Water Separation. In *Membrane and Desalination Technologies*; Wang, L. K.; Chen, J. P.; Hung, Y.-T.; Shammas, N. K., Eds.; Springer, 2011; pp 639-668.

5. Gao, W.; Liang, H.; Ma, J.; Han, M.; Chen, Z.-l.; Han, Z.-s.; Li, G.-b. Membrane Fouling Control in Ultrafiltration Technology for Drinking Water Production: A Review. *Desalination* **2011**, *272*, 1-8.

6. Guo, W.; Ngo, H.-H.; Li, J. A Mini-Review on Membrane Fouling. *Bioresour. Technol.* **2012**, *122*, 27-34.

7. Meng, F.; Chae, S.-R.; Drews, A.; Kraume, M.; Shin, H.-S.; Yang, F. Recent Advances in Membrane Bioreactors (MBRs): Membrane Fouling and Membrane Material. *Water Research* **2009**, *43*, 1489-1512.

8. Yan, L.; Li, Y. S.; Xiang, C. B. Preparation of Poly (Vinylidene Fluoride) (PVDF) Ultrafiltration Membrane Modified by Nano-Sized Alumina (Al_2O_3) and Its Antifouling Research. *Polymer* **2005**, *46*, 7701-7706.

9. Chang, Y.; Ko, C.-Y.; Shih, Y.-J.; Quémener, D.; Deratani, A.; Wei, T.-C.; Wang, D.-M.; Lai, J.-Y. Surface Grafting Control of Pegylated Poly (Vinylidene Fluoride) Antifouling Membrane Via Surface-Initiated Radical Graft Copolymerization. *J. Membr. Sci.* **2009**, *345*, 160-169.

10. Rahimpour, A.; Madaeni, S.; Zereshki, S.; Mansourpanah, Y. Preparation and Characterization of Modified Nano-Porous PVDF Membrane with High Antifouling Property Using UV Photo-Grafting. *Appl. Surf. Sci.* **2009**, *255*, 7455-7461.

11. Rana, D.; Matsuura, T. Surface Modifications for Antifouling Membranes. *Chem. Rev.* **2010**, *110*, 2448-2471.

12. Lewandowski, A. F., Collant Filter and Oil Coalescer. U.S. Patents 5,454,937, October 3, 1995.

13. Li, J.; Huang, S.; Wang, X. Experimental Research of Separation Efficiency on Steam-Water Separator with Corrugated Plates. *Nuclear Power Engineering* **2007**, *28*, 94-97.

14. Cairo Jr, J. A.; Young, J. A., Induced Gas Liquid Coalescer and Flotation Separator. U.S. Patent 5,080,802, January 14, 1992.

15. Moosai, R.; Dawe, R. A. Gas Attachment of Oil Droplets for Gas Flotation for Oily Wastewater Cleanup. *Sep.Purif. Technol.* **2003**, *33*, 303-314.

16. Leech III, C. A.; Radhakrishnan, S.; Hillyer, M. J.; Degner, V. Performance Evaluation of Induced Gas Flotation Machine through Mathematical Modeling. *J. Petrol. Technol.* **1980**, *32*, 48-58.

17. Hoffmann, S.; Nitsch, W. Membrane Coalescence for Phase Separation of Oil-in-Water Emulsions Stabilized by Surfactants and Dispersed into Smallest Droplets. *Chem. Eng. Technol.* **2001**, *24*, 22-27.

18. Tan, K. Y.; Hughes, T. L.; Nagl, M.; Huck, W. T. Nonfouling Capture–Release Substrates Based on Polymer Brushes for Separation of Water-Dispersed Oil Droplets. *ACS. App. Mater. Interfaces* **2012**, *4*, 6403-6409.

19. Hu, D.; Li, X.; Li, L.; Yang, C. Designing High-Caliber Nonwoven Filter Mats for Coalescence Filtration of Oil/Water Emulsions. *Sep. Purif. Technol.* **2015**, *149*, 65-73.

20. Agarwal, S.; von Arnim, V.; Stegmaier, T.; Planck, H.; Agarwal, A. Role of Surface Wettability and Roughness in Emulsion Separation. *Sep. Purif. Technol.* **2013**, *107*, 19-25.

21. Agarwal, S.; von Arnim, V.; Stegmaier, T.; Planck, H.; Agarwal, A. Effect of Fibrous Coalescer Geometry and Operating Conditions on Emulsion Separation. *Ind. Eng. Chem. Res.* **2013**, *52*, 13164-13170.

22. Hong, A.; Fane, A.; Burford, R. Factors Affecting Membrane Coalescence of Stable Oil-in-Water Emulsions. *J. Membr. Sci.* **2003**, *222*, 19-39.

23. Kobayashi, M.; Terayama, Y.; Yamaguchi, H.; Terada, M.; Murakami, D.; Ishihara, K.; Takahara, A. Wettability and Antifouling Behavior on the Surfaces of Superhydrophilic Polymer Brushes. *Langmuir* **2012**, *28*, 7212-7222.

24. Kobayashi, M.; Ishihara, K.; Takahara, A. Neutron Reflectivity Study of the Swollen Structure of Polyzwitterion and Polyelectrolyte Brushes in Aqueous Solution. *J. Biomat. Sci.-Polym. E* **2014**, *25*, 1673-1686.

25. Shah, R. R.; Merreceyes, D.; Husemann, M.; Rees, I.; Abbott, N. L.; Hawker, C. J.; Hedrick, J. L. Using Atom Transfer Radical Polymerization to Amplify Monolayers of Initiators Patterned by Microcontact Printing into Polymer Brushes for Pattern Transfer. *Macromolecules* **2000**, *33*, 597-605.

26. Tummons, E. N.; Tarabara, V. V.; Chew, J. W.; Fane, A. G. Behavior of Oil Droplets at the Membrane Surface During Crossflow Microfiltration of Oil–Water Emulsions. *J. Membr. Sci.* **2016**, *500*, 211-224.

27. Lee, H.; Dellatore, S. M.; Miller, W. M.; Messersmith, P. B. Mussel-Inspired Surface Chemistry for Multifunctional Coatings. *Science* **2007**, *318*, 426-430.

28. HMKTest. What Is Particle Size Distribution D50, D50 Particle Size Distribution. http://www.aimsizer.com/faqs-What-is-D50.html (accessed Aug 13, 2017).

Chapter 5. Summary and Future Work

5.1. Research Summary

This dissertation summarizes my Ph.D. research, which includes an in-depth study of the swelling of polyelectrolyte brushes in both water and surfactant solutions, fabrication of polyanionic brush-modified membranes with nearly 100% oil rejection and strong fouling resistance, and development of a superoleophobic membrane that can potentially resist fouling and prompt oil coalescence simultaneously.

Chapter 2 describes the superoleophobicity of polyanionic brushes and their application as an anti-fouling layer in the filtration of O/W submicron emulsions. The poly(3-sulfopropyl methacrylate potassium salt) (PSPMK) brush swells by up to 280% and is superoleophobic in water. The density of PSPMK brushes created through surface-initiated atom transfer radical polymerization increases with polymerization time. Due to electrostatic repulsion, the anionic PSPMK brushes completely resist the adsorption of anionic surfactants. Moreover, microfiltration membranes modified with PSPMK brushes show almost 100% oil rejection and minimal fouling during dead-end filtration of emulsions stabilized with anionic surfactants. Nevertheless, strong electrostatic attraction induces adsorption of cationic surfactants as well as positively charged oil droplets on the brush layer, leading to brush collapse and membrane fouling. Ellipsometric data further show that less dense brushes at low cationic surfactant concentrations are more likely to collapse.

Chapter 3 focuses on the swelling of zwitterionic poly(solfobetaine methacrylate) (PSBMA) brushes in ionic surfactant solutions. Similar to the effect of inorganic salts, both anionic and cationic surfactants adsorb to PSBMA brushes and change swelling

significantly. The extent of PSBMA swelling or collapse depends on the surfactant charge and concentration, as well as the brush thickness. These changes of brush swelling may stem from a combination of charge-screening, disordering of water molecules around zwitterions and the surfactant hydrophobicity. Filtration of surfactant solutions with PMEDSAH brush-modified membranes confirms high swelling of thin brushes with anionic surfactants and less swelling with cationic surfactants.

Chapter 4 presents my attempts to modify surfaces with zwitterionic PSBMA brushes to achieve fouling resistance and oil coalescence simultaneously. Both dead-end and cross-flow filtrations of submicron emulsions with different membranes show the effect of the membrane substrate on oil coalescence. As the preliminary data demonstrate, oil coalescence occurs on PSBMA brush-modified nylon membranes, whereas track-etched membranes with the same coating do not induce oil coalescence. This may result from the higher roughness on the nylon membrane surface. It also implies zwitterionic PSBMA brushes cannot completely resist oil adsorption due to the lack of strong electrostatic repulsion. Nevertheless, this weaker fouling resistance allows oil droplets to attach to the membrane, coalesce with other droplets and finally detach from the membrane.

5.2. Future Work: Membrane Modification with Zwitterionic Brushes for Oil Coalescence and Fouling Resistance

As described in Chapter 4, membrane-induced oil coalescence depends on various factors such as surface roughness, pore size and filtration pressure.[1-3] To fabricate a surface coating for both oil coalescence and fouling resistance, all of these factors may need to be considered, which requires a deeper understanding of oil coalescence, especially on

membrane surfaces. In addition, more experiments are needed to optimize the surface coating and evaluate the resistance to fouling and oil coalescence.

5.2.1. Membrane Characterization

The preliminary data mainly focus on membrane filtration, but an explanation for these filtration results requires more information about the membrane. Scanning electron microscope (SEM) and atomic force microscope (AFM) can provide morphology information, such as the roughness and the pore size and porosity changes after membrane modification. Determination of zeta potentials of membranes is also important for this research, since it can identify the sign and estimate the magnitude of the charge that the zwitterionic PSBMA brushes carry. Such information will help us to understand the interaction between oil droplets and membrane surfaces. I hypothesize that a nearly neutral membrane surface may be a good choice for providing some fouling resistance while enhancing coalescence. Firstly, less charge ensures that the surface will not completely repel oil droplets with the same charge. This is vital since weak oil attachment on membrane surface is the first step of coalescence.[4] In contrast, when the oil and the surface are oppositely charged, a nearly neutral surface will avoid extensive oil adsorption or even oil saturation.[5]

5.2.2. Dead-End and Cross-Flow Filtrations of the Same Emulsion.

Due to the invisibility of submicron oil droplets, we employed another emulsion with much larger oil droplets (~ 10 μm) for DOTM experiments, as Chapter 4 describes. To compare the effects of dead-end and cross-flow filtration on oil coalescence on membranes, emulsions employed in the two filtrations should be the same. Thus, dead-end filtrations of emulsions with larger oil droplets are necessary. From another point of view, this

experiment is also helpful to observe the coalescence of oil droplets in different sizes during dead-end filtrations.

5.2.3. Compare Zwitterionic Brushes with Neutral Hydrophilic Brushes

As discussed earlier, the nearly zero net charge on zwitterionic brush surfaces may allow both anti-fouling and oil coalescing purposes. However, neutral hydrophilic brushes such as poly(poly(ethylene glycol) methacrylate) (PPEGMA) and poly(2-hydroxyethyl methacrylate) (PHEMA) also have that potential.[6] Unlike zwitterionic brushes, these neutral brushes don't have the strong intra-group, inter-or intra-chain interactions,[7, 8] and this may lead to a less hydrated brush layer. Thus, these brushes may foul more easily, or even saturate with oil like traditional hydrophobic membranes.[5] This hypothesis needs to be verified by experiments.

REFERENCES

REFERENCES

1. Hong, A.; Fane, A.; Burford, R. Factors Affecting Membrane Coalescence of Stable Oil-in-Water Emulsions. *J. Membr. Sci.* **2003**, *222*, 19-39.

2. Agarwal, S.; von Arnim, V.; Stegmaier, T.; Planck, H.; Agarwal, A. Role of Surface Wettability and Roughness in Emulsion Separation. *Sep. Purif. Technol.* **2013**, *107*, 19-25.

3. Agarwal, S.; von Arnim, V.; Stegmaier, T.; Planck, H.; Agarwal, A. Effect of Fibrous Coalescer Geometry and Operating Conditions on Emulsion Separation. *Ind. Eng. Chem. Res.* **2013**, *52*, 13164-13170.

4. Hoffmann, S.; Nitsch, W. Membrane Coalescence for Phase Separation of Oil-in-Water Emulsions Stabilized by Surfactants and Dispersed into Smallest Droplets. *Chem. Eng. Technol.* **2001**, *24*, 22-27.

5. Hu, D.; Li, L.; Li, Y.; Yang, C. Restructuring the Surface of Polyurethane Resin Enforced Filter Media to Separate Surfactant Stabilized Oil-in-Water Emulsions Via Coalescence. *Sep. Purif. Technol.* **2017**, *172*, 59-67.

6. Barbey, R.; Lavanant, L.; Paripovic, D.; Schüwer, N.; Sugnaux, C.; Tugulu, S.; Klok, H.-A. Polymer Brushes via Surface-Initiated Controlled Radical Polymerization: Synthesis, Characterization, Properties, and Applications. *Chem. Rev.* **2009**, *109*, 5437-5527.

7. Kobayashi, M.; Ishihara, K.; Takahara, A. Neutron Reflectivity Study of the Swollen Structure of Polyzwitterion and Polyelectrolyte Brushes in Aqueous Solution. *J. Biomater. Sci. Polym. Ed.* **2014**, *25*, 1673-1686.

8. Kudaibergenov, S.; Jaeger, W.; Laschewsky, A., Polymeric Betaines: Synthesis, Characterization, and Application. In *Supramolecular Polymers Polymeric Betains Oligomers*, Springer: 2006; pp 157-224.